BONE RESONANCE ANALYSIS, HISTOMORPHOMETRY AND THE MECHANICS OF FRACTURE HEALING

MELLICK JOSEPH CHEHADE (MBBS)

Department of Orthopaedics and Trauma

Royal Adelaide Hospital

Thesis submitted for the degree of

Doctor of Philosophy

in

The University of Adelaide

(Faculty of Medicine)

June 1997

TABLE OF CONTENTS

ABSTRACT

The overall aim of this thesis was to assess the use of bone resonance analysis (BRA) as an indicator of fracture healing. BRA measures the resonant frequency of the fractured bone and may be compared to the contra-lateral bone as a reference of normality. No studies have previously correlated in-vivo resonant frequency changes with the mechanical and histomorphometric properties of healing fractures. Also BRA is theoretically a measure of stiffness and techniques using BRA assume a workable correlation between stiffness and strength. This has not, however, been demonstrated in the literature.

Thus the detailed aims of this study were:

1. to assess the validity of using the contra-lateral limb as a control;
2. to develop a reproducible technique of BRA for use in a sheep fracture healing model;
3. to examine the mechanical changes in a sheep fracture healing model and determine the relationship between stiffness and strength;
4. to assess the use of in-vivo BRA as an indicator of fracture mechanical properties;
5. to describe the histomorphometry of the healing fracture callus and adjacent cortex;
6. and, to relate the histomorphometry to both the mechanical and vibrational properties of the healing fracture.

The first part of this study assessed the symmetry of properties between the left and right tibiae of normal sheep. Very strong correlations were found in the resonant frequency values of normal left and right sheep tibiae, justifying the use of the contra-lateral limb as a control for the resonant frequency. Strong left/right concordance was also found in mechanical tests of strength. Left and right stiffness values, however, correlated poorly in individual cases, even though the mean values were symmetrical. The correlation improved as the load used to measure stiffness was increased.

Following this a highly reproducible technique of in-vivo BRA was developed justifying its use in the subsequent fracture study.

The main study subsequently used a sheep fracture healing model. Forty merino wethers were assigned to five groups of eight sheep and were culled at 2, 4, 6, 8 or 10 weeks. The fracture was created with an osteotomy to the tibial midshaft after application of an

external fixator. Resonant frequencies were determined both prior to fracture and at the time of culling and expressed as a ratio of post- to pre-fracture values (FI). This value was squared to give a 'stiffness index' (SI) that was theoretically expected to better reflect mechanical stiffness changes. The mechanical properties were determined from torsional and four-point bending tests on both 'fractured' and normal tibiae and 'healing ratios' were calculated. Histoquantitation was performed of the healing callus and adjacent cortex.

From the mechanical tests, the study found marked variations in stiffness and strength at each duration of healing examined. Stiffness was shown to be load-dependent: measurements at higher loads reflected ultimate strength more accurately. There was a biphasic relationship between stiffness and strength: at first there was a strong correlation regardless of loading conditions, but in the second phase, which included the period of 'clinical healing', stiffness and strength were not significantly correlated.

The BRA indices, FI and SI, were correlated with the mechanical healing ratios. BRA showed only moderate correlations with bending stiffness in the corresponding plane of vibration. The correlation was better with stiffness measured under low loads which was consistent with the unloaded testing conditions of BRA. There was no significant correlation of BRA with strength. Unexpectedly, FI reflected the mechanical ratios better than SI. Reference errors, due to use of the contra-lateral tibia for mechanical control values, were believed to significantly influence the correlations found with BRA.

This study described changes in the microstructure of the healing callus. Bone volume and trabecular thickness increased whereas the surface area and number of trabeculae decreased. Trabecular separation did not change significantly. Callus histomorphometry correlated poorly with the mechanical properties but very strong correlations were found with BRA: bone volume and trabecular thickness showed strong positive correlations; trabecular surface area and number showed strong negative correlations.

In the cortex adjacent the fracture line, porosity increased with healing. The square root of the cortical porosity correlated moderately with stiffness but strongly with strength. It was hypothesised that this association was a reflection of the regional acceleratory phenomenon.

It was concluded from this study that BRA and techniques that monitor bending stiffness were inherently limited in the assessment of strength at the time of clinical union but would be useful primarily in showing a progression (or failure to progress) towards union. Any assessment of stiffness must take into account the loading conditions. In-vivo BRA was shown to be a valid indicator of fracture healing; at least at the early callus microstructual level. Monitoring cortical porosity changes may have clinical application in the assessment of fracture strength: either independently or in conjunction with other monitoring techniques.

DECLARATION

This work contains no material which has been accepted for the award of any degree of diploma in any university or other tertiary institution and, to the best of my knowledge and belief, contains no material previously published or written by another person, except where due reference has been made in the text.

I give consent to this copy of my thesis, when deposited in the University Library, being available for loan and photocopying.

Mellick J Chehade

2 June, 1997

ACKNOWLEDGEMENTS

It is impossible to adequately acknowledge the help of the many people who have been instrumental in this thesis and to whom I am deeply indebted.

Mr Anthony P Pohl, the Director of Trauma at the Royal Adelaide Hospital and the "father" of this project, has been my guide and mentor throughout. The ability to take even the seemingly most difficult concepts and break them down into simple, logical steps is the rare and wonderful gift of a great teacher. His clarity of thought and ability to "laterally" extend an argument have been inspirational. I am privileged to have had the opportunity to work with him and my indebtedness to him extends well beyond this thesis.

Professor Mark J Pearcy (Biomedical Engineering) supervised and directed me in the biomechanical aspects of this work and spent many hours reading through successive drafts. His kindness and help throughout the years have also been instrumental and I am very thankful.

My undergraduate training was in medicine, not engineering, Without the training and knowledge gained from Professor Colin Hansen (Mechanical Engineering) in dynamic analysis and vibrations in engineering, this project would not have been possible.

The histomorphometric analysis in this thesis was only possible because of the expertise and efforts of Dr Nicola L Fazzalari (Chief Scientist, Division of Tissue Pathology). His advice on the statistics and presentation of this work was also invaluable.

For the design and development of the bone resonance analysis equipment used in this study; the late nights of software programming; the rapid repair of the many overused instruments; and the early morning swims to prepare the body for long days of sheep testing, I must thank my research assistant and good friend, Tim Lawes (Mechanical Engineer).

To Namal Nawana (Mechanical Engineer) for his work in the mechanical testing; Ian Parkinson (Senior Technical Officer, Tissue Pathology) and Margaret McGee (Hospital Scientist, Orthopaedic Department) for their assistance with the bone

histomorphometric analysis; and Krysten Willsen (Statistician) for her help with the statistical analyses, I would also like to extend my gratitude.

Tim Kuchel (Chief Veterinary Surgeon), Denise Noonan (Veterinary Surgeon), Patricia Little (Animal Research Theatre Supervisor), Brain Lewis (Animal Housing Officer), Karyn Keiser (Research Assistant) and Geoff Siedel (Theatre Assistant) were responsible for the excellent care and health of the sheep throughout the study.

The Adelaide Bone and Joint Research Foundation funded the initial research and development of the vibrational analysis apparatus and helped to feed my family in the first year of the project.

To my parents, Karl and Delele, for the years of love and support through very challenging times, their undying faith in me and the "never give up" attitude instilled by example - thank you.

John and Vicki, my other parents, thank you for your friendship and support and allowing me to spend more time on the research instead of on keeping the house together.

Finally I must acknowledge the incredible support and understanding of my wife, Vicki, and our children, Karl and Natalia: for years they have been hearing "...it's nearly finished..." - now it is and we all thank God!

DEDICATION

To Vicki, Karl and Natalia

PUBLICATIONS ARISING

Chehade MJ, Pohl AP, Pearcy MJ, Nawana N.

Clinical implications of stiffness and strength changes in fracture healing.

J Bone Joint Surg [Br] 1997; 79-B: 9-12.

Chehade MJ, Fazzalari NL, Pearcy MJ, Lawes TJ, Pohl AP.

Relationship of in-vivo bone resonance analysis to healing callus microstructure.

Transactions XVIth Congress of the International Society of Biomechanics - Tokyo, Japan; 1997: (in publication).

Chehade MJ, Fazzalari NL, Pearcy MJ, Lawes TJ, Pohl AP.

Relationship of in-vivo bone resonance analysis to healing callus microstructure.

Transactions Combined Scientific Meeting of Australian and New Zealand Orthopaedic Associations -Perth, Australia; 1996: 218

Chehade MJ, Pohl AP, Pearcy MJ, Nawana N.

Stiffness and strength changes in a sheep fracture healing model: the implications in clinical fracture assessment.

Transactions 42nd Annual Meeting Orthopaedic Research Society- Atlanta, USA; 1996: 625.

Chehade MJ, Nawana N, Pearcy MJ, Pohl AP.

Stiffness and strength changes in a sheep fracture healing model: the implications in clinical fracture assessment.

Transactions XVth Congress of the International Society of Biomechanics - Jyväskylä, Finland; 1995: 168-9.

AWARDS

The following awards were received for original work in this thesis:

"International Society of Biomechanics Young Investigators Award"
(XVth Congress of the International Society of Biomechanics, Jyväskylä, Finland, 1995)

"International Society of Biomechanics Clinical Biomechanics Award **- Runner-up**
(XVth Congress of the International Society of Biomechanics, Jyväskylä, Finland, 1995)

"Orthopaedic Research Society Young Investigator Award"
(Combined Scientific Meeting of Australian and New Zealand Orthopaedic Associations, Perth, 1996)

"R. J. Bauze Award"
(Annual State Meeting of the Australian Orthopaedic Association, Adelaide, 1995)

LIST OF FIGURES

LIST OF TABLES

CHAPTER ONE

INTRODUCTION AND LITERATURE REVIEW

1.1 INTRODUCTION

The aim of this research was to address the assessment of fracture healing, which remains one of the most difficult and important challenges facing orthopaedic research and clinical practice today.

This chapter reviews traditional fracture assessment techniques and discusses their shortcomings with emphasis on the need to assess the mechanical properties of healing fractures. The structure and biology of normal long bones are outlined and a synopsis of our current understanding on the biology of fracture healing is presented. Particular reference is made to the known mechanical changes that occur during fracture healing. Techniques researched to monitor bone mechanical properties are discussed with reference to some of their shortcomings. Bone resonance analysis (BRA), a form of vibrational analysis, is then discussed at length as it was the principal aim of this research to assess the role of BRA in the assessment of fracture healing. The role of symmetry in determining control or healing endpoint values is examined and the validity of extrapolating refracture risk from stiffness monitoring techniques is questioned. Finally, the use of an ovine model for fracture healing studies is considered.

The first step in this thesis was to look at the issue of symmetry in normal tibiae in terms of both the in-vitro mechanical and vibrational properties. The next step was to develop a reproducible technique of BRA applicable to in-vivo monitoring of sheep. The final step was to develop a fracture healing model of sheep tibia in which the mechanical, vibrational and histomorphometric properties could each be determined. For ease of organisation and discussion, these properties are presented separately. The mechanical properties are presented first and form the foundation of the fracture healing study. The histomorphometric and vibrational analysis data are then presented, both of which have also been assessed with relation to the mechanical findings. In the final chapter these healing fracture properties are summarised and the clinical implications of the findings are presented.

1.2 ASSESSMENT OF FRACTURE HEALING

Currently, fracture healing is assessed by clinical and radiological assessment and with the empirical passage of time. This assessment has remained essentially unchanged since radiology was first introduced one hundred years ago and so has our inability to accurately determine fracture healing.

1.2.1 Clinical Assessment

Healing is usually defined clinically as stability to manual testing and painless weight bearing, without the use of a cast (Christensen et al 1986). Fracture stability, determined by gross movement, is only helpful in monitoring fracture healing in the early phase of treatment. Pain on stressing a healing bone is unhelpful as even many non-unions are pain free (Matthews et al 1974) and early manual testing for stability may even damage the healing fracture (Brandon and Richards 1989).

1.2.2 Radiological

Radiologically, a fracture is "healed" when there is solid callus formation and obliteration of the fracture lines. However, this does not appear until several weeks after clinical healing allowing weight bearing (Christensen et al 1983; Christensen et al 1986). Radiographs provide an accurate assessment of the structural anatomy of the human skeleton and the position and alignment of the fracture fragments. They do not, however, allow the differentiation between primary and secondary callus in the early stages of healing (Brandon and Richards 1989), nor do they provide any information about the mechanical status of the healing fracture. Radiographs provide a two dimensional representation of the fracture site and cannot be reliably used to distinguish union from partial union or even non union (Burturla and Pope 1973). Even with multiple views, a pseudo-arthrosis may not be evident (Matthews et al 1974). Hypertrophic non-union exemplifies how an abundance of callus may have no correlation with the state of healing.

1.2.3 Empirical Healing Time

Most orthopaedic textbooks will give expected healing times for different fracture types. These times do not take into account many important variables such as age, metabolic or systemic diseases, head injuries, vascular conditions, trauma severity, soft tissue interposition, nutrition or fracture treatment. The empirical passage of time thus offers no more than a guideline to fracture healing assessment.

1.2.4 Problems

Current fracture assessment has been considered as "adequate" in the majority of cases, however there are many shortcomings. Kenwright (1985) suggests that the combination of clinical and radiological assessment is satisfactory for defining the endpoint of fracture healing for an average long bone fracture in approximately 90% of cases with an accuracy of ± 3 weeks. Both the radiological and clinical assessments of fracture healing are subjective and therefore open to misinterpretation (Hammer and Norrbom 1984). Current definitions are dependent upon their assessment technique and the "endpoint" from one assessment modality does not necessarily correspond to the "endpoint" of another.

It is likely that many fractures are functionally healed earlier than their "empirical healing time" and are therefore subjected to an unnecessarily long period of immobilisation (Burturla and Pope 1973) with all of the potential accompanying complications. Disuse osteoporosis, reduced range of adjacent joint mobility, increased cost of medical care (Pelker and Saha 1985) and the prolonged time off work, with all its associated problems, are but a few obvious examples.

On the other hand there is the problem of insufficient fracture immobilisation. Refracture and/or malunion may complicate premature resumption of activity. Refracture rates of "clinically healed" tibial fractures have been reported at 3% (Chrisman and Snook 1968). Seimon (1964) reported a refracture rate of up to 8% for the shaft of femur. The risk of refracture following the removal of plate fixation from "healed" tibial or femoral diaphyseal fractures is 2% (Kenwright 1985).

Our current assessment of delayed and non union relates exclusively to the passage of time. Treatment for a non-union cannot occur before the time determined diagnosis has been made. If fractures not progressing to union could be identified at an early stage, treatment could be instigated much earlier, saving many months delay and all the associated problems of prolonged immobilisation.

A fracture which is sufficiently healed to allow the resumption of normal living activities for an office worker or for home duties may not have sufficient strength for patients returning to strenuous work or professional sport.

Our current assessment of fracture healing is clearly inadequate.

1.2.5 Healing Endpoint

When is a fracture healed? Before an assessment of the endpoint of fracture healing can be made, the "endpoint" needs to be defined. The problem lies in the fact that there is no exact definition of fracture healing. If one were to use the restoration of the prefracture anatomy to define fracture healing, it could take several years and very few fractures would ever be "healed".

Any definition of "endpoint" is useless from a practical perspective if it cannot be related to function i.e. *"The fracture is healed enough for what?"* Thus, what is required is a means of fracture assessment that relates to the mechanical properties of the bone. The potential advantages of being able to assess the mechanical properties are extensive as they would enable the objective determination of common endpoints to fracture treatment. This would not only help to optimise current fracture treatment but it would also allow the objective comparison between different treatment modalities.

1.2.6 Ideal Method

In searching for a suitable definition for an ideal method of fracture assessment I could not go past one given by Kenwright (1985) who stated that "... The ideal method would be non-invasive, rapidly performed, and give an immediate result which would represent in a repeatable way the biomechanical quantities of the

healing fracture at that time. The biomechanical profile should allow accurate prediction of the safe time of removal of fracture immobilisation or predict the occurrence of non-union..."

1.3 BONE BIOLOGY AND BIOMECHANICS

As this research is concerned primarily with the assessment of healing *long* bone fractures the following discussion will be restricted to long bones. Except where otherwise referenced, the following information is from text book chapters by Buckwalter et al (1991) and Tencer et al (1993).

1.3.1 Structure Of Bone: Macroscopic

Long bones are comprised of a thick-walled tubular diaphysis with a widened metaphysis and epiphysis at each end. Macroscopically there are two forms of bone tissue: cortical (compact) and cancellous (trabecular). Most of the cancellous bone is contained in the metaphysis where the cancellous bone is arranged in plates to support the subchondral bone that underlies the articular cartilage. The cortical bone increases in thickness away from the metaphysis to become maximal at the mid-diaphysis.

Although dissimilar on gross visual inspection, cortical and cancellous bone are identical in both composition and material properties. It is the distribution and arrangement of the bone that differs between the two types and is responsible for differences in their mechanical properties. Cortical bone is of much denser and hence less porous (usually less than 15 per cent porosity) than cancellous bone which can be up to 70 per cent (Schaffler and Burr 1988). The thick, dense diaphyseal cortical bone is arranged in a manner that allows optimal resistance to torsion and bending and can have up to ten times the ultimate compressive strength of a comparable volume of cancellous bone. Strength refers to the ability of a material to absorb the applied energy by deforming to the load without fracturing. Cortical bone is generally strongest in compression, followed by tension and then shear. While having a tensile strength almost as great as cast iron, bone is only one third as heavy and ten times more flexible.

The stiffness and strength of whole bones are not just a function of their material properties but also of geometric characteristics of the bone such as the length-to-diameter ratio and of several aspects of the cross sectional geometry of the cortex. These include the cross-sectional area (A) and the second moment of area (I). The moment of inertia is an expression of the shape of the cross section and the particular distribution of the cross-sectional area with respect to the applied bending loads.

At the structural level, the cylindrical tube shape of long bone is the most efficient shape to resist the compression, bending (multiple directions) and torsional loads.

Because of the viscoelastic nature of bone, the ultimate strength and stiffness properties are influenced by the rate of strain (Reilly et al 1974; Reilly and Burstein 1975; Wright and Hayes 1976). Bone which is very rapidly loaded will be stiffer, absorb more energy and have a greater ultimate strength than bone which is loaded more slowly. Carter and Hayes (1977) found approximately a 2 fold increase in both the elastic modulus stiffness and ultimate strength when strain rate was increased from 0.001 to 10.0/sec. Therefore strain rate must be taken into consideration when testing mechanical properties.

Cortical bone is also *anisotropic* with a stress-strain behaviour which is strongly dependent upon the orientation of the bone with respect to the direction in which it is loaded. It is stiffest when loaded axially in the direction of the osteon. When loaded perpendicular to the osteons, it is not only less stiff but it is also more brittle in that it fails with much less plastic (non elastic) deformations after yielding. Because of these complex anisotropic and viscoelastic properties, any meaningful description of bone material behaviour must include the strain rate and the direction of loading.

1.3.2 Structure Of Bone: Microscopic

At the microscopic level bone can be either woven (primary) or lamellar (secondary). Woven bone is found in the embryonic skeleton and in fracture callus. In both cases it is replaced by the mature lamellar form of bone.

Woven bone has an irregular arrangement of collagen fibrils and an irregular pattern of mineralisation. It also has a relatively high cell and water content. Mechanically, it is much more easily deformed and weaker than lamellar bone. Because of the random type nature of the collagen distribution it behaves in an isotropic manner when loaded in that it reacts in a similar fashion regardless of the direction in which the forces are applied.

By contrast, lamellar bone has a highly organised arrangement of collagen fibrils in a tight sheet like distribution and mechanically it behaves anisotropically.

Lamellar bone has various forms depending on the arrangement of the lamellae. Apart from the trabecular form that exists in the cancellous bone there are, in cortical bone, the inner and outer circumferential lamellae, interstitial lamellae and the lamellae of the osteons. These lamellae all lie parallel to the bone axis but with the collagen fibrils within adjacent lamellae running in different directions. The cortex of the diaphysis is comprised predominantly of osteons which are concentrically arranged lamellae disposed around a central channel known as a Haversian canal. These contain blood and lymphatic vessels and occasionally nerves. Volkmann's canals obliquely interconnect the Haversian canals. Osteocytes are contained within lacunae which lie between the lamellae. The cell processes of the osteocytes are contained within canaliculi which extend radially from the central canal and connect the osteocytes with the central canal and with each other.

Bone matrix contributes to approximately 90 per cent of lamellar bone volume with the cells, blood vessel and cell processes making up the rest. Of this matrix approximately 65% is inorganic, 25% organic and 10% water.

Type-1 collagen, which is particularly adept in tissues subjected to large tensile forces, accounts for approximately 90% of the organic component. The other 10% is predominantly comprised of non-collagenous glycoproteins and bone-specific proteoglycans with a few growth factors.

The inorganic component of the matrix is predominantly calcium and phosphorus and is responsible for the majority of the bone stiffness and strength. It is mainly in

the form of bone mineral crystals of hydroxyapatite [$Ca_{10}(PO_4)_6(OH)_2$] which are distributed within specific regions in and between the collagen fibrils.

1.3.3 Bone Modelling And Remodelling

Bone is a living tissue which is constantly being maintained and adapted through the processes of modelling and remodelling. According to Frost (1989) *modelling* refers to a "sculpturing" process by which existing bone is removed or new bone added with a resultant change in the geometry or density of the bone. *Remodelling*, on the other hand refers to the process by which existing bone is removed and replaced. These processes are performed by various cells, intercellular materials and capillaries that communicate with each other and are specially organised in space and time into a functional unit referred to as a Basic Multicellular Unit (BMU). The osteoclast is the first cell to be produced by the BMU to remove the pre-existing bone. With internal (osteonal) remodelling, large cutting cones can be formed leaving large resorption cavities visible on plain radiographs as cortical lucencies. Osteoblasts, spindle cells and small blood vessels follow the advancing group of osteoclasts laying lamellae of new osteoid which subsequently mineralises.

1.4 FRACTURE REPAIR

In this section the histology of fracture repair is examined. The limited research on the microstructure of the healing callus is then considered. Finally, the recognised biomechanical stages of healing fractures are presented.

1.4.1 Histology: Stages Of Repair

Histological descriptions of fracture healing have traditionally included three general phases: inflammation, reparation and remodelling (Cruess and Dumont 1975; McKibbin 1978; Sevitt 1980).

By including the injury impact as a separate stage and subdividing reparation into soft and hard callus stages, five phases of repair were defined. Following the description of the regional acceleratory phenomenon by Frost (1983) a sixth phase can be included.

1.4.1.1 Injury

This stage lasts approximately seven days. The fracture is associated with injury to not only the bone but also the adjacent periosteum, soft tissues and local bone marrow. Local disruption of the blood supply leads to haematoma formation. Necrosis of the bone ends usually occurs for a couple of millimetres. With the injury or death of the local tissue there is both release of local messengers and sensitisation of surviving local cells to differentiate and proliferate into the many cell lines required for eventual repair. These include endothelial and smooth muscle cells required for new capillary formation; fibroblasts, lipoblasts and intercellular materials for the new local connective tissue; and chondroblasts and osteoblasts for cartilage and bone matrices.

1.4.1.2 Granulation tissue

During this stage, which lasts about two weeks, a soft granulation tissue is formed between the fracture ends. This tissue is formed from the sensitised and stimulated precursor cells which have become differentiated and organised. Macrophages, giant cells and other wandering cells also arise in this tissue to invade and remove any haematoma clot while osteoclasts begin to erode into some of the fracture surfaces.

1.4.1.3 Callus

With the continuing cellular proliferation, differentiation and organisation of the granulation tissue there is the production of chondroblasts and osteoblasts. These cells synthesise the chondroid and osteoid (extracellular organic matrices of cartilage and woven bone) thus producing 'soft callus'. This begins to mineralise from after a week or so and is usually completed between four and sixteen weeks, forming woven bone.

1.4.1.4 Remodelling

In fracture healing the BMU described above is responsible for remodelling of the callus. In a sequential process of resorption and formation, the different

components of the callus are removed and replaced with new bone, the type of which depends on what was removed: mineralised cartilage is replaced with woven bone and woven bone is replaced with lamellar bone. Any callus between the ends of the cortices is replaced with lamellar bone which is aligned parallel to the local peak longitudinal compression and tension strains. In addition, callus plugs in the medullary cavity are usually removed. This process may take one to four years.

1.4.1.5 Modelling

The modelling or reshaping process in fracture healing occurs concurrently with the remodelling process. It commences after the stage of callus formation and may take several years. Bone modelling drifts acting on both the endosteal and periosteal surfaces of the cortex contour the gross shape. Following fractures in children the normal bone shape is usually regained but in adults there is usually some residual abnormality (Courpron 1981; Frost 1989). Similarly, but through a different process, there is a "mini-modelling" of the trabeculae inside the bone in which they are realigned to the direction of the major local mechanical strains (Frost 1988).

1.4.1.6 Regional acceleratory phenomenon

The regional acceleratory phenomenon was first described by Frost in 1983 although he acknowledged that Kolar and his associates in Czechoslovakia had described many of its effects as early as 1965. Rather than being a separate process, the RAP has the effect of accelerating fracture healing by between two and ten fold. It can act on any of the five healing stages between the time of injury and final healing (Figure 1.1). Beginning within days of the initial injury, and peaking at one to two months, it takes between six months and over two years to subside. Its effect on the increased intra-cortical bone remodelling is indicated by the radiological appearance of "tunnelling" within the cortices.

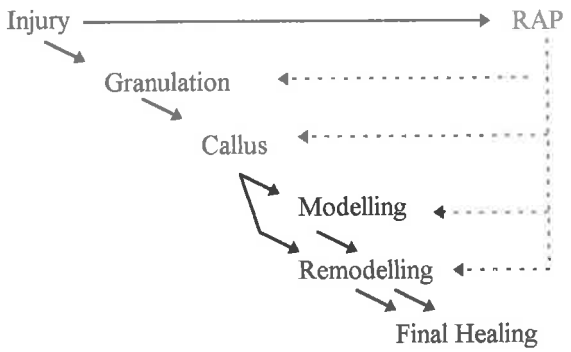

Figure 1.1 Influence of the Regional Acceleratory Phenomenon

1.4.2 Callus Histomorphometry

Whereas the biology of normal fracture healing has been well described, there is a paucity of work detailing the histomorphometry of new bone formation in fracture healing.

Markel et al (1991) used a canine gap healing model to study the histomorphometry of fracture callus and to relate this to the local indentation stiffness, torsional stiffness and torsional strength of the bone. Using the standardised parameters recommended by Parfitt et al (1987), they described changes in osteoid surface and volume, osteoblast surface and number, osteoclast number, trabecular bone volume and thickness as well as anisotropy. They found that the number of osteoblasts increased between two and eight weeks but decreased at twelve weeks. The number of osteoclasts however increased throughout the twelve weeks of the study. The volume of trabecular bone, osteoid surface and osteoid volume increased up to eight weeks and then levelled off by twelve weeks. Trabecular width and anisotropy increased for the twelve weeks.

When the histomorphometry was correlated with the biomechanical properties of the healing fracture it was found that increases in indentation stiffness were mildly related to increases in the trabecular thickness ($r = 0.55$, $p = 0.09$), both of which increased throughout the study. Torsional stiffness and strength which levelled off after eight weeks however seemed to relate better to callus volume which decreased between eight and twelve weeks.

In a similar previous study by the same authors, Markel et al (1990), the cortical porosity of the bone ends was also measured. Cortical porosity was found to increase with fracture healing and was associated with a decrease of the indentation stiffness of the cortex.

Cortical porosity was also measured by Aro et al (1990) in a closed fracture model of rat tibiae. A continuous increase in porosity was demonstrated for the six weeks of the study and was believed to be due to a time-related change in the balance of periosteal bone formation and resorption during fracture repair.

No studies have correlated fracture histomorphometry with bending stiffness techniques or with vibrational analysis techniques which form the basis of most fracture assessment research. In addition there are no studies that have correlated the cortical porosity changes with the mechanical properties of the healing fracture.

1.4.3 Biomechanical Stages Of Healing

The stiffness and strength of bone are its prime qualities as the fundamental functions of bone are to carry load, to support and protect organs, and to enable locomotion. The principal aim of fracture healing, therefore, is to restore these qualities. In the absence of early rigid fixation considerable movement is possible at the fracture site. This movement needs to be accommodated by the fracture healing process until sufficient stiffness has been restored to allow further healing of bone under more rigid conditions. During the process of callus formation and maturation there is considerable change in the tolerance of the healing tissue to strain (Perren 1979). Granulation tissue can deform to twice its original length (100% strain), cartilage will tolerate about 10% strain and finally the strain tolerance of bone is only 2%. Each tissue stage imparts a degree of rigidity to the tissue that allows the differentiation and formation of the next stage.

White et al (1977) described four distinct biomechanical stages of fracture repair based on the site of failure, torque-angle curves and energy to failure in healing rabbit tibial fractures:

In stage 1 the fracture site has a low stiffness, "rubbery " deformation pattern and failure is through the original fracture site.

In stage 2 the stiffness has increased and there is considerably less deformation at yield which still occurs through the fracture site.

In stage 3 there has been little change in stiffness but the strength is greater and failure occurs partly through the original fracture site and partly through adjacent intact bone.

In stage 4 the strength has further increased and failure is now entirely through previously intact bone.

This descriptive classification based on destructive testing, however, has no practical clinical application.

1.5 BIOMECHANICAL ASSESSMENT OF FRACTURE HEALING

With the limitations of current fracture assessment techniques, many alternatives have been researched. Some of these techniques involve the direct or indirect assessment of stiffness. This is achieved by measurement of movement at the fracture site or of fracture fixation in response to a known load. Vibrational analysis techniques such as wave propagation and resonant frequency analysis have also been studied. This section discusses these biomechanical assessment techniques and some of their shortcomings.

1.5.1 Mechanical Measurements

Edholm et at (1984) described a technique to assess fracture union with a deflection ratio which was determined by radiographic measurement of the tibial deflection to an applied bending moment. When this ratio fell below a given value (which took into account the patient's weight) union was considered to be stable enough for full weight bearing during walking.

Studies by Burny and associates reported a reduction in the displacement of the fracture/ fixator system with progressive fracture healing. This was determined by

the use of strain gauges attached to external fixator rods (Burny 1968; Burny et al 1985; Burny et al 1984), plates (Burny et al 1985), proximal femoral nail plates (Burny et al 1985) and intramedullary nails (Burny et al 1971). Unfortunately strain gauges bonded to the fixation device for the period of treatment were subjected to mechanical and environmental damage during the surgical operation and in every day use. Calibration of the gauges was also difficult making large-scale patient testing impractical.

Jernberger (1970) developed a method to measure the stiffness of tibiae with the use of a strain-gauged frame attached via bone screws inserted percutaneously under local anaesthesia. Even though no complications were reported from the study, the invasive nature of this procedure made it unsuitable for routine clinical use.

Jörgensen (1972) assessed the stiffness of healing tibial fractures by substituting the supporting bar from a Hoffman unilateral external fixator with a dial gauge micrometer which measured the deflection of the fracture site to a known applied bending load. This left the fractures without stabilisation during testing.

Evans et al (1985) developed a removable fixator transducer which was attached to the column of an external fixator and was able to measure bending in two perpendicular planes and torsion about the centre line of the fixator column. Calibration was carried out on a standard frame prior to attachment to the fracture fixator. The fixator did not require disassembly for testing and fracture stabilisation was therefore not compromised. From clinical studies using this method, Richardson et al (1987) measured the sagittal stiffness of healing tibial fractures. They concluded that 15Nm/deg could safely be used to define clinical tibial fracture healing.

Instrumentation of external fixators has proved to be a very useful technique and much useful information has been obtained. It is non invasive in that the external fixator is already in use for the fracture treatment. It is however limited in its application to the small percentage of fractures treated by this method. In most techniques accurate measurements are only possible with well fixed bone pins and a

stiff fixation frame. The loosening of a single pin will result in a 10% reduction of the measurement accuracy and if more than one pin is loose the measurement accuracy is reduced to "...an unmanageable degree" (Harris et al 1985). Measurements are only valid with a unilateral frame configuration and any changes in the configuration of the system during treatment make subsequent monitoring very difficult (An et al 1988).

1.5.2 Wave Propagation Analysis

In engineering, vibrational analysis is used to determine the mechanical properties of structures by measuring their response to vibrations. Recent research has been aimed at applying vibrational analysis to human long bones.

Stress wave propagation of long bones is an application of vibrational analysis that has been investigated by several researchers as a means of assessing the mechanical properties of intact normal and osteoporotic bone (Pelker and Saha 1975; Chen and Saha 1987; Wong et al 1983; Pelker and Saha 1983; Saha and Lakes 1977; Cheng et al 1989; Guzelsu and Saha 1981) and in the monitoring of fracture healing (Burturla and Pope 1973; Wong et al 1976; Pelker and Saha 1985; Sonstegard and Matthews 1976). The vibrations were generated by impacting the bone and the bone's response was measured with bonded strain gauges or piezoelectric transducers. The flexural wave velocity and peak accelerations were the main factors measured and used as indicators of the mechanical bone properties.

The absence of a model for *in vivo* bone to allow interpretation of the results in terms of mechanical properties, poor reproducibility and problems with soft tissue, have restricted the usefulness of this type of analysis for human *in vivo* studies (Cornelissen et al 1986).

1.5.3 Resonant Frequency Analysis

1.5.3.1 Technique

Another application of vibrational analysis is resonant frequency analysis. This utilises the resonant frequency of a healing long bone fracture as an indicator of bone healing. Several different techniques have been described for resonance analysis.

The resonant frequency is determined by measuring the vibrational response of the bone to a given force input. Random force inputs have generally been achieved by impacting the bone with hammers (Burturla and Pope 1973; Christensen et al 1986; Van der Perre et al 1983). A Fast Fourier Transform (FFT) is then utilised to determine the resonant frequency from the frequency domain modal information. (In addition to the resonant frequencies, the modal parameters include modal shapes and damping coefficients.) Alternatively, a steady state approach has been employed in which the bone is excited with a time varying sinusoidal force from an electromagnetic shaker (Markey and Jurist 1974; Christensen et al 1986; Collier and Donarski 1987).

When compared to the steady state techniques, FFT analysis requires much more expensive equipment, greater analysis time, and is less accurate (Nokes et al 1994). However, with the rapid advances in electronic and computing technology which are becoming increasing more affordable, this disadvantage may soon cease to apply.

In order that tests be non invasive, they must be performed in the presence of intervening soft tissue. Due to their predominantly subcutaneous location, the ulna and tibia are the most accessible long bones and have therefore been the focus of most studies (Nokes et al 1984). Vibrational analysis studies on the ulna have usually been centred on determination of generalised bone properties and osteoporosis whereas fracture healing studies have been focused on the tibia.

An accelerometer is used to measure the bone's response. Resonant frequencies can be determined from either the peaks of impedance curves or directly from peak

accelerations if the input force amplitude is constant throughout the frequency sweep.

The shaker can be applied by hand or with a mechanical holding device. Hand application allows greater versatility in application however there is no literature comparing the accuracy of measurements using these two techniques.

The position and angle of shaker application will influence the vibrational response of the bone (Borgwardt Christensen et al 1982). Individual modes of vibration are more easily excited at points where the modal deflection is greatest whereas excitation of a mode from a nodal point is not possible.

The sensitivity of an accelerometer to a modal vibration is maximal when positioned directly in its plane of vibration and away from nodal points. In this way the influence of modes vibrating in other planes is also minimised. The bone response has been measured from the shaker driving point (Thompson et al 1976; Thompson 1973; Larsen et al 1985; Borgwardt Christensen et al 1982) or, more commonly, from a location which is at a distance from the force input. To avoid the detection of signals not originating in bone, Collier and Donarski (1987) advise placement of the accelerometer at least 3cm away from the shaker in the case of "normal" skin and 8cm in oedematous cases.

Critical to the valid interpretation of results from any technique is the reproducibility. Boundary conditions are the most important factor in the determination of resonant frequencies (Hight et al 1980; Jurist and Dymond 1970; Borgwardt Christensen et al 1982). In the tibia, limb position and quadriceps tension are the two most important factors in boundary condition variability and therefore must be controlled (Borgwardt Christensen et al 1982). The use of soft tibial splints aids in muscle relaxation during testing has been used to improve reproducibility (Larsen et al 1985; Ammitzboll et al 1985; Cornelissen et al 1985).

1.5.3.2 Models

Several mathematical models have been developed to interpret resonant frequency data in terms of the mechanical properties of intact bones (Thompson et al 1976;

Orne and Mandke 1975; Orne 1974; Orne and Young 1976; Jurist and Kianian 1973; Spiegl and Jurist 1975; Collier et al 1982; Hight et al 1980; Khalil et al 1980; Lowet et al 1993; Thomsen 1990; Van der Perre et al 1983). These models vary in complexity and most assume linearity in a system for which there is increasing evidence of non-linearity (Brandon and Richards 1989; Richards et al 1989). The greater the complexity of the model the more difficult it is to obtain accurate values for the constants required in the models.

However, the simple beam model based upon the Euler-Bernouilli approach that was proposed and tested by Van der Perre and Cornellisen (1983) has been shown to be useful. In this model the resonant frequencies of the flexural vibration modes are given by:

$$f_k = \alpha_k \sqrt{\frac{EI}{\mu l^4}}$$

where f_k = natural cyclic frequency of k^{th} mode (Hz)

E = Young's modulus of elasticity (Nm^{-2})

I = area moment of inertia about the bending axis through the centroid (m^4)

μ = mass per unit length (kgm^{-1})

l = length (m)

α is a dimensionless proportionality factor determined by the boundary conditions and the mode (subscript k).

The product EI is an index of the bending stiffness and is proportional to the square of the frequency:

$$f^2 \propto EI$$

Mathematical models to interpret healing fractures are far fewer in number. A model, also based on Euler-Bernouilli beam theory, was proposed by Lewis (1975) and was used to calculate mode shapes and frequencies given a fracture located in the middle of a long bone. To be used as a clinical tool, however, this model required the shape of the tibia to be known accurately.

Markey and Jurist (1974) suggested that, based on standard engineering principles, the square of the resonant frequency ratio (fractured versus intact bone) would indicate the relative strength of union. They also suggested that this would allow for comparisons between healing in different individuals as structural differences would be compensated for.

Cornelissen et al (1982) presented a fracture healing model in which mechano-dynamic relations are defined. The dynamic ratio (DR) is used as an index of the state of fracture repair as determined by the vibration data and is the ratio of measured resonant frequency of fractured limb to that of the normal, control contra-lateral limb. The buckling strength ratio (RBS) and the transverse bending stiffness ratio (TSR) are used to describe the mechanical properties at the fracture zone. Using a mathematical model DR is related to RBS and TBS.

The influence of several modal variables and fracture parameters on these mechano-dynamic relations were also included in the model (Cornelissen et al 1985). Analysis of fracture healing using this model indicates that the first single bending mode with 'free-free' end conditions is the most sensitive to mechanical property changes during fracture healing. This is supported with experimentally derived data (Cornelissen et al 1985; Cornelissen et al 1987). The rigid body mode in an intact bone is an indicator of generalised bone mass rather than bending stiffness. In the presence of a fracture however, it is transformed into a single bending 'hinged-hinged' mode which is sensitive to fracture healing, particularly in the earlier stages (Cornelissen et al 1987).

In all of the bending modes, fracture location significantly affects the sensitivity of the DR to changes in RBS and TBS: -the sensitivity decreasing with increasing distance of the fracture from the bone midpoint. The fracture gap does not affect

the relationship. Callus mass was believed to influence the relation in all modes but was not quantified.

1.5.3.3 Modal analysis

In the intact human tibia, several resonant frequencies can be identified depending on both the plane and mode of vibration (Vandecasteele et al 1981; Christensen et al 1986). The lowest resonance (120 Hz) has been identified as a rigid body mode in the sagittal plane. Next are the first (220 Hz) and second (350 Hz) single bending modes which occur respectively in the plane approximately perpendicular to the anteromedial surface (frontal plane) and in the anteroposterior (sagittal) plane (Cornelissen et al 1988). These planes represent the planes of minimum and maximum stiffness respectively (Vandecasteele et al 1981). In sheep tibiae however, the frontal plane is slightly stiffer than the sagittal plane (Cornelissen et al 1988).

Higher frequencies represent multiple bending and torsional modes. Most studies have confined analyses to the rigid body mode and/or single bending modes which all usually occur below 1000 Hz.

Cornelissen et al (1988) found that the determination of modes above the single bending modes is difficult in vivo, particularly in elderly patients. The second single bending mode was the most readily identified in vivo. The accurate determination of the single bending mode frequencies can sometimes be difficult due to the coupling that can occur between these two modes which increases the scatter (Cornelissen et al 1988; Evans 1985; Cornelissen et al 1985).

The resonant frequencies are also dependent on the end conditions with the resonant frequency for a given mode being highest vibrating under free-free end conditions; intermediate for free-hinged; and least for hinged-hinged end conditions (Van der Perre 1984). Positioning the tibia to hang freely over the side of a bed, or giving it generalised support without constraints, allows near free-free end conditions (Christensen et al 1986).

1.5.3.4 Skin and soft tissue

In order that the dynamic testing of the bone by impedance or frequency measurement be "non-invasive", the testing must be done though intervening skin and soft tissue. The soft tissue could potentially effect results either by altering the recorded input force or the measured response and several studies have looked specifically at this issue (Sonstegard and Matthews 1976; Thompson 1973; Saha and Lakes 1977; Thompson et al 1976; Ziegert and Lewis 1979; Cornelissen et al 1986; Van der Perre et al 1983; Nokes et al 1984; Collier and Donarski 1987; Lim 1989). Using modal analysis on amputated lower limbs Cornelissen et al (1986) examined the influence of soft tissues and joints on the vibration of the human tibia. The soft tissues and the fibula were dissected gradually and measurements were made using a hammer impact technique. The accelerometer was manually applied to the skin. They found that stripping of the skin did not induce any significant changes in the modal parameters with resonant frequency changes never greater than 5%. They stated that this was because the skin added little mass and no stiffness to the bone. As the skin acted as a damper to the system, the damped frequencies increased with skin removal. While the force applied directly to the bone was different to the force on the bone when there was intervening skin, the difference was insignificant. The skin was likened to the tips and extenders used on impulse hammers with hard tips being used for high frequency measurements and rubber tips for low frequencies. They concluded that the skin prolonged the waveform when interposed between hammer and bone thus limiting the usable frequency range but did not introduce errors in impedance or frequency response measurements within that usable frequecy range. This was in agreement with the model proposed by Thompson (1973) where the skin acted as a spring and also with the spring-spring damper model proposed by Orne (1974). In general, preloading the skin using a low diameter and low mass interface instrument increased its stiffness allowing unaltered force transmission from shaker to bone (Thompson et al 1976; Thompson 1973). The amount of preload required varied depending on factors such as skin thickness (Nokes et al 1984) and oedema (Collier and Donarski 1987) and sufficient preload time must be allowed for adequate equilibration of the skin fluid.

With respect to measurement of the acceleration signal through skin, Cornelissen (1986) concluded that the compressibility of the skin alters the signal. Preloading the skin can reduce this effect but may also cause a shift in the resonant frequencies: preloading with a weighted arm can decrease the resonant frequency through a mass loading effect whereas applying the preload by adding an elastic support can change the boundary conditions. The determination of the resonant frequencies per se was not influenced by the skin compressibility. When the accelerometer was held manually against normal skin with a preload force of about 18 N, an almost unaltered signal was obtained between the bone and skin in the range between 40 to 1000 Hz. Thus for slim, non oedematous skin the accurate dynamic analysis of the bone is not significantly hindered. Collier and Donarski (1987) however state that thick, oedematous skin can affect accelerometer measurements of the bone response by both limiting the measurable frequency range and by introducing a skin resonance in the 50 to 1000 Hz range which may be difficult to distinguish from a bone resonance. They stated that by knowing the total impedance, (skin plus accelerometer), a correction can be made for movement distortion due to skin. This would allow accurate measurements to be extended by a factor of 3 to 5 depending on the signal to noise ratio.

Cornelissen et al (1986) also showed that muscle surrounding the tibia decreased the resonant frequency and increased the damping of the tibia whereas the presence of the fibula had a stiffening effect which accounted for 5 to 11% of the observed natural frequency.

Thompson et al (1976) suggested that due to soft tissue atrophy resulting from inactivity of the injured limb during fracture healing, differences would emerge between the soft tissue responses of normal and fractured limbs. This would potentially compromise the use of the unfractured limb as a control.

Overall, these studies suggest that the influence of skin and soft tissue complicates resonant frequency interpretations. However, with adequate skin preloading; appropriately sized and weighted measuring equipment; and referencing of the opposite limb in fracture monitoring, meaningful measurements should be possible.

1.5.3.5 Fracture models

Several groups have developed experimental fracture models to examine the relationship between the resonant frequency and fracture stiffness. Benirschke et al (1993) simulated a healing fracture with a thawing rubber insert in cadaver tibiae. Fracture stiffness was determined with four-point bending tests and correlated with resonant frequency determinations on these excised tibiae.

Cornelissen et al (1988) correlated resonant frequency data with four-point stiffness measurements of metal rods with weakened sections which were used to model healing long bone fractures. A modal analysis was also performed on each of three excised healing sheep tibial fractures which were at varying stages of healing. The stiffness of these fractures however was not measured.

Cornelissen et al (1983) monitored three patients with tibial fractures treated with external fixation. Vibration data were correlated with indirect stiffness measurements obtained from strain gauge readings from the fixation bar.

A fracture healing simulation technique has been developed by Cornelissen et al (1988) utilising heat shrinkable hoses and silicon rubber with the advantage that callus can be simulated. This has been used in studies utilising both dry bone and in-situ tibial fractures of amputated limb specimens.

Based on the Bernouilli-Euler beam theory, Lowet et al (1992) derived a theoretical relationship between torsional stiffness and the resonant frequencies of the two single bending modes. Frequency analysis and mechanical torsional stiffness tests were undertaken on 142 long bones from different animals and with different mechanical features in order to evaluate this relationship. Strong correlations were recorded but the vibration data were obtained from excised bones.

To date there have been no published studies in which vibration data obtained from healing fractured bones in vivo have been correlated with direct mechanical tests of stiffness and strength. Nor has there been any attempt to correlate resonant frequency data with histomorphometric studies.

1.5.3.6 Fracture fixation

The effect of the method of fracture fixation on interpretation of resonant frequency data also needs consideration. Plaster cast fixation in conservatively treated tibial fractures has been shown to not significantly effect results (Collier and Donarski 1987; Briggs et al 1988; Matthews et al 1989).

Other fixation devices such as plates, reamed or locked intra-medullary nails and external fixators cause coupling of the fractured bone ends, thus masking the stiffness at the fracture site (Cunningham and Kershaw 1991; Benirschke et al 1993). Removal of the external fixator connecting bar may overcome this problem in some cases but this may leave the fracture vulnerable to handling during testing. Although not conclusive, there is evidence from some studies (Benirschke et al 1993; Tower et al 1993) to suggest that resonant frequency assessments can also be used in fractures fixed with unreamed, unlocked nails.

Plate and unilateral fixation devices would be expected to preferentially increase the bending stiffness of one plane relative to another. As resonant frequency analysis has the potential to differentially monitor bending stiffness in the plane of vibration, it is conceivable that monitoring of fracture healing with such fixation devices may be possible in the plane least affected by the fixation.

1.5.3.7 Vibrational symmetry

Fracture monitoring with referenced indices is based on the assumption that the contra-lateral limb is a valid control. Support for this has been derived from correlations of resonant frequencies between normal left and right limbs. Christensen (1983) obtained a correlation coefficient, r, of 0.99 from studies of 50 healthy individuals in which the rigid body mode of the tibia was measured. The validity of extrapolating this correlation to the bending modes is questionable. Benirschke et al (1993) compared the first single bending mode frequencies of 107 patients and concluded, on the basis of a comparison of their means, that there was no significant difference. Inspection of their plotted data however showed a large amount of scatter in the results suggesting a large standard deviation and raising

serious doubts about the confidence with which indices referenced on the "normal" limb can be used on an individual patient basis. In other studies (Cunningham 1988; Cornelissen et al 1988), tabulated left and right frequency values of single and double bending mode frequencies also showed considerable scatter in the examples given. Whether these differences were real or merely reflected measurement inaccuracies was not clear. Another factor not addressed with this assumed symmetry was the potential for frequency asymmetry secondary to dominance of a lower limb resulting from its preferential use in activities such as football. This asymmetry has already been demonstrated in the ulna of the dominant upper limb of professional sportsmen as well as in tests of unilateral limb disuse (Steele et al 1988).

1.5.3.8 Mechanical symmetry

In assessing relative changes in the mechanical properties of a healing long bone fracture towards union, knowledge of the prefracture or "normal" properties is required. For this reason use of the unaltered, contra lateral limb as a control is common practice. It does, however, assume symmetry of the mechanical properties of the left and right bones in an individual. Several studies have tested this assumption but the results have been variable.

Studies looking at human bone and muscle weight have found significant asymmetry in both upper and lower limbs (Chibber and Singh 1970; Dogra and Singh 1970; Dogra and Singh 1971; Chibber and Singh 1971). Asymmetry of functional mechanical properties, however, has not been as evident.

Mather (1967) used bending tests to compare the mechanical properties of left and right bones in 28 pairs of human femora. He looked at ultimate load, energy absorbed to failure, tensile strength and Young's modulus. Except for the mean energy absorbed to failure, which was slightly higher on the left (18.7 SD 6.99 vs 17.3 SD 6.93), no significant difference was found between mean left and right values. From this he concluded that the properties were symmetrical even though the differences between left and right in some of the individual pairs exceeded 10%.

White et al (1974) looked at the symmetry of rabbit long bones by mechanically testing in them in torsion. Using a constant rate of torsional deformation, they looked at maximum torque, torsional deformation, stiffness and energy absorbed to fracture. Two experiments were performed. In one of experiments both left and right bones were tested in external rotation. In the other experiment, the right bone was tested in internal rotation and the left bone in external rotation. In both tests considerable variation was found within the pairs but no significant differences were found between the mean values to suggest left or right dominance. They also found no significant difference between testing in internal or external rotation.

These studies have focused on symmetry within a population. They have not addressed the issue of confidence in symmetry on an individual case basis which is essential if the contra-lateral limb is to be considered for use as a control in the clinical setting.

1.5.3.9 Healing endpoint

Based on relative indices, several investigators have suggested dynamically determined endpoints to indicate clinical or functional healing. Cunningham (1989) suggested that clinical healing could be indicated when the resonant frequency had attained 90% of that of the contra-lateral normal tibia. This was based on a study in which 20 patients with tibial fractures were monitored with resonance analysis. Christensen et al (1983) suggested 80%. Markey and Jurist (1974) suggested clinical healing had occurred when the square of the frequency ratio was 0.5.

This variation in suggested "endpoints" is not surprising given that they have been determined by correlations with imprecise clinical healing determinants. No endpoints have been defined on the basis of mechanical correlations.

1.6 RELATIONSHIP BETWEEN STIFFNESS AND STRENGTH

The biomechanical assessment of fracture healing is largely based around techniques which either directly or indirectly measure stiffness. Refracture risk at the time of clinical healing however is ultimately a function of fracture strength. There has been very little research however establishing the relationship between

stiffness and strength. Richardson et al (1994) cited the work of Lettin (1965) as justification for the use of stiffness to monitor fracture healing since it reflected changes in both the quantity and quality of the repair tissues. The relationship between stiffness and strength however was not examined in that work.

Henry et al (1968) examined stiffness and strength changes in healing fractures of rabbit radii and looked at the correlation between them. They concluded that there was a good linear correlation ($r = 0.92$) but this was on the basis of fractures that had been tested at 5 weeks only. Stiffness and strength data for fractures at nine and ten weeks was also obtained but not included in the correlation analysis.

The only other reference found was the study by Markel et al (1990) who correlated the indentation stiffness of the healing gap tissue with the torsional strength. They found a logarithmic association ($R^2 = 0.50$) but inspection of the graph shows marked scatter of the results.

1.7 OVINE FRACTURE MODEL

Destructive tests to measure the strength or other properties of healing fractures are obviously not feasible in human studies. Sheep are a well-established experimental animal (Hecker 1983) and have been successfully used in fracture healing studies (Thompson 1973; Nunamaker and Perren 1979; Perren and Rahn 1980; Mayer and Wolf 1983; Goodship and Kenwright 1985; Braunstein et al 1986; Cornelissen et al 1988; Kenwright and Goodship 1989). Ovine research is also much less emotive than research with primate and canine species. In Australia a further advantage for the use of the ovine model is that sheep are readily available and relatively inexpensive to both obtain and maintain. The use of sheep for in-vivo assessment of fracture healing with vibrational analysis however has not been established.

1.8 SUMMARY

It is clear from the literature that there is a need for a non invasive tool to objectively and reproducibly monitor mechanical changes during fracture healing. Resonant frequency analysis is one approach which has shown much promise but is still in its infancy with respect to research and development. Several techniques are in use but none has been shown to be clearly superior.

There have been numerous *in-vitro* studies correlating resonant frequency changes with long bone mechanical properties but no studies to date have correlated *in-vivo* resonant frequency monitoring with direct mechanical testing.

Current fracture monitoring theory relies heavily on the use of the "normal" limb as a control. Confidence in this relationship has not been adequately established with respect to bending mode frequencies or bone mechanical properties.

Whereas the relationships between histomorphometric features and mechanical properties are well established in normal and osteoporotic bone, there is a paucity of work examining this relationship in healing fractures and no studies which have correlated histomorphometry with vibrational analysis or other mechanical fracture assessment techniques.

An understanding of the relationship between stiffness and strength during fracture healing is crucial in determining the role of stiffness monitoring techniques in fracture healing assessment. This relationship is yet to be adequately defined and requires further assessment.

The first step in this thesis was to examine the issue of symmetry between contra-lateral limbs which is described in the next chapter.

CHAPTER TWO

SYMMETRY

2.1 INTRODUCTION

Assessing changes in the mechanical properties during fracture healing requires a reference of normality. Use of the unaltered contralateral limb as a control is the obvious choice. No data are currently available on symmetry of the physical and mechanical properties in sheep.

2.2 AIMS

The aim of this study was to examine symmetry of the physical, mechanical and vibrational properties in sheep tibiae and to determine the validity of using an unaltered tibia as a control for the contralateral tibia in a sheep fracture healing model.

2.3 METHODS

2.3.1 Study group

This study used ten pairs of sheep tibiae. The sheep were all six tooth (2.5 - 3 years old) Merino wethers.

2.3.2 Collection and preparation of specimens

After culling by lethal injection of phenobaritone, both tibiae were excised by careful disarticulation at both the knee and ankle joints using sharp dissection. The specimens were frozen immediately after culling and were stored at -20° Celsius for a period of up to two weeks prior to testing. The muscles and soft tissues around the tibiae were left in situ to prevent the bones from drying and consequently behaving in a more brittle manner (Burstein et al 1972). The specimens were thawed on the evening prior to the day of testing.

2.3.3 Mass and length determination

After dissection of all soft tissue, the mass and length of the tibial bones were recorded. Length was measured from the most proximal point of the medial tibia to the tip of the medial malleolus and recorded to the nearest millimetre. The tibiae were then weighed and recorded to the nearest milligram. Thereafter, throughout the testing, drying of the bones was prevented by regular spraying with a 0.9% saline solution.

2.3.4 Vibrational testing

The tibial pairs were tested to determine their vibrational characteristics. Resonant frequency data was obtained from the tibiae in both the anteroposterior (AP) and mediolateral (ML) planes. Figure 2.1 shows the setup for testing.

The bones were mounted from a simple metal frame using fishing line which was passed through holes drilled in both the AP and ML planes at the proximal tibia. This created free-free boundary conditions on the bone. Two further holes were drilled and tapped eight centimetres proximal to the distal end of the tibia. One was along the anterior ridge of the tibia in the AP plane and the other on the anteromedial surface in the ML plane. These holes allowed the stud mounted accelerometers to be screwed into the bone allowing full contact of the accelerometer with the bone surface. Brüel & Kjær Type 4382 piezoelectric accelerometers were used (Nærum, Denmark).

A Brüel & Kjær Type 8202 Impact Trigger Hammer (Nærum, Denmark) was used to excite the bone at a point approximately six centimetres distal to the proximal end of the tibia. The impact hammer, with a built in transducer and rubber tip, generated frequencies in the lower frequency range with the aim of measuring the first bending mode frequency in each plane. Initially the bone was excited with the accelerometer mounted in the AP plane of the tibia. The bone was excited ten times and the results recorded. The accelerometer was then removed and placed in the ML plane and a further ten measurements were obtained.

The force and acceleration signals were amplified via a Brüel & Kjær, type 2635 preamplifier (Nærum, Denmark) and recorded simultaneously with a Brüel & Kjær, type 2032, Dual Channel Spectrum Analyser (Nærum, Denmark). The coherence function was calculated for impulse excitations where a value of 1 indicated perfect coherence. Measurements were only accepted where the coherence was greater than 0.95 in the frequency range of interest thus ensuring accuracy of the results (Figure 2.2). The resonant frequencies in each plane were then determined from a curve fitting procedure using a modal analysis program.

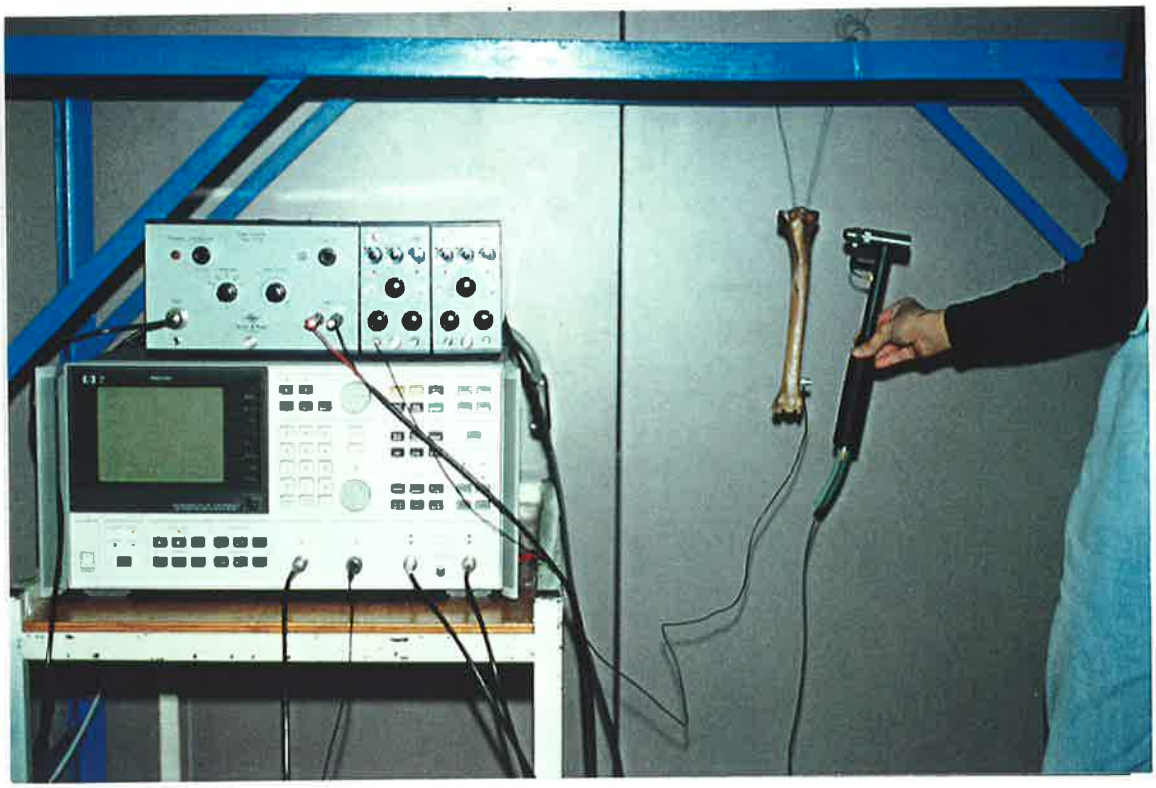

Figure 2.1 Typical setup of equipment for hammer excitation technique

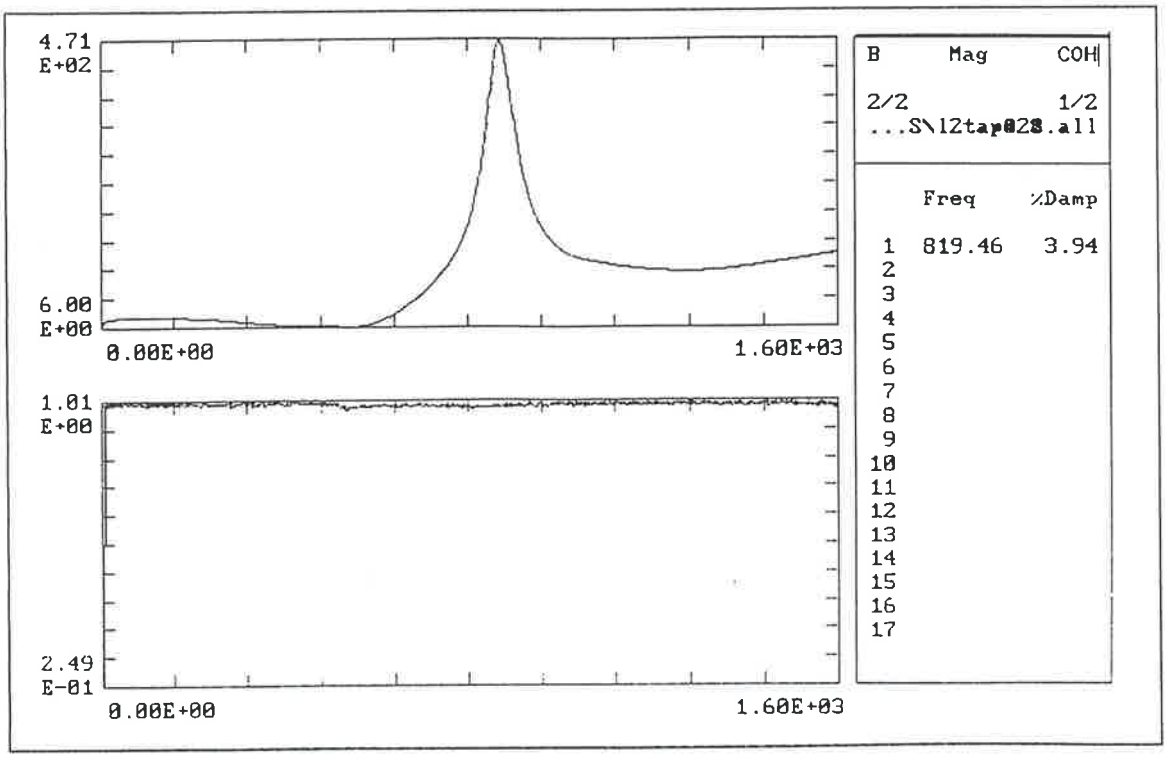

Figure 2.2 Typical coherence observed for the resonant frequency response generated for the sheep tibiae

2.3.5 Mechanical testing

Following vibrational testing, mechanical testing of the sheep tibiae was undertaken. Four point bending stiffness and ultimate bending strength were measured. The four-point bending tests were applied in the anteroposterior (AP) and mediolateral (ML) planes. Ultimate bending strength was determined in the ML plane. The stiffness in the ML plane was also determined at the higher loads in the failure tests.

Mechanical testing was performed with a Hounsfield H25KM Universal Testing Machine (Hounsfield, High Wycombe, UK) fitted with a custom built, four-point bending rig (Figure 2.3). This was set up with a 200mm distance between the outer two pins and 100mm between the inner pins. Control of the machine was achieved with a 386 IBM compatible computer using custom-designed software to analyse and record the data.

The sequence of testing was AP stiffness, ML stiffness and ML fail test. In the stiffness tests, the load was applied to the tibiae by the machine's crosshead which was moved at a rate of 10mm/min until a total load of 150N was achieved. The specimen was then unloaded at the same rate and this cycle was repeated for a total of 5 cycles. The stiffness values were determined from the fifth cycle by calculating the maximum slope of the resultant bending moment / displacement curve (Figure 2.4). The fifth load cycle was used for measurements as this enabled consistent results to be obtained following initial visco-elastic deformation of the specimens and embedding of the loading rollers into the periosteum. Results were recorded as bending moment per unit displacement of the testing machine cross-head: Nm/mm. The bending stiffness was measured in these terms because the complex shape of the tibiae rendered it meaningless to consider stress. The method described gave a means of providing comparative results across specimens and time of healing.

The strength and the ML "fail loading" stiffness (FLS) were determined by a further test in which the increasing load was continued in the ML plane at the same rate until the bone fractured. Strength was determined from the highest bending moment sustained by the bone before failure and FLS was calculated from the maximum slope of the bending moment / displacement just prior to failure (Figure 2.5).

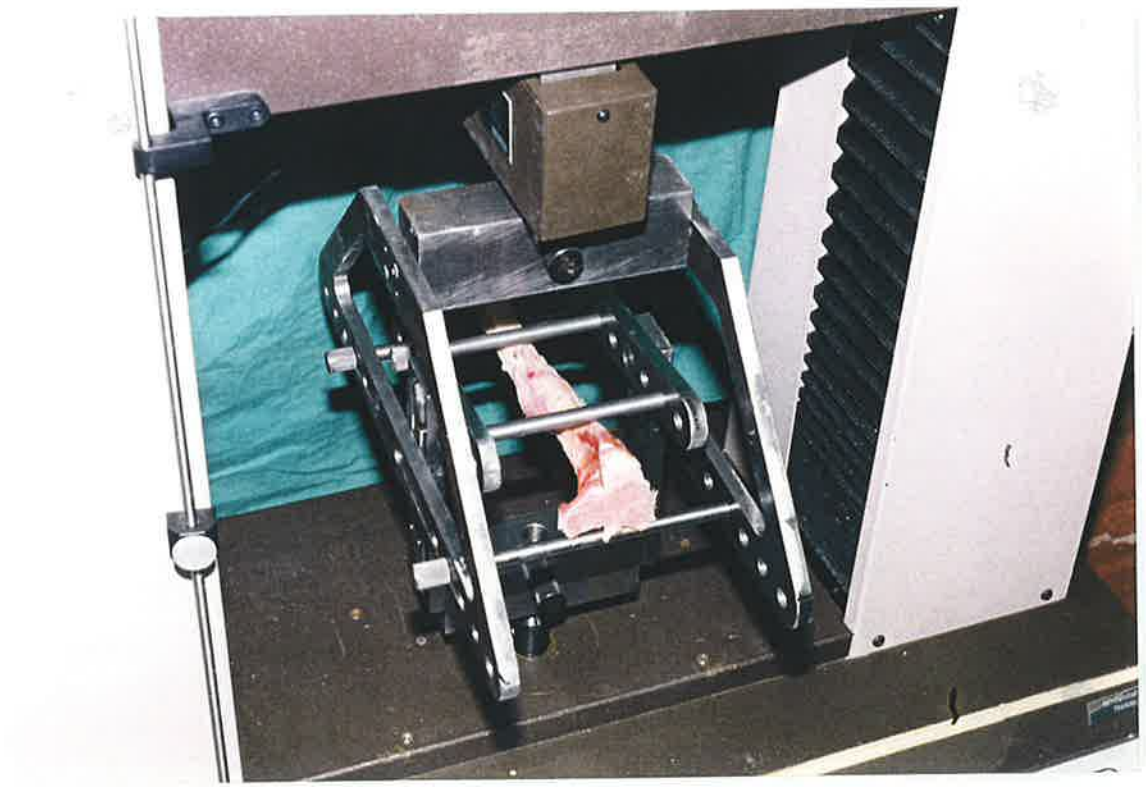

Figure 2.3 Setup for AP bending test with the four-point bending rig mounted in the Hounsfield H25KM Universal Testing Machine

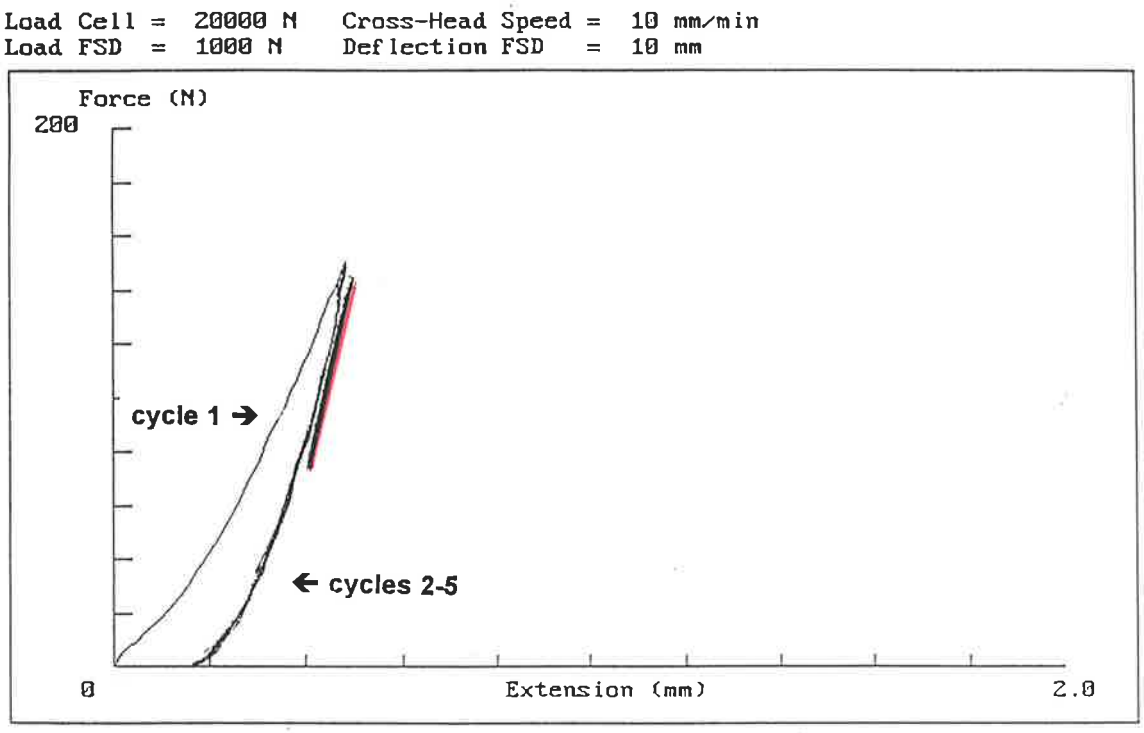

Figure 2.4 Typical bending moment / displacement curve generated by the four-point bending test. The stiffness values were determined from the maximum slope of the fifth cycle.

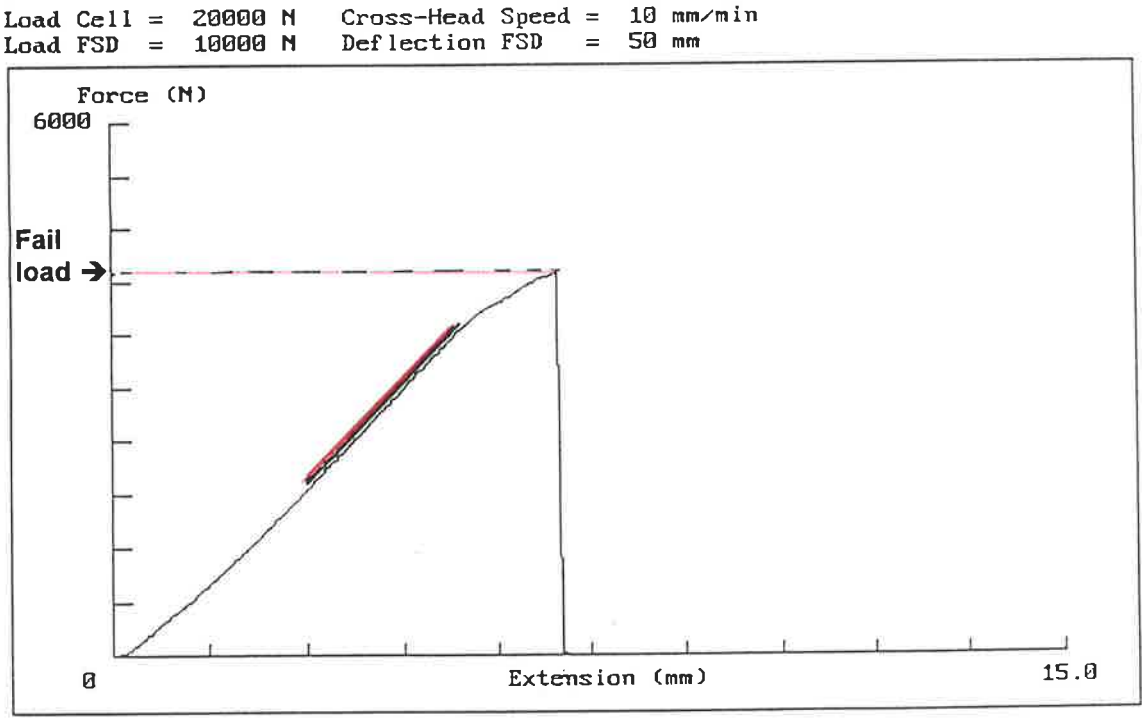

Figure 2.5 Bending moment/ displacement curve showing the loading to failure from which strength and FLS were determined.

2.4 RESULTS

The results were analysed using the analysis package of Excel version 5 (Microsoft, USA) and the mean values and standard deviations (SD) were calculated. Students t-tests were performed to compare the means with an hypothesised difference between left and right being zero. A difference was to be considered as statistically significant where $p<0.05$. A percentage variation value (%Var) was calculated by expressing the difference between the individual left and right tibiae as a percentage of the mean value of the individual pairs:

$$\%Var_{pairX} = \frac{\left(left_{pairX} - right_{pairX}\right)}{\frac{(left_{pairX} + right_{pairX})}{2}} x100\%$$

2.4.1 Mass

The mean mass of left tibiae was found to be 128.0 (SD 14.2) x 10^{-3} Kg as compared to 127.7 (SD 13.5) x 10^{-3} Kg for the right tibiae (Table 2.1). Student's t-test showed no significant difference between the two sides ($p = 0.80$). The mean %Var was 1.8 (SD 0.07) whereas the maximum %Var within any pair of tibiae was 2.9%. Pearson's correlation between left and right tibial bone mass was very strong with $r = 0.98$ (Figure 2.6)

Table 2.1 Left and right tibial masses

Sheep Pair	Mass ($x10^{-3}$ Kg) Left	Right	%VAR
1	118.8	121.3	2.1
2	106.1	108.0	1.8
3	136.2	139.1	2.1
4	114.2	116.0	1.6
5	157.5	155.9	1.0
6	130.4	131.4	0.8
7	125.5	122.6	2.3
8	134.6	133.5	0.8
9	133.5	129.7	**2.9**
10	122.7	119.9	2.3
Mean	128.0	127.7	1.8
SD	14.2	13.5	0.7
Pearson Correlation	0.98		
P(T<=t) two-tail	0.80		

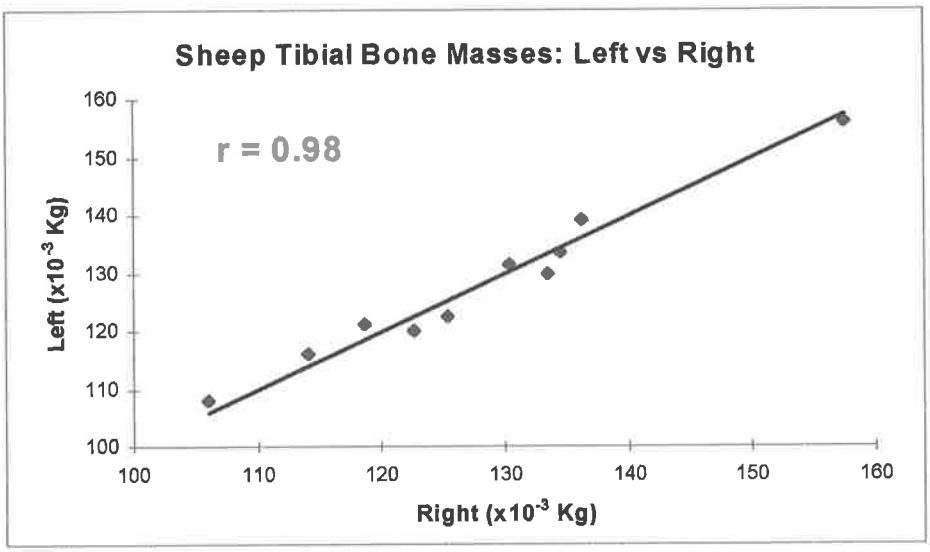

Figure 2.6 Correlation of left and right tibial masses

2.4.2 Length

The mean length of left tibiae was 236 (SD 10) mm as compared to 236 (SD 11) mm for the right tibiae (Table 2.2). Student's t-test showed no significant difference between the two sides (p = 0.24). The mean %Var was 0.5 (SD 0.4) % whereas the maximum %Var within any pair of tibiae was 1.3%. Pearson's correlation coefficient between left and right tibial lengths was very strong with r = 0.99 (Figure 2.7).

Table 2.2 Left and right tibial lengths

Sheep Pair	Length (mm)		
	Left	Right	%VAR
1	223	222	0.4
2	235	238	1.3
3	226	228	0.9
4	234	234	0.0
5	251	252	0.4
6	252	254	0.8
7	224	224	0.0
8	239	240	0.4
9	236	236	0.0
10	237	235	0.8
Mean	236	236	0.5
SD	10	11	0.4
Pearson Correlation	0.99		
P(T<=t) two-tail	0.24		

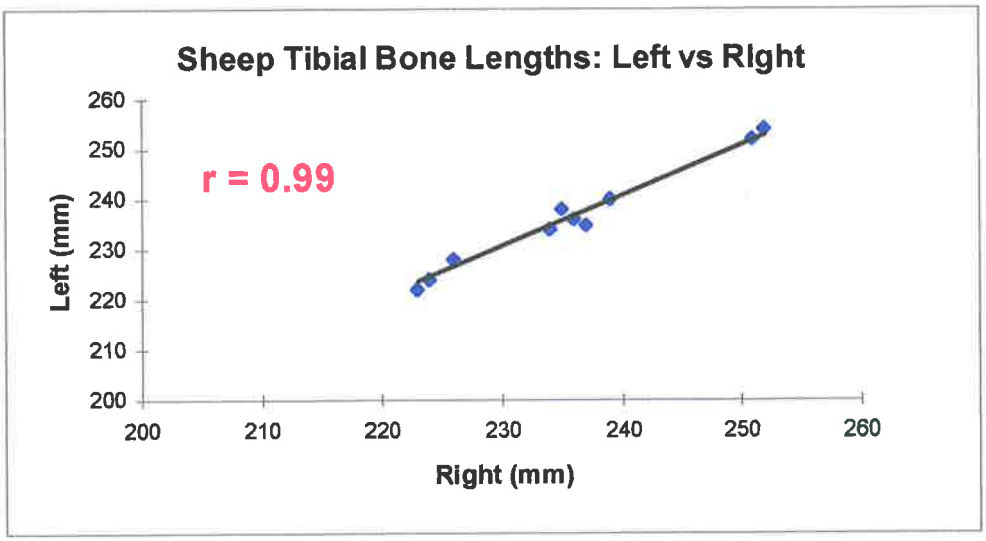

Figure 2.7 Correlation of left and right tibial masses

2.4.3 Vibrational analysis

The mean resonant frequency in the ML was 893 (SD 72) Hz for the left tibia and 900 (SD 77) Hz for the right (Table 2.3). Student's t-test showed no significant difference between the means (p = 0.29). The mean %Var was 1.9 SD 2.0 % and the maximum %Var was 5.3 %. Pearson's correlation was strong with r = 0.96 (Figure 2.8).

Table 2.3 Left and right tibial resonant frequency data from first single bending modes in ML and AP planes

Sheep Pair	ML Resonant Frequency (Hz)			AP Resonant Frequency (Hz)		
	Left	Right	%VAR	Left	RIght	%VAR
1	932	953	2.1	866	887	2.3
2	927	922	0.4	819	813	0.8
3	993	995	0.2	853	856	0.4
4	810	816	0.8	716	732	2.3
5	833	790	**5.3**	697	691	0.9
6	806	814	1.0	706	697	1.2
7	920	942	2.4	888	852	4.0
8	958	975	1.8	795	746	**6.4**
9	945	956	1.1	808	792	1.9
10	802	835	4.1	736	724	1.5
Mean	893	900	1.9	788	779	2.2
SD	72	77	2	71	71	2
Pearson Correlation	0.96			0.96		
P(T<=t) two-tail	0.29			0.20		

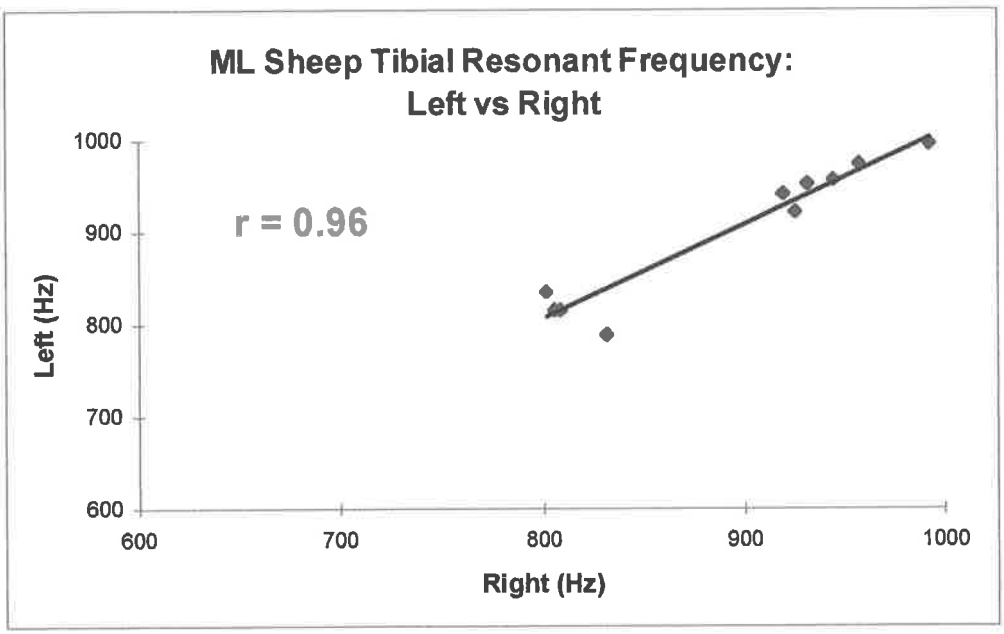

Figure 2.8 Correlation of left and right first ML single bending mode resonant frequencies

The mean AP resonant frequency was 788 (SD 71) Hz for the left and 779 (SD 71) Hz for the right. Again no significant difference was found between the means with the Student's t-test ($p = 0.20$). The mean %Var was 2.2 (SD 2.0) % and the maximum %Var was 6.4 %. Pearson's correlation was strong with $r = 0.96$ (Figure 2.9).

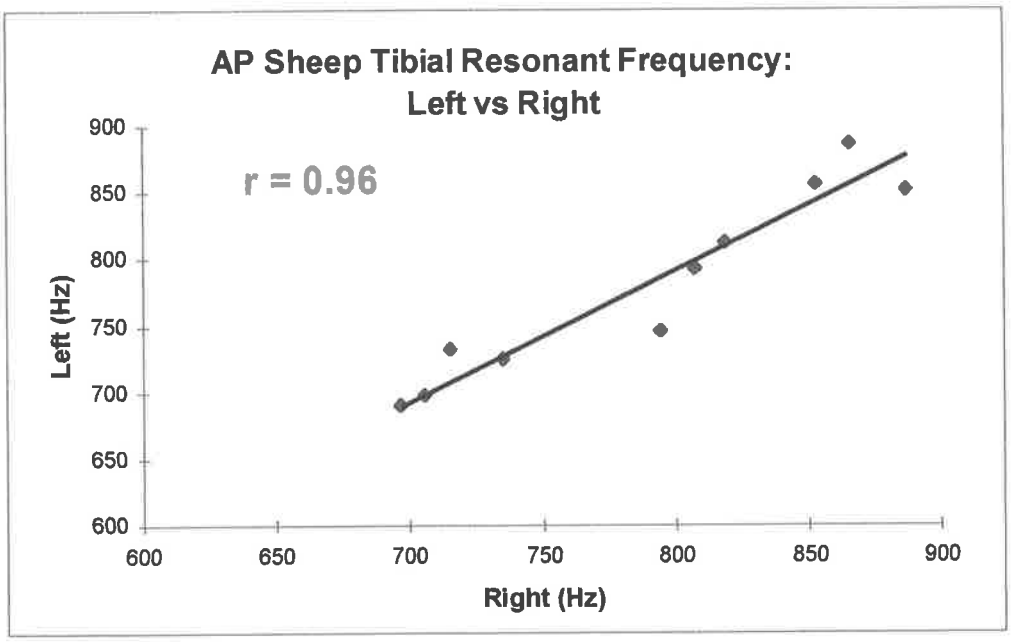

Figure 2.9 Correlation of left and right first AP single bending mode resonant frequencies

2.4.4 Mechanical testing

The bending moments presented were calculated assuming the bone between the inner pins of the four-point bending rig was a homogeneous rod. For comparative purposes the bending stiffness was calculated as the ratio of calculated bending moment to cross-head movement giving units of Nm/mm.

Table 2.4 Stiffness and strength data from left and right sheep tibiae

Sheep Pair	AP Stiffness (Nm/mm)			ML Stiffness (Nm/mm)			ML Fail Stiffness (Nm/mm)			Strength (Nm)		
	Left	Right	%VAR	Left	Right	%VAR	Left	Right	%VAR	Left	Right	%VAR
1	9.3	9.0	3.1	11.4	10.8	5.8	12.5	12.0	3.9	77.3	68.8	11.6
2	8.4	9.3	9.6	9.7	10.4	7.5	10.3	11.5	11.2	56.8	64.4	12.6
3	10.1	9.3	8.5	12.9	12.7	1.2	14.3	13.7	4.4	82.8	83.9	1.4
4	9.0	10.5	15.1	8.1	9.5	16.6	9.5	11.2	16.2	51.6	55.3	6.8
5	11.5	11.2	2.6	12.6	12.2	3.5	14.3	13.6	5.3	82.8	75.5	9.2
6	9.6	10.2	6.3	7.9	11.2	34.2	9.5	11.8	21.4	48.9	54.9	11.6
7	9.6	8.0	17.3	9.8	10.6	7.2	10.8	12.0	9.9	100.5	94.3	6.4
8	11.1	7.3	40.7	14.0	9.3	40.5	15.6	11.1	33.4	103.8	110.5	6.3
9	11.1	9.0	21.0	10.8	11.7	8.3	11.6	12.7	8.3	98.9	89.0	10.5
10	7.0	7.2	3.7	7.7	9.2	17.8	8.8	10.6	17.8	97.4	90.0	7.9
Mean	9.7	9.1	12.8	10.5	10.8	14.3	11.7	12.0	13.2	80.1	78.6	8.4
SD	1.4	1.3	11.7	2.2	1.2	13.3	2.3	1.0	9.2	21.0	18.1	3.4
Pearson Correlation	0.33			0.39			0.55			0.95		
P(T<=t) two-tail	0.29			0.69			0.67			0.54		

The mean AP bending stiffness was 9.7 (SD 1.4) Nm/mm for the left and 9.1 (SD 1.3) Nm/mm for the right (Table 2.4). The difference was not statistically significant with the Student's t-test ($p = 0.29$). The mean %Var was 12.8 (SD 11.7) % and the maximum %Var was high at 40.7 %. Pearson's correlation was poor with $r = 0.33$ (Figure 2.10).

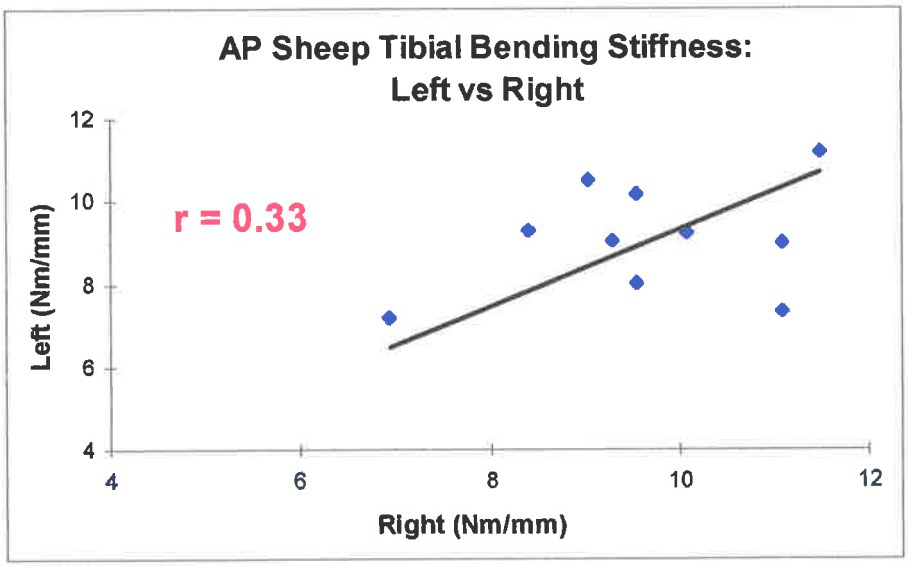

Figure 2.10 Correlation of left and right AP bending stiffness

For the ML bending stiffness loaded to 150 N the mean stiffness was 10.5 (SD 2.2) Nm/mm for the left and 10.8 (SD 1.2) Nm/mm for the right. The difference was not statistically significant with the Student's t-test ($p = 0.69$). The mean %Var was 12.8 (SD 11.7) % with the maximum %Var again high at 40.7 %. Pearson's correlation was poor with $r = 0.33$ (Figure 2.11).

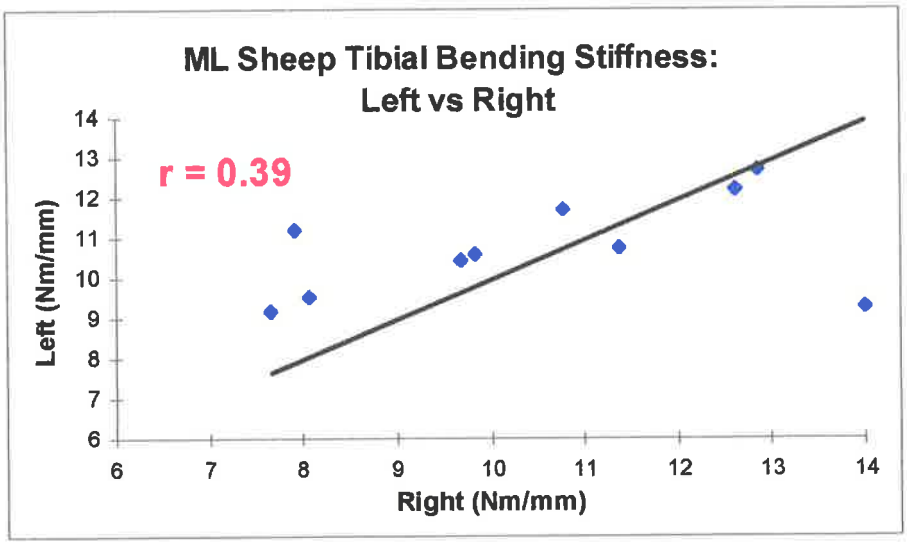

Figure 2.11 Correlation of left and right ML bending stiffness

At the loads to failure the mean stiffness (FLS) in the ML plane was 11.7 (SD 2.3) Nm/mm for the left side and 12.0 (SD 1.0) Nm/mm for the right. Student's t-test failed to show any significant difference between left and right mean values ($p = 0.67$) and the mean %Var was 13.2 (SD 9.2) %. The maximum %Var was 33.4 % and Pearson's correlation was not high with $r = 0.55$ (Figure 2.12).

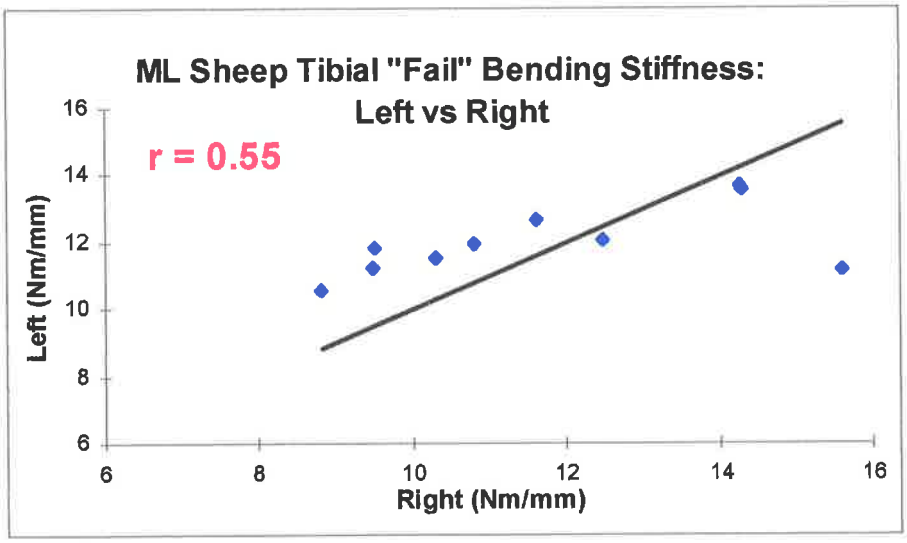

Figure 2.12 Correlation of left and right ML "fail" bending stiffness

From the maximum bending moments in the ML plane the strength was 80.1 (SD 21.0) Nm on the left side and 78.6 SD (18.1) Nm on the right. No significant difference was indicated between left and right means with the Student's t-test ($p = 0.29$). The mean %Var was 8.4 (SD 3.4) % and the maximum %Var at 12.6 % was much lower than for the bending stiffness tests. Pearson's correlation was strong with $r = 0.95$ (Figure 2.13).

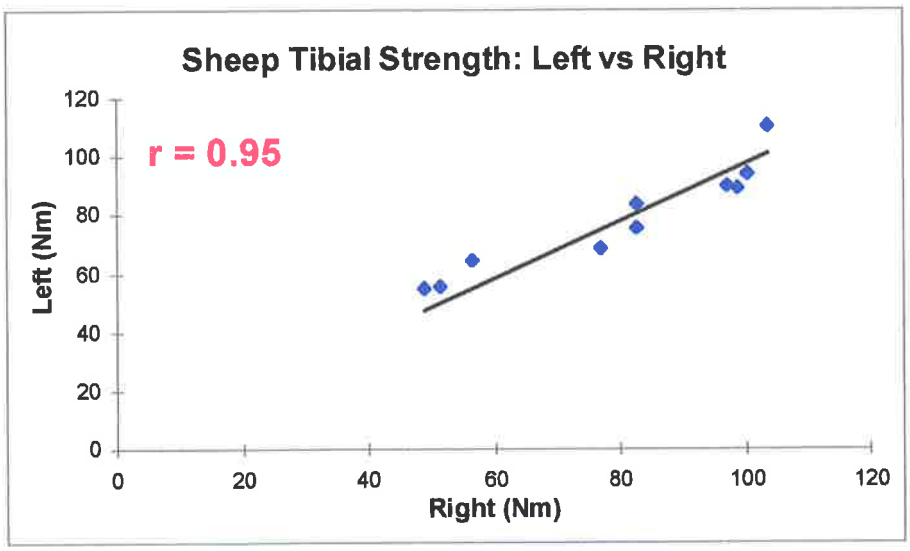

Figure 2.13 Correlation of left and right ML bending strength

2.5 DISCUSSION

These results are in keeping with most other studies of symmetry with no significant differences being found between left and right *mean values* with the t-tests. In addition, the physical properties (mass and length) and the resonant frequency data have shown strong correlations between left and right. The mechanical data however is less convincing, particularly when the amount of variation between left and right individual pairs is considered. If we consider pair 8 we find a greater than 40% variation between left and right in both the ML and AP bending tests. This difference is reduced to 33% when tested at loads to failure and when the ultimate bending strengths were compared, the difference was only 6%. As the mass and length show such little variations between sides, why such individual asymmetry should exist in the mechanical properties is not evident. Why bending strength should show greater symmetry than bending stiffness is also not immediately evident.

As the bending mode resonant frequency is supposedly an index of bending stiffness, it is noteworthy that the individual asymmetry found in the mechanical data is not also reflected in the vibrational data. Inaccuracies in the mechanical measurement technique using the four-point bending tests must be considered as a possible explanation but would seem unlikely given the strong symmetry found in the mechanical strength measurements.

Another possibility to be considered is that the resonant frequencies may not be as sensitive to bending stiffness differences as mechanical testing. Consider the mathematical relationship between frequency and bending stiffness:

$$f \propto \sqrt{EI}$$

- the resonant frequency is proportional to the square root of bending stiffness. Thus changes in the bending stiffness are reflected by relatively smaller changes in the resonant frequency. This sensitivity difference may explain some of the symmetry difference noted between the mechanical stiffness and resonant frequency data but does not explain differences as great as 40 percent.

If a comparison is made between the stiffness values calculated from the bone displacements to both the high loads to failure and the relatively low loads to 150N, it can be seen that the stiffness was always greater for any given bone when measured at the higher loads. This indicates non-linearity in the bending stiffness properties of the bone. The differences in symmetry noted between the resonant frequency data may be a reflection of the loading conditions under which the tests are undertaken. The resonant frequencies were determined from the bones in an unloaded condition. The mechanical tests for stiffness require measurement of deflection under load. Thus it is possible that the stiffness is symmetrical when the bone is not loaded but is more variable under load.

Testing this hypothesis would be somewhat difficult with mechanical methods: - what is a bending test without a load to bend? An alternative would be to test for resonant frequency symmetry with the bone under load. The difficulty in this situation would be in accurately matching both the loading and boundary conditions in the pairs during testing.

These results indicate that the ipsilateral unaltered tibia can be used with confidence as a control for resonant analysis data in isolated bones. Asymmetry in sheep tibiae where the bone is unaltered *in-vivo* would therefore be due to differences in boundary conditions or soft tissue.

Even though "statistical" symmetry has also been demonstrated in the mechanical stiffness properties, only limited confidence can be placed on the use of the unaltered tibia as a control in the consideration of *individual* cases.

CHAPTER THREE

BONE RESONANCE ANALYSIS:

SHEEP TECHNIQUE

3.1 INTRODUCTION

The bone resonance analysis (BRA) technique developed at the Royal Adelaide Hospital (Pohl et al 1991) forms the basis of this study. The equipment consists of a hand held shaker to generate the force and an accelerometer to record the response. In human studies, the BRA technique uses a standardised measurement protocol in which the human tibia is supported along a foam splint. A hand held shaker vibrates the tibia from the area of the medial tibial prominence and an accelerometer at the medial malleolus measures the response. This technique is highly reproducible in human testing (Chehade and Pohl 1992; Lawes and Chehade 1993) but the proposed sheep studies required a new technique.

3.2 AIMS

The aim of this study was to develop a reproducible technique for monitoring the resonant frequency of tibiae in sheep.

3.3 METHODS

3.3.1 Study sample

Six skeletally mature, six tooth (2.5 - 3 years old) Merino wethers were chosen for the study. To determine both inter- and intra-observer reproducibility, two observers performed each BRA test. Testing of each sheep occurred three times per day and on three separate days. A total of nine tests were therefore performed per sheep by each observer.

3.3.2 Anaesthesia

The sheep were fully anaesthetised for the testing. After induction with slow external jugular intravenous injection of 5mg sodium pentothal, the sheep were intubated. Anaesthesia was maintained with nitrous oxide and halothane.

Figure 3.1 (above)
Outline of subcutaneous medial surface of sheep tibia

Figure 3.2 (left)
BRA setup and technique for monitoring sheep tibiae

3.3.3 Positioning

In the standard testing position the sheep were placed flat against the table on their left side and the left leg was shaved. The right leg was secured with masking tape and retracted forward. This allowed unobstructed access to the medial aspect of the left tibia which lay flat against the table (Figure 3.1). The entire length of the tibia was thus evenly supported throughout under general support conditions.

3.3.4 BRA setup

In performing BRA (Figure 3.2), a custom built hand held electromagnetic shaker was used to input constant amplitude sine waves. The coil from a Brüel & Kjær Type 4810 shaker (Nærum, Denmark) was used in the custom built shaker which also incorporated a linear variable differential transducer (LVDT) to allow monitoring of the static preload during testing. The shaker housing was designed to facilitate hand held operation. The vibrational response was measured with a Brüel & Kjær Type 4393 accelerometer (Nærum, Denmark). A Brüel & Kjær Type 2635 charge amplifier (Nærum, Denmark) was used to both drive the shaker and amplify the accelerometer signal. Custom written software (Applied Development and Design, Adelaide, Australia) and an A/D card (analogue to digital conversion) on a 286 IBM compatible laptop computer was used to perform the resonance analysis.

3.3.5 BRA technique

The tests involved the input of sine swept, constant amplitude waves through the hand held electromagnetic shaker to the medial tibial prominence of the proximal tibia (Figure 3.2). A frequency sweep from 50 to 1000Hz was used with a resolution of 4 Hz. The static preload of the shaker was maintained at 10 ± 0.5 Newton (Chehade et al 1993) and was indicated by a bar plot on the computer monitor (Figure 3.3). The shaker was positioned against the skin such that the preload was applied at 90 degrees to the underlying anteromedial bone surface.. The response of the tibia to this force input was measured with a hand held accelerometer firmly applied over the medial surface of the distal tibia 4cm proximal to the medial malleolus. This generated a plot of frequency versus amplitude of vibration which was displayed on the computer monitor (Figure 3.3). The frequency sweeps were repeated until there was visible reproducibility of the obtained plot (referred to as a scan). Measurements were then repeated four times. The resulting four scans were saved as a single file. The average resonant frequency of the four scans constituted one test and was used for statistical analyses. With each anaesthetic the sheep were tested three times by each observer and the tibia was repositioned after each test.

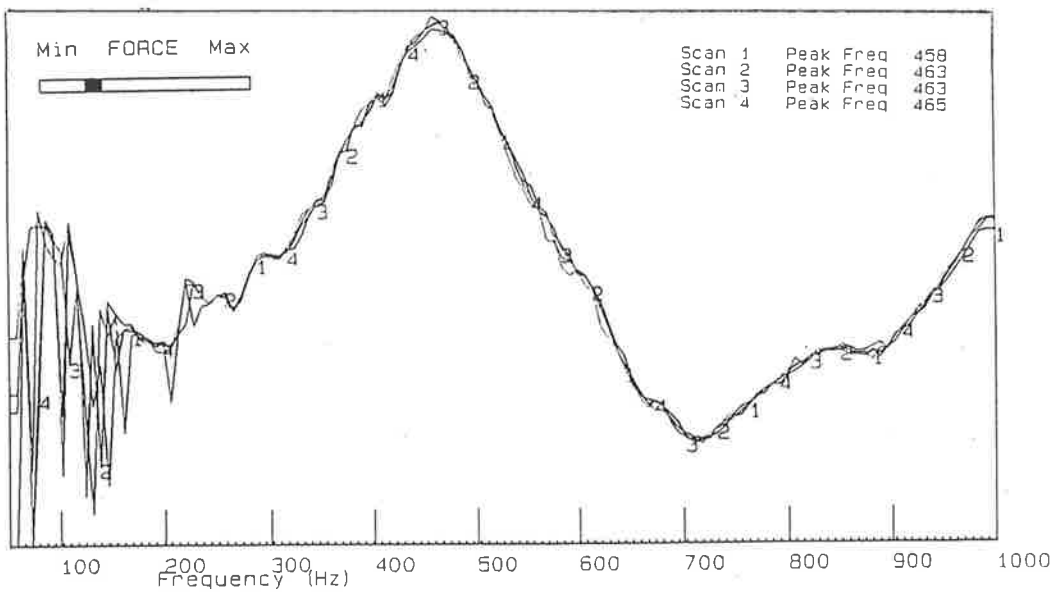

Figure 3.3 Typical BRA scans showing the average of resonant frequency peaks. The static preload is indicated by the bar plot in the left top corner.

3.4 RESULTS

The coefficient of variation (CV) was calculated as an indicator of intra-observer reproducibility and expressed as a percentage:

$$CV = \frac{STD}{mean} \times 100\%$$

To assess inter-observer reproducibility a percentage variation value (%Var) was calculated by expressing the difference between observers as a percentage of the mean resonant frequency measured between the observers:

$$\%Var_{\text{interobservor}} = \frac{(frequency_{observer1} - frequency_{observoer2})}{\frac{(frequency_{observer1} + frequency_{observer2})}{2}} x100\%$$

The results of the individual tests for each sheep are tabulated in Appendix B.

Table 3.1 summarises the intra-observer reproducibility data for each of the observers. For both observers the mean CV of all tests of all sheep was only 1.2%. The maximum CV for any series of tests was 1.5%.

Table 3.1 Summary of data of all BRA intra-observer reproducibility tests

	Observer 1			Observer 2		
Sheep	*Mean*	*SD*	*CV*	*Mean*	*SD*	*CV*
1	590	5.8	1.0	588	6.1	1.0
2	565	8.3	1.5	564	6.8	1.2
3	576	5.2	0.9	570	8.1	1.4
4	512	5.4	1.1	516	6.5	1.3
5	627	8.9	1.4	623	6.4	1.0
6	568	8.1	1.4	566	6.0	1.1
Mean	573	7	1.2	571	7	1.2

Inter-observer reproducibility was also good (Table 3.2). The mean %Var for each test ranged between 0.9 and 1.7% and the maximum recorded %Var was only 3.4%.

Table 3.2 Summary %Var data as an index of inter-observer reproducibility

	%Var		
Sheep	*Mean*	*STDev*	*Max*
1	1.5	1	3.1
2	1.7	1	3.2
3	1.7	1	3.3
4	1.3	1	3.3
5	0.9	0.6	1.9
6	1.2	1.1	**3.4**

3.5 DISCUSSION

This study has demonstrated a technique of BRA on normal sheep tibiae that has both intra- and inter-observer reproducibility. This technique should therefore be suitable to assess the use of resonant frequency monitoring during fracture healing in a sheep tibial fracture healing model.

CHAPTER FOUR

FRACTURE HEALING STUDY:

OVERVIEW AND MECHANICAL PROPERTIES

4.1 INTRODUCTION

To assess the use of BRA as a monitor of fracture healing, resonant frequency changes need correlation with the mechanical and histomorphometric properties of the healing fracture. This requires a live animal model. As demonstrated in the previous chapter, a reproducible technique of BRA is possible using sheep tibiae in-vivo. This suggests that an ovine fracture healing model is appropriate. The usual options for management of a fractured bone during healing include cast fixation, internal fixation or external fixation. Cast fixation is technically possible in sheep but does not allow sufficient control of movement at the fracture site to confidently maintain anatomical reduction or to standardise the healing environment. Management of a sheep with a cast also poses practical problems in keeping the cast dry, in preventing pressure areas and in allowing normal weight bearing. Both plate fixation and external fixation allow early restoration of function. Testing the mechanical properties of the fracture, however, requires the prior removal of the fixation. Removing a plate results in unavoidable damage to some of the surrounding new bone and thus potentially influences the mechanical properties to be tested.

External fixation has been used in ovine tibial fracture studies (Kenwright and Goodship 1989; Goodship et al 1993). Although more cumbersome, an external fixator can be removed without disturbing the fracture healing site and also allows healing by callus formation. Goodship et al (1993) showed that increasing the fixator frame offset by 10mm resulted in a 40% reduction of the stiffness of the fixation and also significantly reduced the rate of fracture healing. Therefore, to standardise the mechanical environment of the healing fracture, the application of the external fixator must also be standardised.

The decision was made, therefore, to proceed with a sheep tibial fracture model to study and correlate the vibrational, mechanical and histomorphometric properties of healing fractures. In this chapter the sheep tibial fracture model is presented first with a general overview of the study plan. The mechanical properties are then presented in detail and act as a frame-work on which the vibrational and histomorphometric properties are correlated in subsequent chapters.

As discussed in section 1.6, the assessment of refracture risk with stiffness monitoring techniques assumes a workable correlation between stiffness and strength. Therefore, this study was also undertaken to test the hypothesis that this assumed correlation between stiffness and strength is valid.

4.2 AIMS

The aims of this section were:

1. To examine the mechanical properties of normal sheep tibiae;
2. To study the time related stiffness and strength changes that occur in a healing sheep tibial fracture; and
3. To assess the relationship between stiffness and strength.

4.3 METHODOLOGY

The following account gives a general overview of the methodology of this fracture healing study. The creation and stabilisation of the tibial fracture is then detailed. This is followed by a description of the methodology employed in the mechanical testing.

4.3.1 Fracture Model

4.3.1.1 Overview

The sheep were all initially anaesthetised and the initial "prefracture" BRA tests were performed. Under this anaesthetic, an external fixator was then applied and an osteotomy of the tibia was performed. At a designated culling time the sheep were again anaesthetised, the external fixator was removed and further BRA testing was undertaken. The sheep were then culled and the tibiae were removed for the mechanical and histomorphometric studies.

4.3.1.2 Study Group

Forty skeletally mature, six tooth (2.5 - 3 years old), Merino wethers were chosen for the study. All sheep weighed between 42 and 46 Kg. Ethical approval was obtained from the South Australian Institute for Medical and Veterinary Science and the research was undertaken under the supervision of its veterinary staff. In accordance with advice from the research statistician, the sheep were randomly allocated to 5 groups of 8 sheep destined for culling at 2, 4, 6, 8 or 10 weeks (Appendix C). All surgery was performed by the one surgeon and without prior knowledge of group allocation.

4.3.1.3 Anaesthesia

The sheep were fully anaesthetised for the procedure. Induction was performed with 5mg sodium pentothal injected slowly into the external jugular vein. After endotracheal intubation, anaesthesia was maintained with nitrous oxide and halothane.

4.3.1.4 Positioning

Both the BRA testing and the application of the external fixator were performed with the sheep positioned on their left sides in the standard sheep testing position outlined in chapter 3 (Section 3.3.3, Figure 3.2).

4.3.1.5 BRA Testing

The BRA testing was performed using the BRA equipment and technique outlined in the BRA technique chapter under sections 3.3.3 and 3.3.4. This part of the study is detailed in chapter five.

4.3.1.6 External Fixator

The external fixators were custom built for the purpose of this study (Figure 4.1). They were all configured in a standardised manner such that the three pins of the proximal clamp were in exact alignment with those of the distal clamp. A 32mm gap separated the inner two pins (distal pin of the proximal clamp and the proximal pin of the distal clamp). The clamps fixed to the fixator body were used as the alignment jig for the pin insertion.

Full surgical aseptic technique was used in the application of the external fixator and prophylactic intramuscular penicillin was administered prior to surgery. The tibial outline was marked on the skin and the fixator was centrally positioned on the tibia. A one centimetre stab incision was made for the distal pin insertion. Using a trochar inserted through a 5mm (inside diameter) cannula, the position for the distal fixator pin was determined. The trochar was then removed from the cannula and replaced with a smaller inner cannula and a 4mm drill bit. A hole was drilled through both tibial cortices passing through the centre of the medullary canal perpendicular to the longitudinal axis of the tibia and inclined 45 degrees posterior to the mediolateral plane. The inner cannula was removed and a Hoffman 5mm, self tapping, half threaded fixation pin (Howmedica, USA) was inserted to a standardised depth of 3.5 turns into the distal cortex (Figure 4.2).

With the distal pin now in position, the corresponding distal hole of the fixator was placed over the distal pin and the fixator was used as a jig for insertion of the remaining five pins (starting with the most proximal pin and working distally). With all six pins inserted, the external fixator was secured to the pins with the centre of the fixator body positioned 5 cm from the skin at the level of the third pin from the proximal end (Figure 4.3).

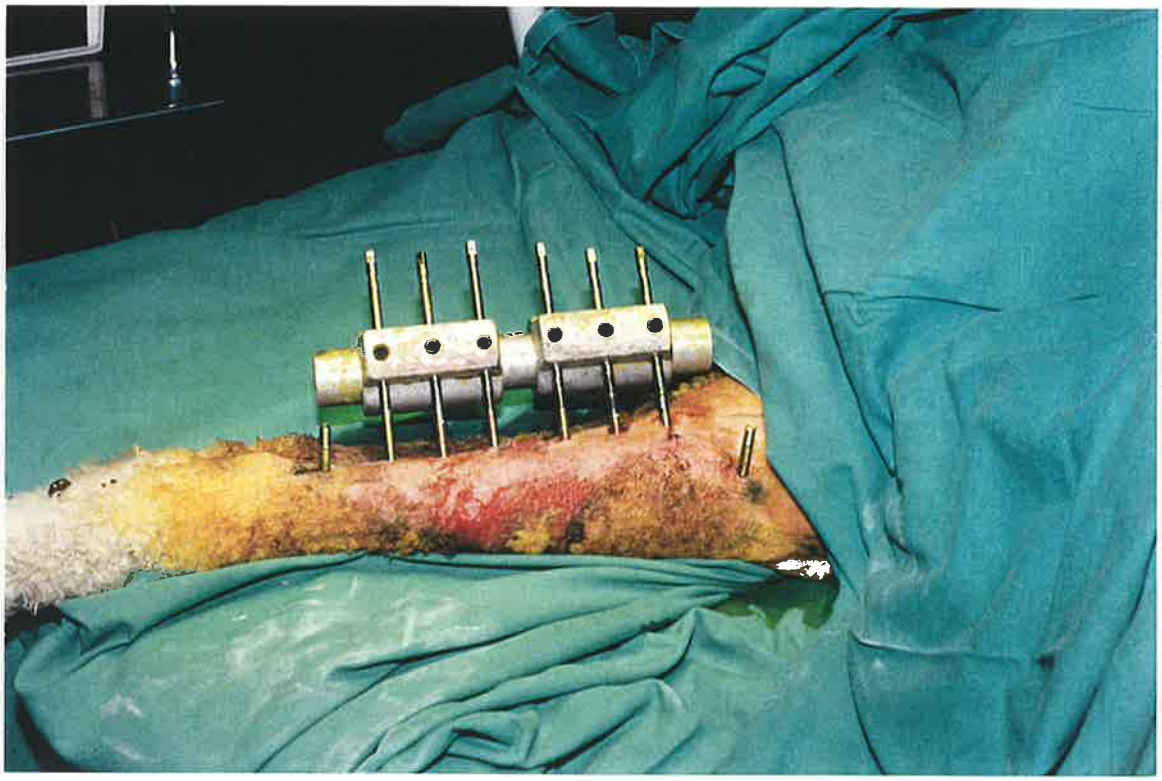

Figure 4.1 Custom built external fixator used with standardised clamp position and pin alignment

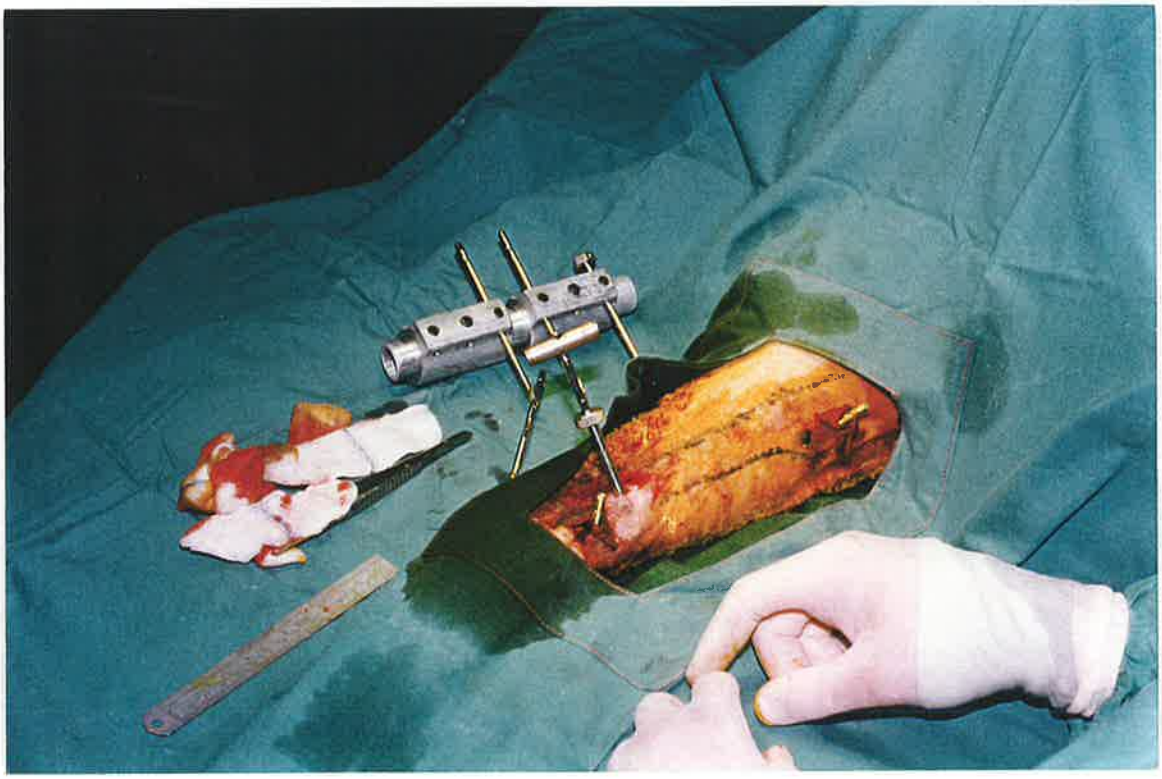

Figure 4.2 Position of initial distal pin reference for external fixator placement

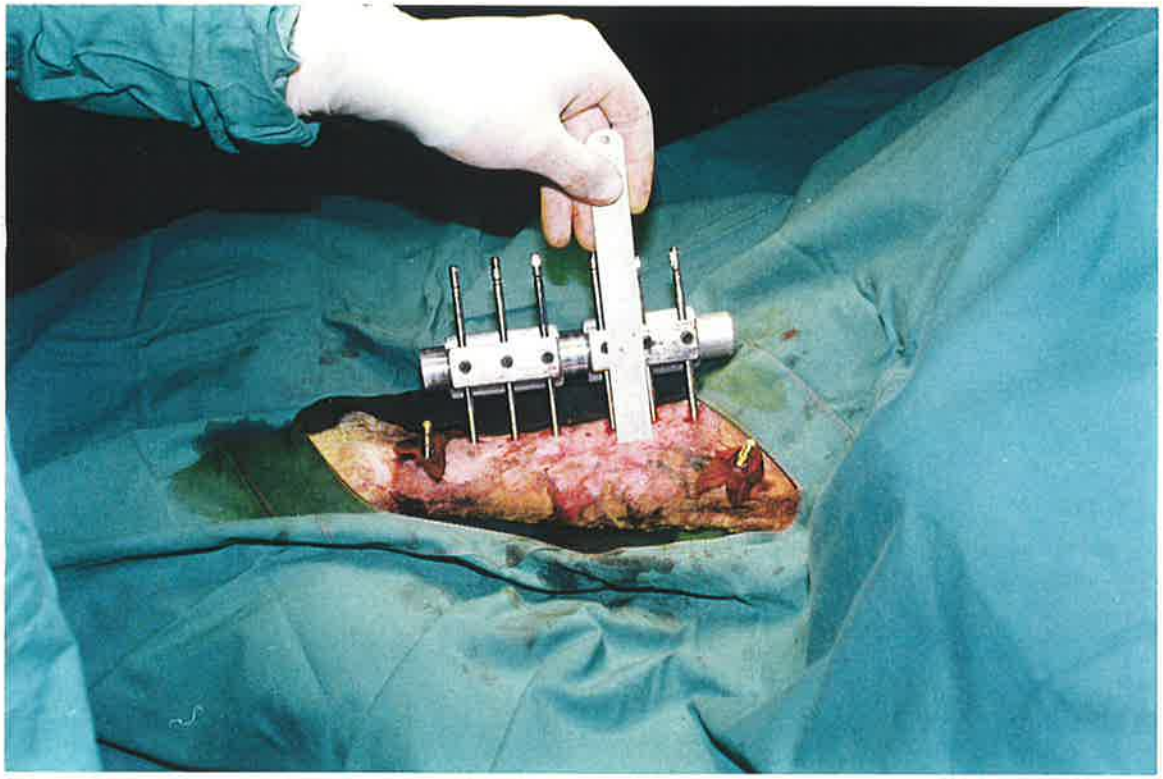

Figure 4.3 Standardised position of external fixator body

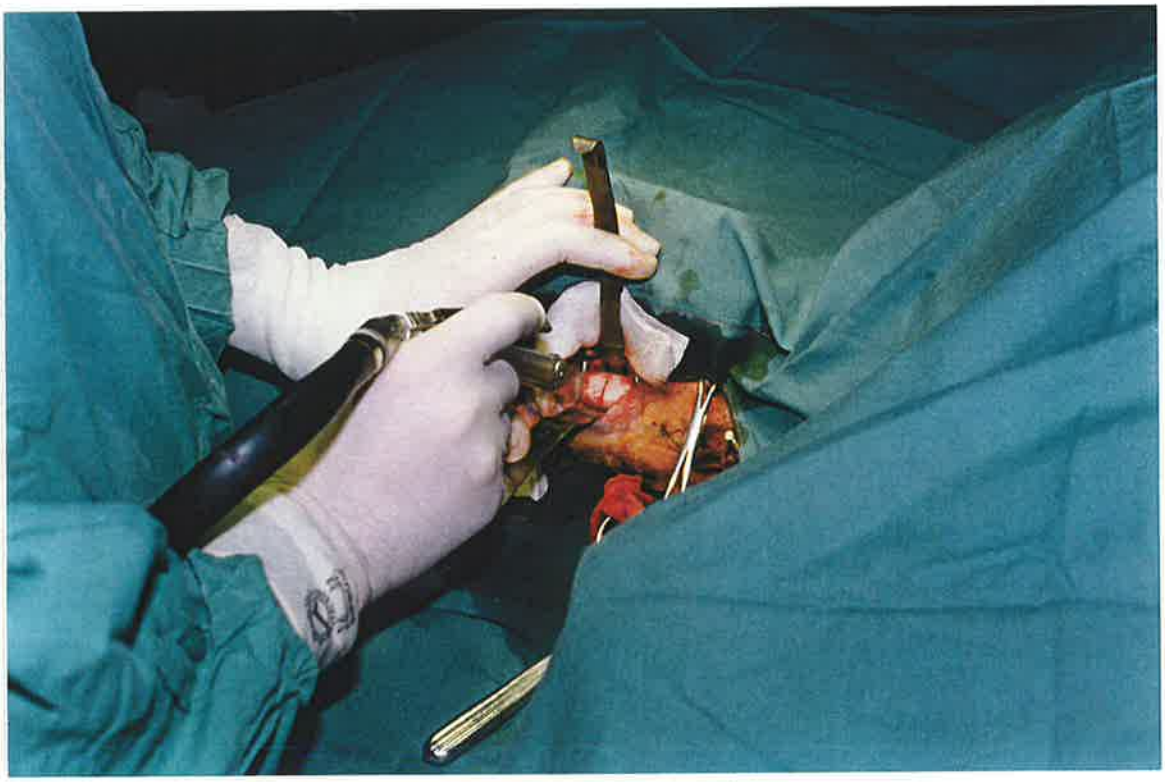

Figure 4.4 Osteotomy to tibial midshaft

4.3.1.7 Osteotomy

With the external fixator in place, a skin incision was then made between the inner 2 pins and continued through the periosteum onto the bone. Using a periosteal elevator, the periosteum was then lifted from the bone around its entire circumference without further cutting it. Two steel spatulae were positioned between the bone and periosteum to protect both the surrounding soft tissue and the periosteum. A transverse osteotomy was then performed midway between the two inner pins using a 2mm thick oscillating saw (Figure 4.4).

The periosteum was closed using simple interrupted 2/0 Vicryl sutures. Skin closure was achieved with 2/0 Prolene interrupted, vertical mattress sutures. The wounds were dressed with gauze soaked in betadine solution. Combine dressings, crepe bandage and a complete outer layer of masking tape were then used to further cover both the wound and the external fixator.

4.3.1.8 Post Operative Care

The sheep were kept in a special recovery pen for three days. Intramuscular penicillin was continued for 24 hours post operatively. Intramuscular methadone (25mg) was administered until the sheep were able to ambulate on the fractured tibia without evidence of distress. The sheep were then housed in larger pens with up to 3 sheep per pen. They were maintained in these pens until the time of their culling and were monitored for evidence of wound or pin tract infection.

4.3.1.9 Culling

On the day of culling, the sheep were anaesthetised and the external fixator was carefully removed. The BRA testing was then performed (see chapter 6). Whilst still under anaesthesia the sheep were culled by intravenous injection of phenobarbitone.

4.3.1.10 Specimen Collection

Both tibiae were excised for mechanical and histomorphometric testing, the right tibia acting as a control. With their muscles and soft tissues left in situ, the tibiae were carefully disarticulated from both the knee and ankle joints using sharp dissection with a scalpel blade. The specimens were then frozen and stored at -20° Celsius for a period of up to a month prior to undergoing mechanical testing and histomorphometric analysis.

4.3.2 Mechanical Testing

Torsional and bending stiffness were measured as well as the ultimate bending strength. The torsional tests were applied in internal rotation (IR) and external rotation (ER) and the four-point bending tests were applied in the anteroposterior (AP) and mediolateral (ML) planes. In the BRA testing the ML plane was the plane of vibration used for the resonant frequency analysis. As one of the principal aims of this thesis was to correlate BRA with the mechanical properties of the healing bone, the ML plane was chosen for the destructive strength tests.

4.3.2.1 Specimen Preparation

The frozen specimens were thawed on the evening prior to the day of testing with the muscles and soft tissues helping to keep the bones moist. On the morning of testing the bones were stripped of all soft tissues and muscles. The samples were then immediately wrapped in tissue paper soaked with 0.9% saline solution. Throughout testing the bones were sprayed with the saline solution every 10 minutes to prevent drying of the bones.

4.3.2.2 Torsion Tests

The bone ends were excised perpendicular to the long axis of the bone at lengths of at least 21cm to fit in the four point bending rig (which was utilised after the torsion testing). Special care was taken with the fractured bone to ensure that no extraneous load was applied through the fracture site. A minimum of bone was removed whilst still allowing a flat surface for mounting in the aluminium cups for torsional testing. Transfixation bolts with sharpened points were used to secure the bones as close to the centre of the cups as possible. Polymethyl methacrylate (PMMA) bone cement was

used to fix the bones in place. The specimen was then mounted in a Hounsfield H25KM Universal Testing Machine (Hounsfield, High Wycombe, UK) using a custom built torsion rig (Figure 4.5). The torsion rig converted the linear motion of the testing machine's cross-head to rotation through the action of angled sliders, mounted on the cross-head, running against rollers on a disc at the top of the rig. The disc was supported on thrust bearings so that only torsion was applied to the specimen. The rotating shaft was coupled to the specimen through a double sliding carriage system to eliminate any lateral bending moment and hence to apply pure torsion to the specimen.

Control of the machine was achieved with a 386 IBM compatible computer using custom-designed software which was also used to record and analyse the data. Care was taken not to apply a compression load and to ensure the specimen was in the neutral torsional position.

A torsion test was undertaken at a speed of 20°/minute. The bone was twisted in one direction until a displacement of 3° was achieved and the direction of the twisting was then reversed. The torsional displacement passed through the neutral position and the bone was then twisted to 3° of displacement in the opposite direction. Five such cycles of full torsion were applied. The torsional stiffness of the fractured and control tibiae was determined using the slope of the load displacement graphs between 1.5° and 2.5° of displacement in each direction and was recorded in Nm/deg. Where the torsion load on the distal tibia was from medial to lateral, it was recorded as external rotation (ER) whereas lateral to medial torsion was recorded as internal rotation (IR).

4.3.2.3 Four-Point Bending Tests

Following completion of the torsion tests, the specimens were removed from the aluminium cups. Special care was taken not to apply any extraneous loads to the bones. The four point bending rig was mounted in the Universal Testing Machine and both the control tibiae and fractured tibiae were tested. The four-point bending tests were undertaken in the identical manner to that outlined for the mechanical tests for symmetry in section 2.3.5. From these tests the ML and AP stiffness, ML fail load stiffness (FLS) and strength were determined. The testing sequence was ML Stiffness, AP stiffness and ML fail test. This was to ensure that if the healing fracture failed during the ML stiffness tests, the fail data could still be analysed for strength.

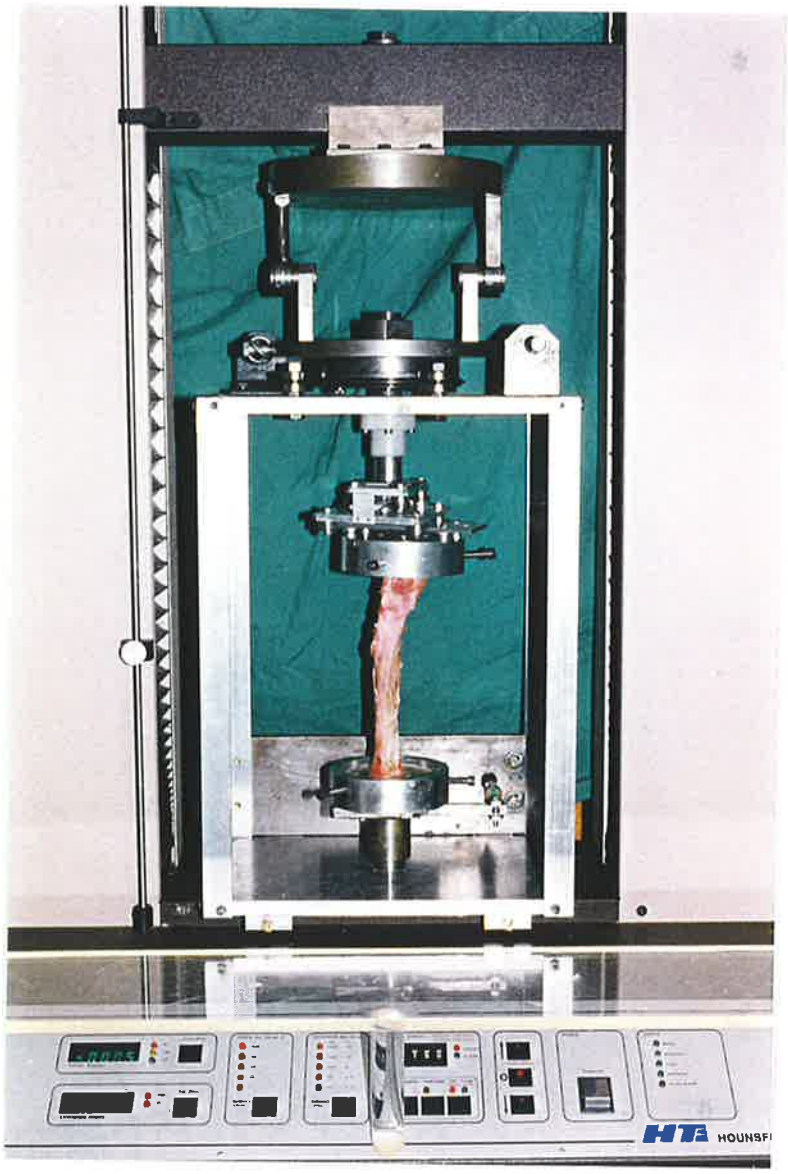

Figure 4.5 Setup for torsional test with the custom rig mounted in the Hounsfield H25KM Universal Testing Machine

4.4 RESULTS

The raw data from all the mechanical tests are tabulated in appendix D

4.4.1 Study Group-

Of the 40 sheep scheduled in this study, 15 were totally excluded from mechanical analysis (Table 4.1). Thirteen sheep (all eight of the 2 week group and five of the 4 week group) could not be tested due to fracturing of the callus at the healing osteotomy site. This occurred whilst the tibiae were being excised from the culled sheep and prior to any mechanical testing. The remaining two tibiae not tested were from the 6 week group. These were culled following falls that resulted in fractures through the distal pin sites of the external fixator.

Table 4.1 Study exclusions (n = 15)

SHEEP	*GROUP*	*REASON*
@04	2	refracture during excision of tibia from leg
@06	2	"
@14	2	"
@26	2	"
@31	2	"
@39	2	"
@42	2	"
@43	2	"
@05	4	"
@08	4	"
@27	4	"
@28	4	"
@30	4	"
@35	6	fracture through pin sites
@41	6	"

The remaining twenty-five sheep were all tested (Tab. 4-2). The ML stiffness data from sheep "@17" and the torsional stiffness data from sheep "@45" was lost due to corruption of the computer file during the saving routine. This was not seen as a reason to totally exclude these sheep from the study and the data from the remaining mechanical tests was included for analysis.

As part of an initial proposal of the study to include radiological assessment of the healing fracture, the sheep were anaesthetised every two weeks to obtain the radiographs. Two of the sheep assigned for the 10 week group ("@03" and "@13")

had been otherwise well but died unexpectedly on anaesthetic induction. Both of these deaths occurred at the 8 week stage and were the result of accidental intra-arterial injection of sodium pentothal. Because of the chance nature of the deaths and the absence of any obvious selection bias, they were added to the 8 week group and included in the study. As a result of these deaths and technical difficulties in obtaining the radiographs, this part of the study was then abandoned.

Table 4.2 Final study group (n = 25)

SHEEP	GROUP	COMMENT
@12	4	
@20	4	
@23	4	
@09	6	
@17	6	ML Stiffness (& Stiffness Ratio) data lost - file corruption
@21	6	
@22	6	
@38	6	
@40	6	
@03	8	accidental premature culling - originally in group 10
@11	8	
@13	8	accidental premature culling - originally in group 10
@15	8	
@16	8	
@19	8	
@24	8	
@25	8	
@36	8	
@44	8	
@07	10	
@18	10	
@29	10	
@32	10	
@33	10	
@45	10	IRC & ERC Stiffness (& Stiffness Ratios) data lost - file corruption

4.4.2 Control Tibiae

Only the right tibia of the remaining 25 sheep suitable for analysis (Table 4.2) were included. Torsional stiffness in IR and ER, low load bending stiffness in the AP and ML planes, ML fail stiffness and strength were all analysed. These have been labelled as IRC, ERC, APC, MLC, FLSC and STRC respectively (Appendix D).

Ultimate failure occurred between the inner two bending pins at the tibial mid diaphysis in all the tested control tibiae.

The mechanical properties of the control sheep in the allocated study time subgroups were compared (Appendix E). The properties within each subgroup were found to be both widely variable and normally distributed. An analysis of variance (ANOVA) failed to detect any significant difference between the study healing time subgroups for any of the mechanical properties tested (Table 4.3).

Table 4.3 Summary ANOVA p values between subgroups of control tibiae

Mechanical Properties	*P values (Alpha 0.05)*
IR Torsion	0.36
ER Torsion	0.51
AP Stiffness	0.97
ML Stiffness	0.72
ML Fail Stiffness	0.47
Strength	0.24

A summary of the control mechanical data is given in Table 4.4 and Student's t-test results are given in Table 4.5. The torsional stiffness in IR was found to be significantly greater than in ER (2.79 v 2.46 Nm/deg, p=0.0012); bending stiffness in the ML plane was found to be significantly greater than in the AP plane (9.95 v 9.03 Nm/mm, p=0.0054); and ML stiffness to failure was found to be considerably greater than ML stiffness at the lower loads to 150N (9.95 v 14.07 Nm/mm, p=1.5E-09).

Table 4.4 Control group mean values

Mechanical Variable	*Mean*	*SD*
IR Torsion (Nm/deg)	2.79	0.90
ER Torsion (Nm/deg)	2.46	0.63
AP Stiffness (Nm/mm)	9.03	1.59
ML Stiffness (Nm/mm)	9.95	1.46
ML Fail Stiffness (Nm/mm)	14.07	2.57
STR (Nm)	99.70	16.92

Table 4.5 Student's t tests show significant differences between tested means

Variables	*P(T<=t) two-tail*
IR vs ER Stiffness	0.0012
ML vs AP Stiffness	0.0054
ML vs ML Fail Stiffness	1.5E-09

In examining the relationship between ER and IR, a strong coefficient of correlation (r=0.90) was found (Figure 4.6). The correlations between ML and AP stiffness (r=0.46) and ML and ML fail stiffness (r=0.54) were low (Figures 4.7 & 4.8).

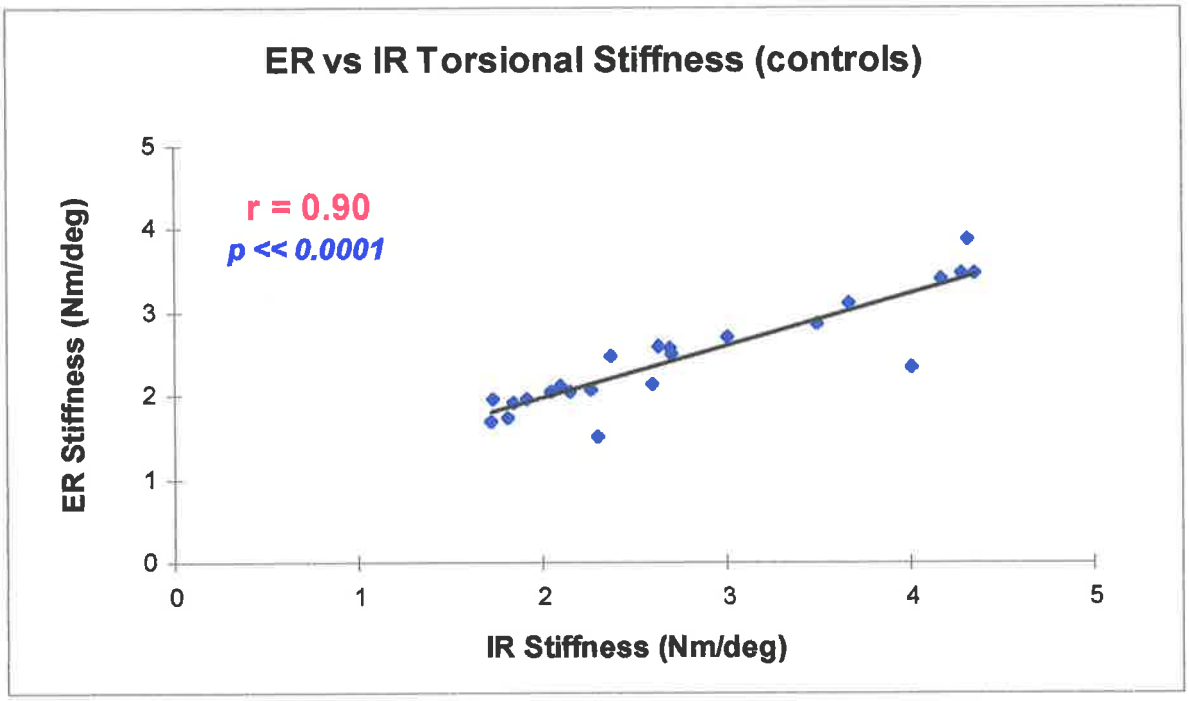

Figure 4.6 Correlation between ER and IR torsional stiffness in control tibiae

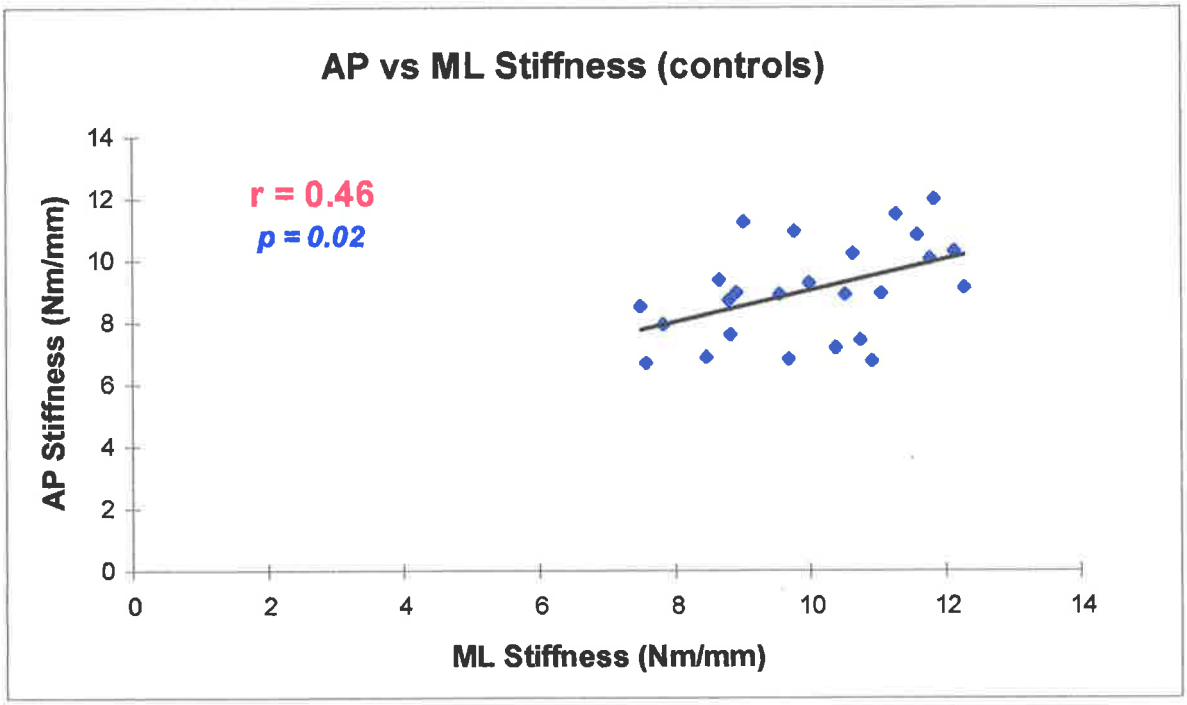

Figure 4.7 Correlation between AP and ML stiffness in control tibiae

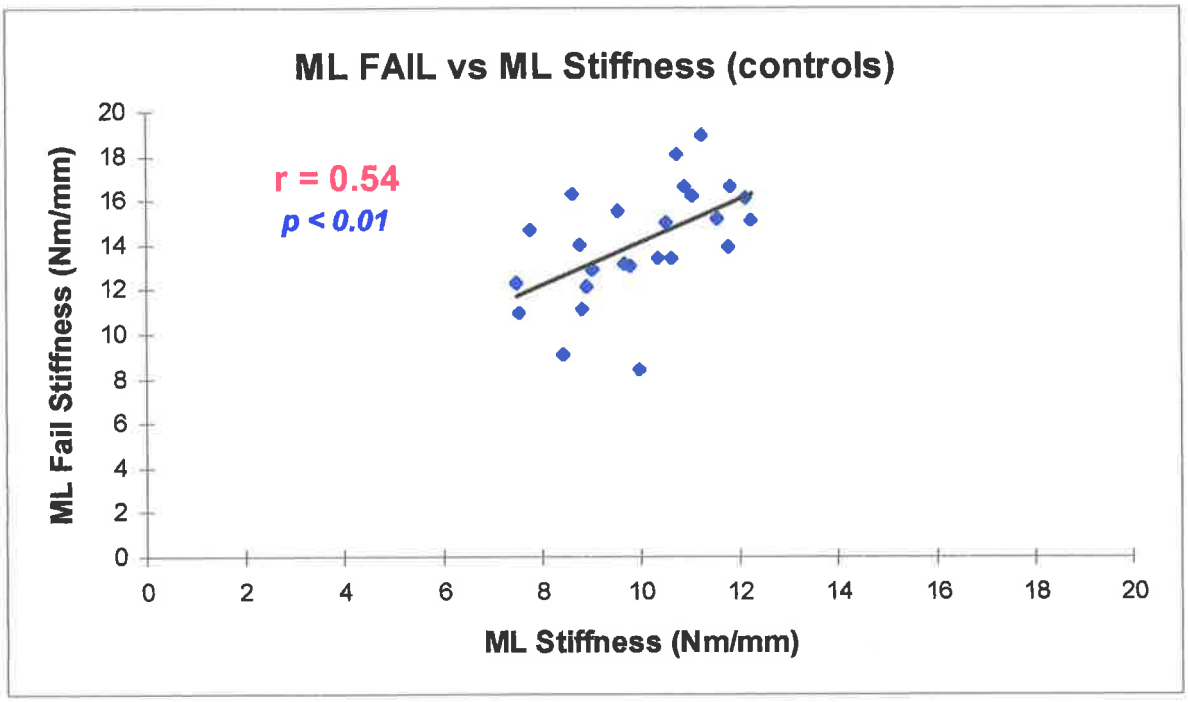

Figure 4.8 Correlation between ML fail and ML stiffness in control tibiae

As the strength value obtained in this study was from the four-point bending tests to failure in the ML plane, only the ML stiffness tests were correlated with strength. In these control tibiae, the correlation of strength with ML stiffness (r=0.39) was shown to be much less than the correlation with ML fail stiffness (r = 0.71, Figures 4.9 & 4.10).

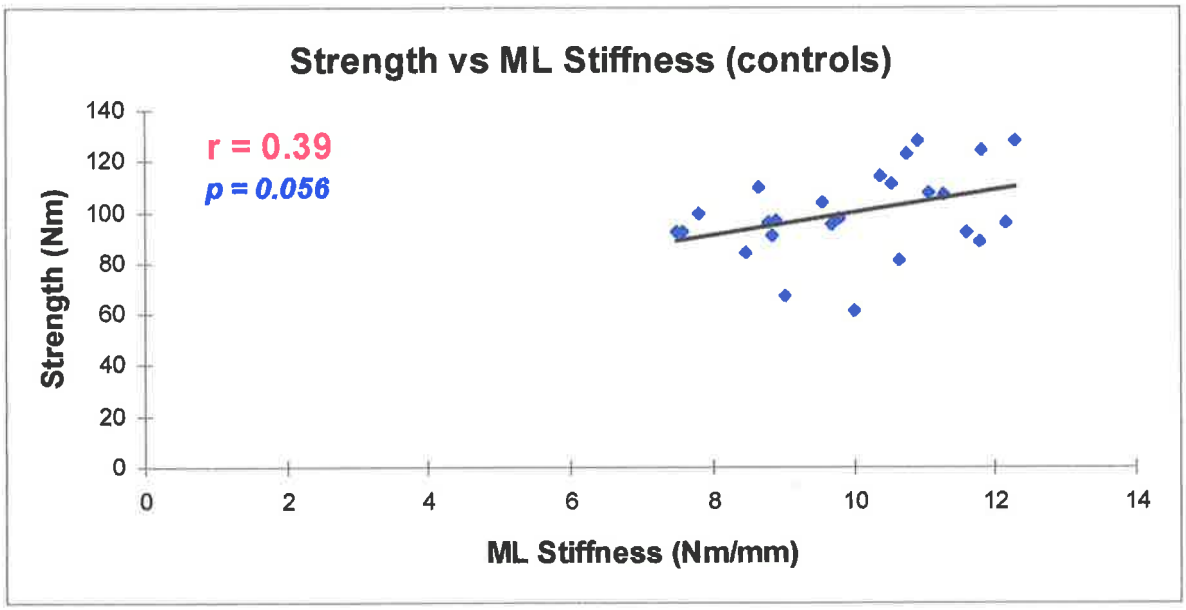

Figure 4.9 Correlation between strength and ML stiffness in controls

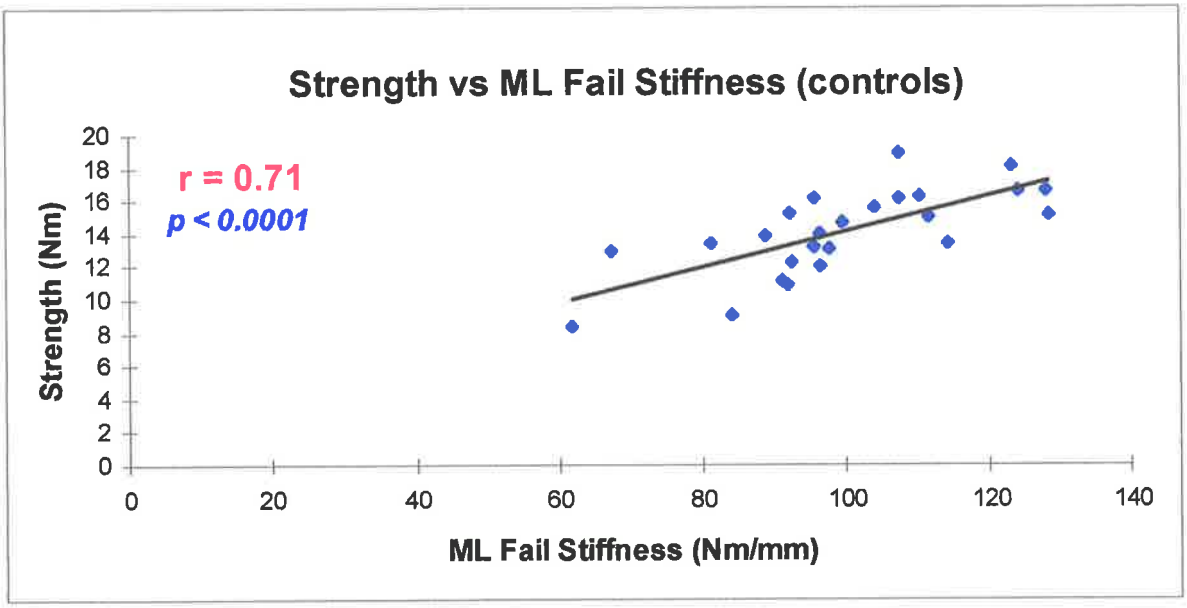

Figure 4.10 Correlation between strength and ML fail stiffness in controls

4.4.3 Fracture Model

Because of the large variability in the mechanical properties of the sheep in this study, stiffness and strength have been normalised with respect to the control tibiae and the results presented in terms of stiffness and strength "healing ratios".

In all cases, testing to failure in the osteotomised tibiae resulted in refracture through the osteotomy site.

4.4.4 Time Related Mechanical Changes

Changes in fracture stiffness and strength healing ratios, as a function of healing time, are shown in Figures 4.11 to 4.16 and are summarised in Figure 4.17. For each of the mechanical properties examined, wide variations were found within the healing time subgroups. Over the 10 week duration of this study, the return towards normal stiffness occurred much more quickly than the return towards normal strength: the mean ML stiffness ratio approached unity (0.95) at the 8 week stage compared to a strength ratio of 0.36 for the same healing time (Figure 4.17). Similarly, the stiffness measured at low loads in the ML plane was quicker to return to normal than the stiffness measured at the higher loads to failure: the ML stiffness ratio was 0.95 at 8 weeks compared to 0.78 at same time for the ML fail stiffness (Figure 4.17). In the ten week period of this study, five sheep achieved stiffness values exceeding that of the unfractured control tibia when measured with low

loads whereas none of the osteotomised tibiae had attained the stiffness of the control leg when measured at loads to failure.

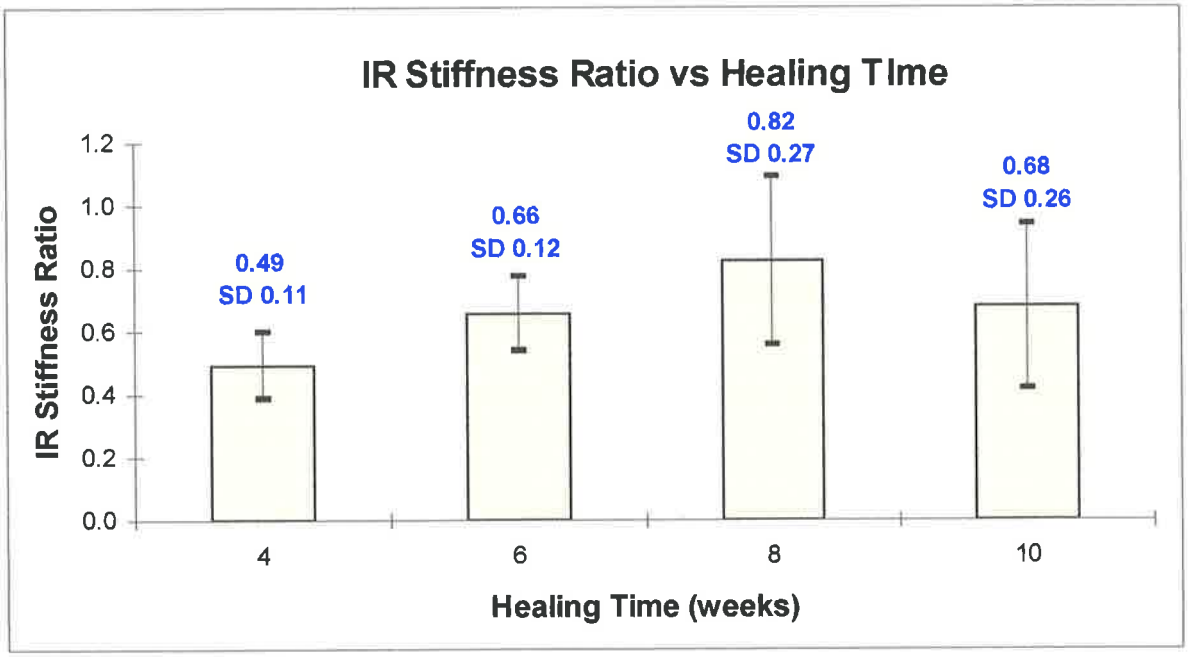

Figure 4.11 Changes in mean IR torsional stiffness during fracture healing

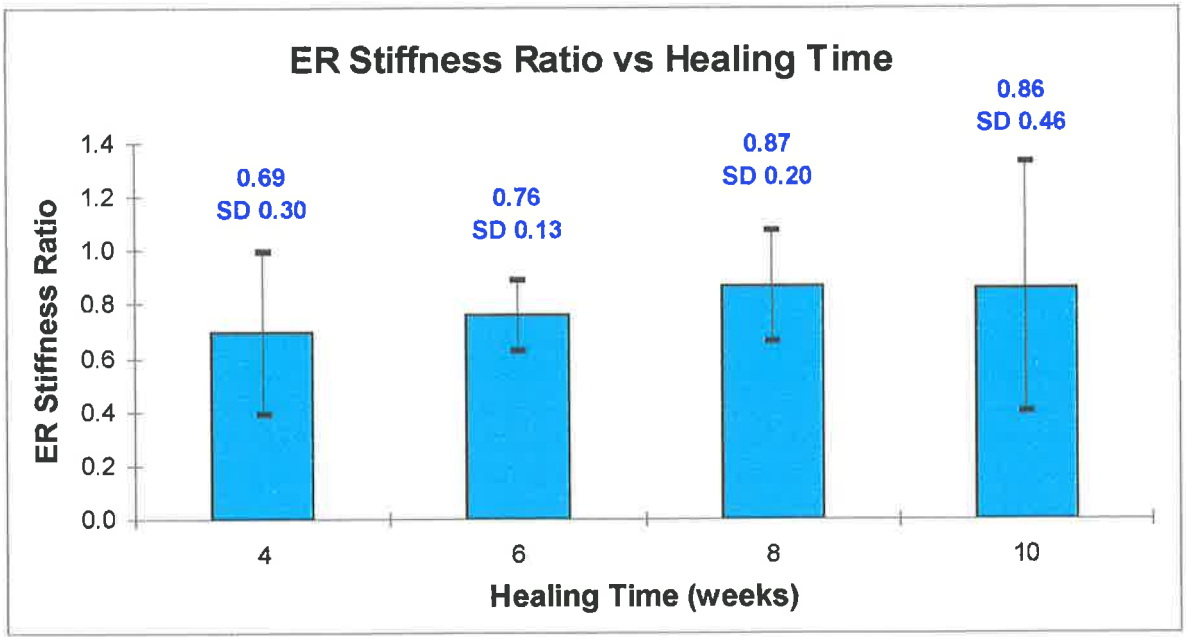

Figure 4.12 Changes in mean ER torsional stiffness during fracture healing

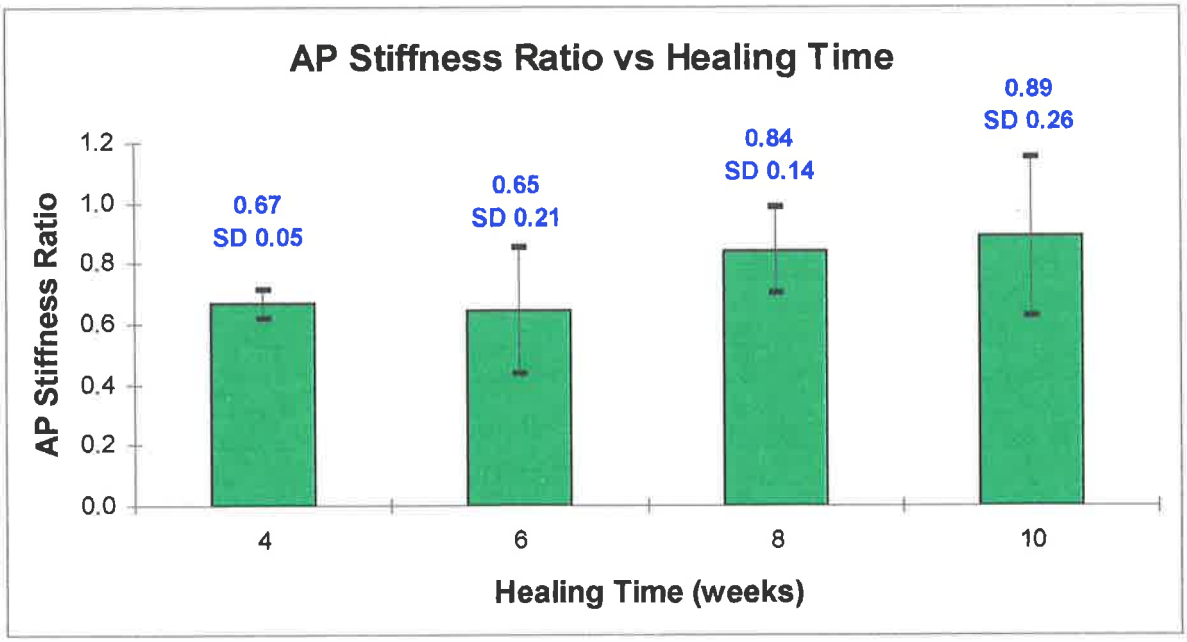

Figure 4.13 Changes in mean AP stiffness during fracture healing

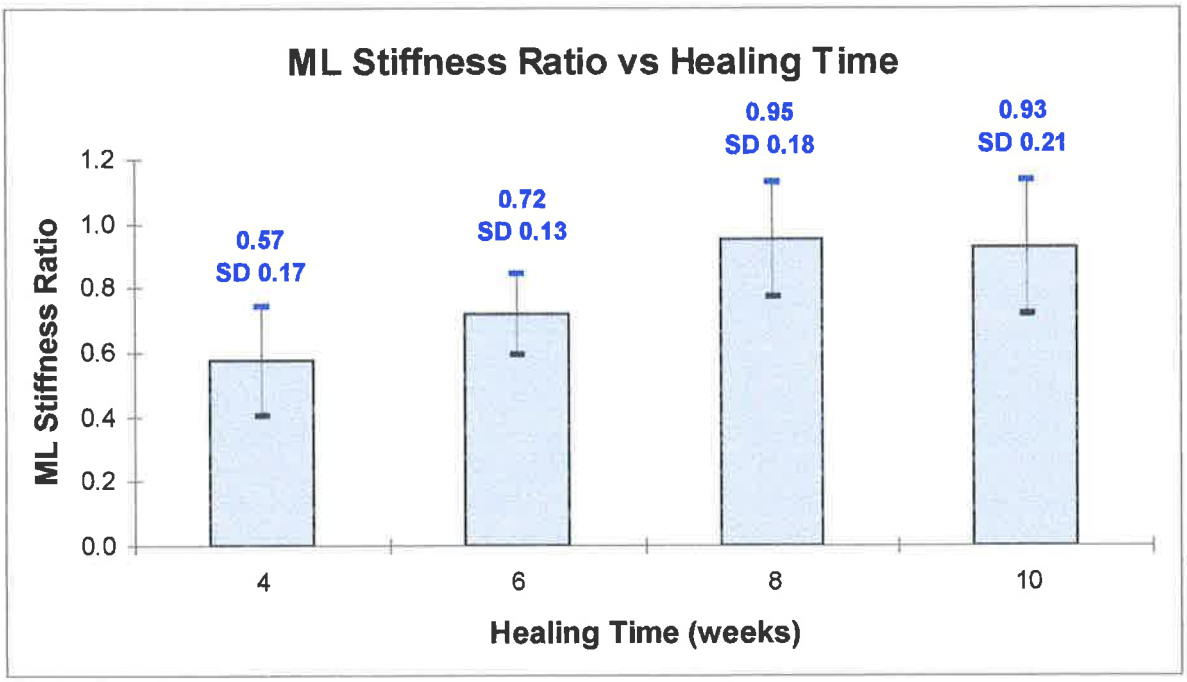

Figure 4.14 Changes in mean ML stiffness during fracture healing

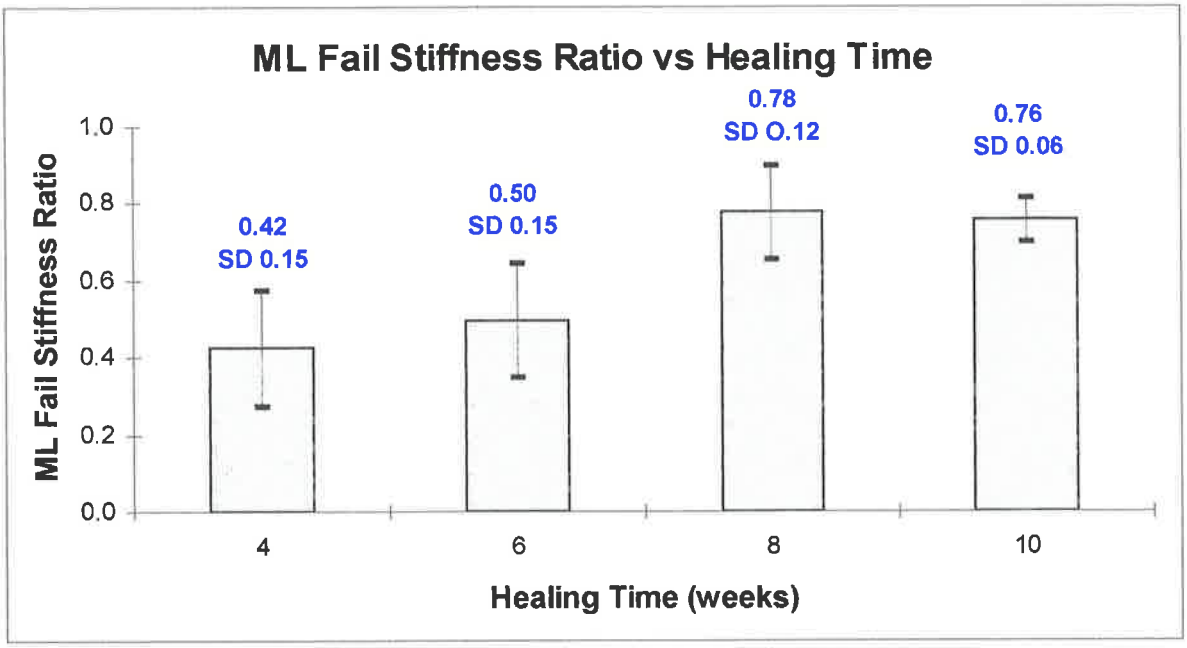

Figure 4.15 Changes in mean ML fail stiffness during fracture healing

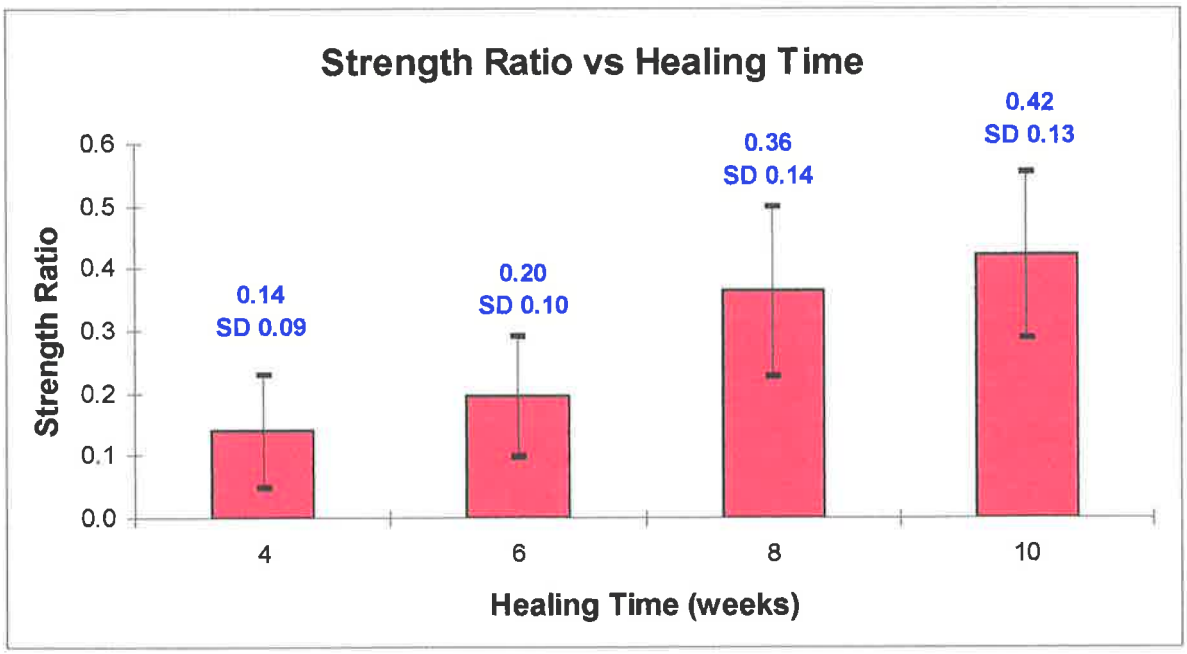

Figure 4.16 Changes in mean strength during fracture healing

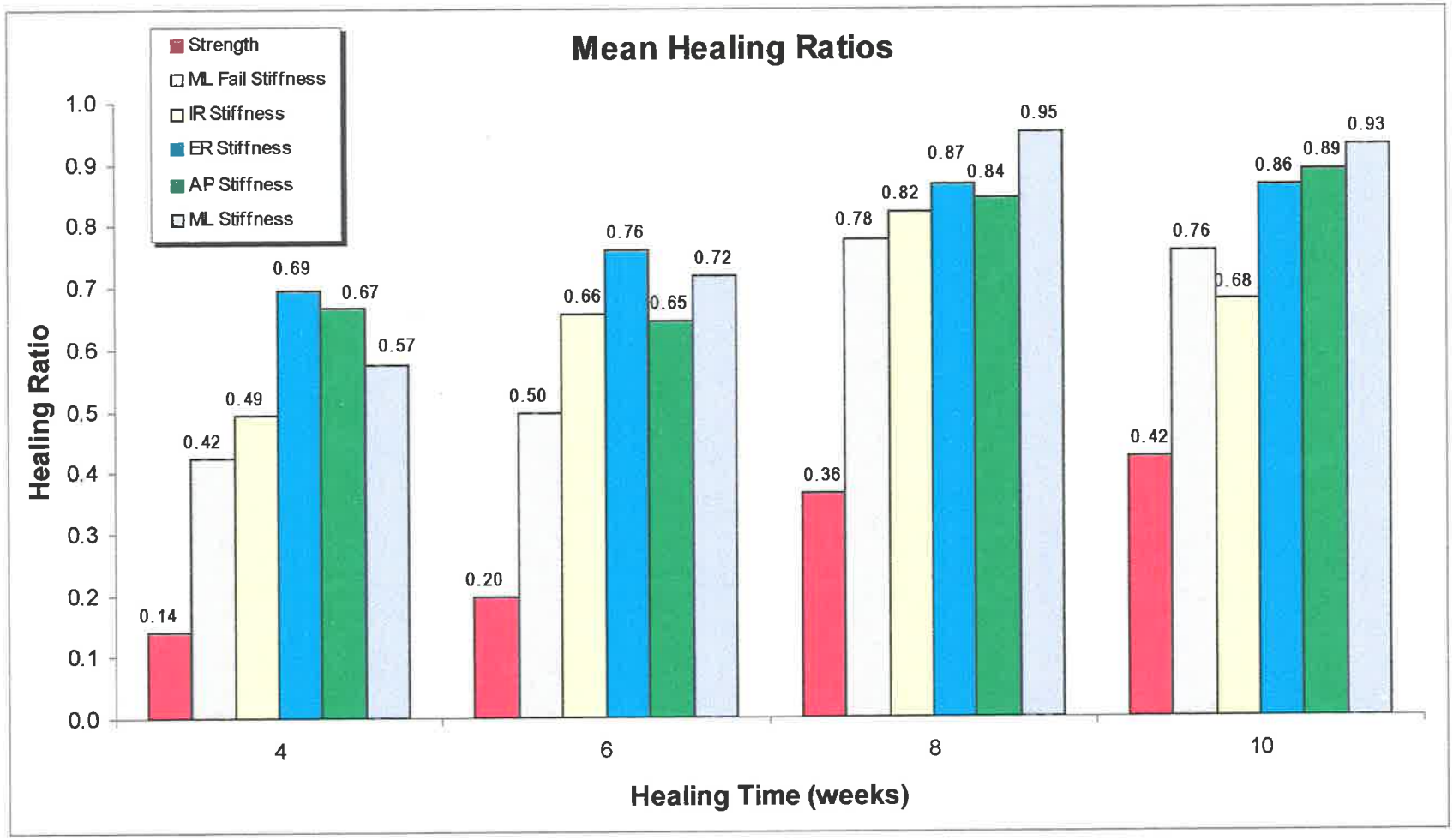

Figure 4.17 Combined mean healing ratios

An analysis of variance showed that between weeks 4 and 10 the only significant differences in the mechanical properties of the healing bone occurred in the ML fail stiffness ratio and in the strength ratio (Table 4.6). Further analysis of the time subgroups using t-tests showed that, over a two week interval, the only significant difference occurred between weeks 6 and 8 (Table 4.7).

Table 4.6 ANOVA of mechanical properties as a function of healing time

Mechanical Property	*p value*
IR Stiffness Ratio	0.16
ER Stiffness Ratio	0.73
AP Stiffness Ratio	0.09
ML Stiffness Ratio	0.94
ML Fail Stiffness Ratio	9.E-05
Strength Ratio	0.0045

Table 4.7 Student's t-tests using pooled variance data from ANOVA tests

Groups	*Interval (weeks)*	*ML Fail Stiffness Ratio*	*Strength Ratio*
4-6	2	0.51	0.44
6-8	2	0.001	0.02
8-10	2	0.72	0.42
4-8	4	0.0014	0.02
6-10	4	0.003	0.01
4-10	6	0.002	0.01

4.4.5 Stiffness v Strength

The correlation between stiffness and strength was considerably stronger when the stiffness was measured at the fail load than at the lower loads ($r = 0.80$ v 0.58, Figures 4.18 & 4.19).

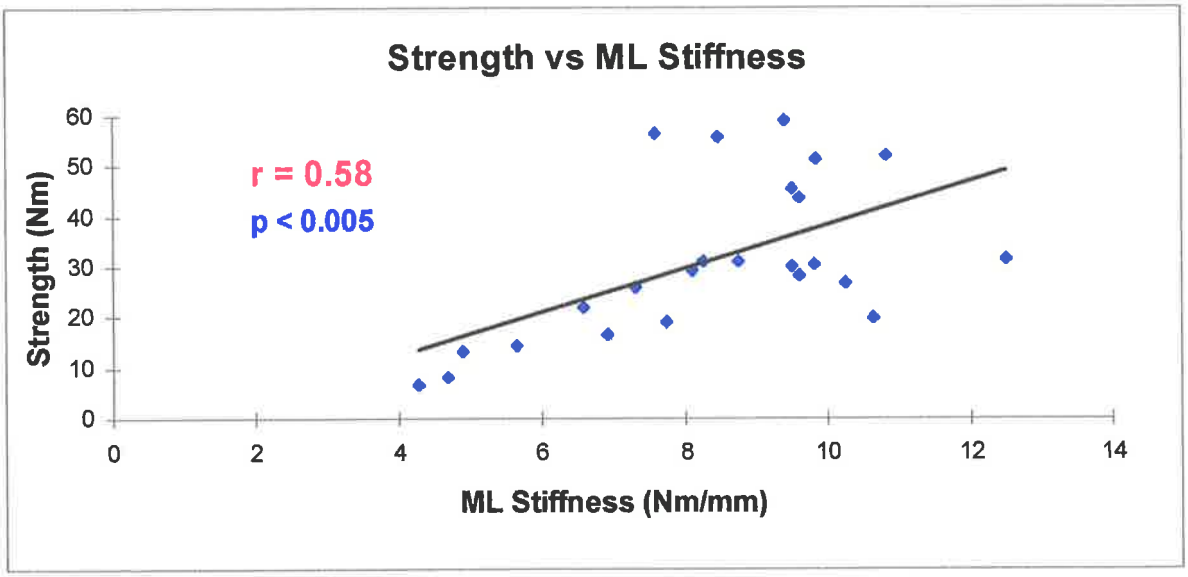

Figure 4.18 Correlation between strength and stiffness at low loads

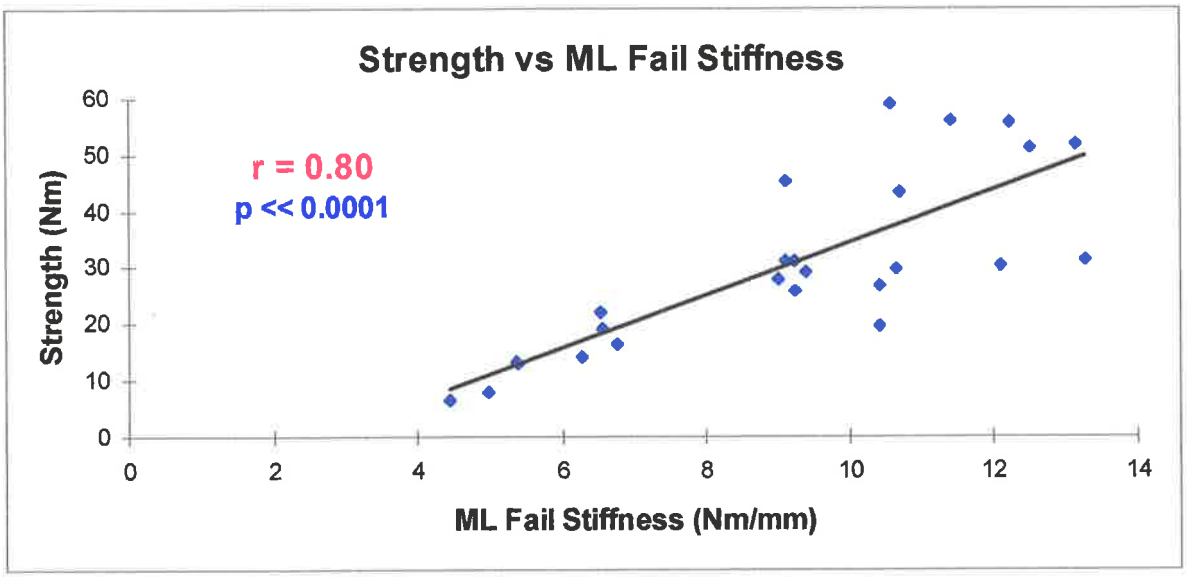

Figure 4.19 Correlation between strength and stiffness at fail loads

Further examination of the relationship between stiffness and strength suggested two separate healing phases (Figures 14.20 &14.21). For both stiffness measured at low loads (ML Stiffness) and stiffness measured at high loads (ML fail stiffness), the correlation with strength was found to be strong at the lower stiffness values below 7 Nm/mm (r = 0.89 and 0.90 respectively). For the higher stiffness values the relationship broke down, particularly with low-load stiffness, and no significant correlation was found (r = 0.00, p=0.99 and 0.44, p=0.074 respectively).

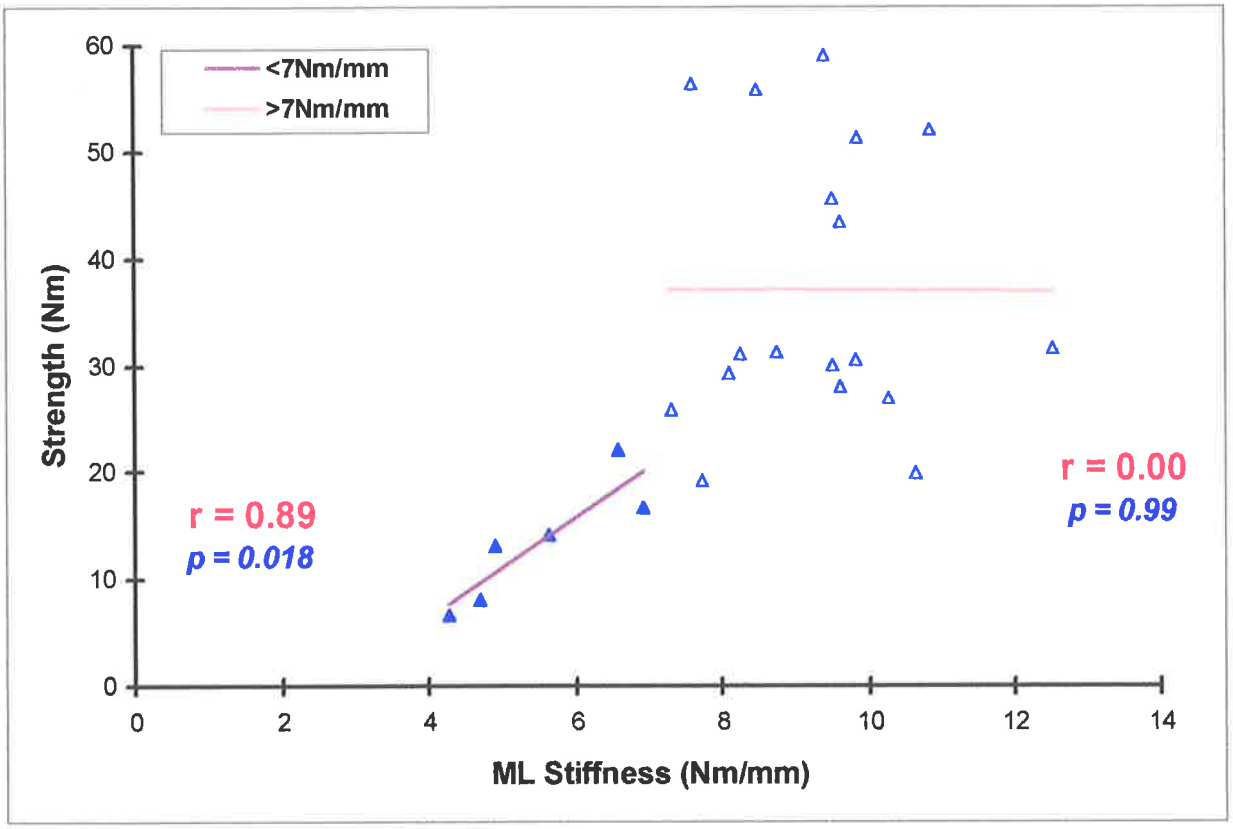

Figure 4.20 Breakdown of data into early and late stiffness phases showing isolated linear correlations with strength for low load ML stiffness

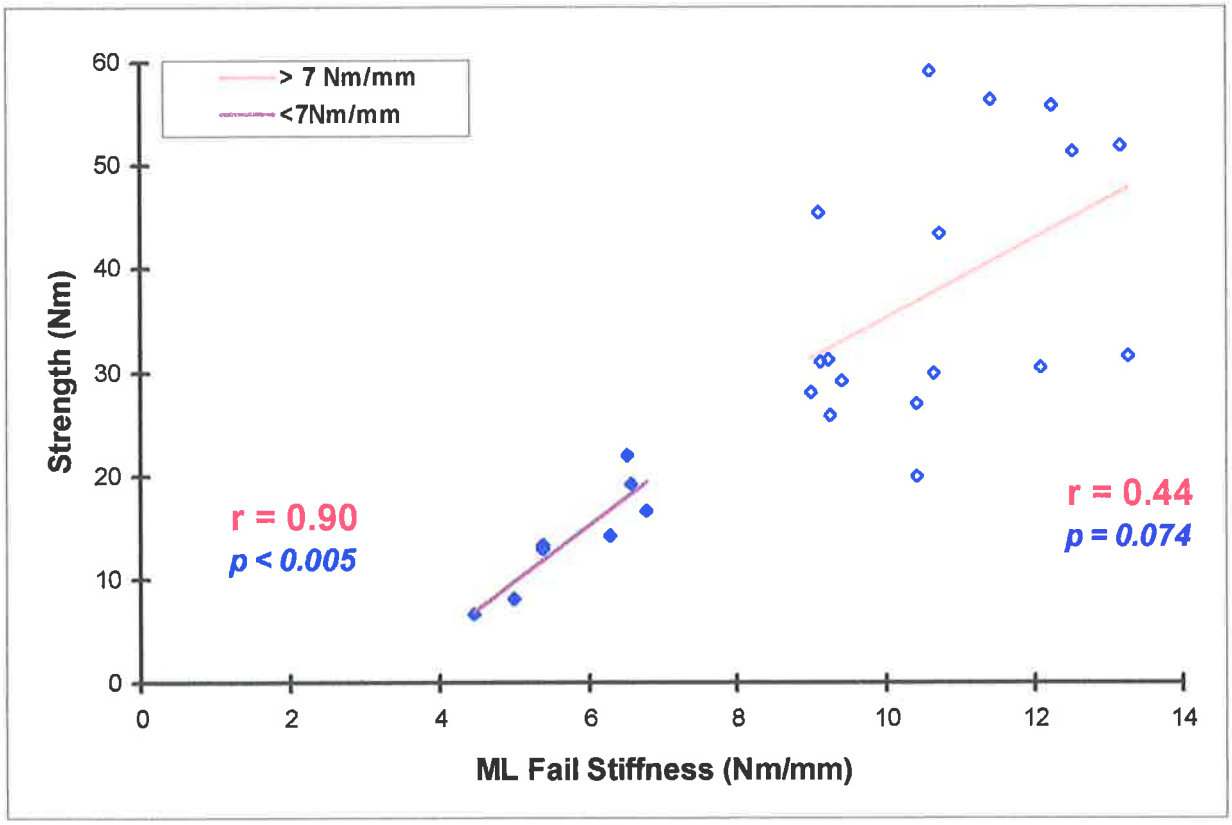

Figure 4.21 Breakdown of data into early and late stiffness phases showing isolated linear correlations with strength for the high load ML fail stiffness

To obtain a greater clinical perspective, the stiffness and strength *healing ratios* were also correlated (Figures 4.22 & 4.23). Differences in the correlations between relative strength and stiffness were again found depending on the loading conditions used to determine stiffness. Healing which achieved the presumed prefracture stiffness under low-loading conditions indicated a relative strength of as little as 0.24 (Figure 4.22). Under loads to failure, no specimen actually reached the stiffness of the control side although one achieved a relative stiffness value of 0.99. The relative strength at this point, however, was higher at O.33 (Figure 4.23). Under both low- and high-loading conditions a wide range in relative strength values was found, with values as high as 0.62 obtained for relative stiffness values still considerably less than one.

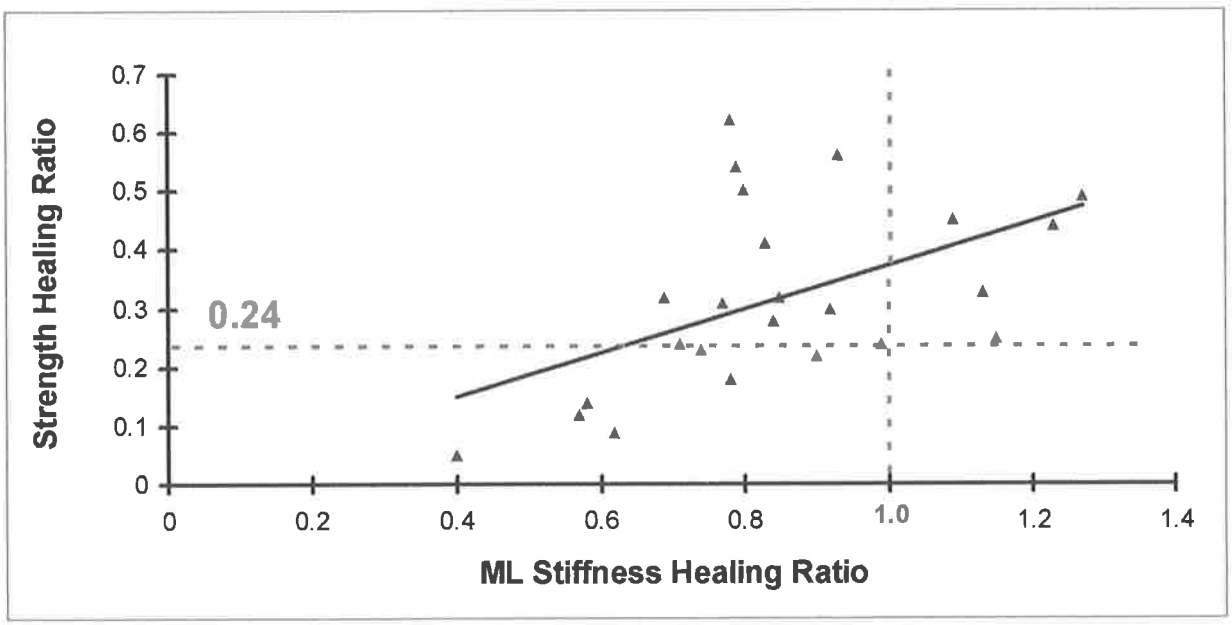

Figure 4.22 Correlation of healing ratios of the low-load ML stiffness and strength showing the 'baseline' relative strength value for a return to prefracture stiffness

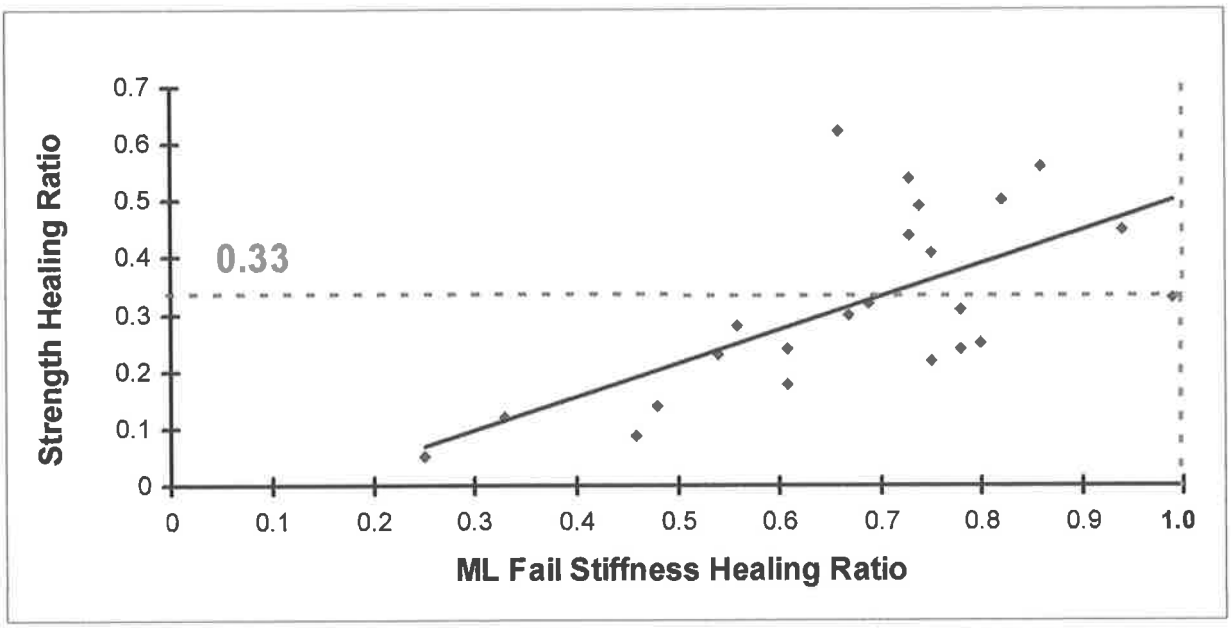

Figure 4.23 Correlation of healing ratios of ML fail stiffness and strength showing the 'baseline' relative strength value for a return to prefracture stiffness

4.5 DISCUSSION

4.5.1 Control Tibiae

There are several points to be noted from the analysis of the mechanical properties of the normal sheep tibiae. The difference measured between the torsional stiffness in IR and ER is not surprising given the non-symmetrical geometry of the tibial shaft. To my knowledge, however, none of the published literature utilising torsional data define the torsional direction that was used. This is obviously a potential source of error if not recognised during testing. The strong correlation between ER and IR, however, infers that correlations with either direction would be possible so long as the chosen direction was consistent throughout testing.

The higher bending stiffness measured in the ML plane compared with the AP plane is in keeping with previously published literature (Cornelissen et al 1988). An interesting finding was the large difference between ML stiffness and ML fail stiffness. This indicates that the ability of the bone to resist a deforming load increases with increasing load. This non-linear behaviour may be in part due to

viscoelastic properties of the bone and/or due to a structural change resulting from the deformation itself.

The low correlations between ML stiffness and AP stiffness and between ML stiffness and ML fail stiffness was an interesting finding. If the stiffness data at low loads was reliably representative of the overall bone stiffness properties, then this would be a very surprising finding, particularly in the case of ML stiffness versus ML fail stiffness. One would expect the difference between these two values to be quantitative only. The poor correlation, however, may merely be a reflection of the large variability in stiffness properties to even small differences in loading conditions when low loads are used. In other words, the non-linear behaviour of bone stiffness may be more pronounced at low loads. The much better correlation of strength with ML fail stiffness in this group of control tibiae (compared to the low-load ML stiffness) adds further support to this explanation. Thus, in comparing the stiffness of one bone with that of another, having comparable loading conditions may be critical but may be difficult to achieve under low-loading conditions. This is an important point because clinical stiffness monitoring techniques are usually performed under low- or non-loading conditions.

The variability in the mechanical properties of the control tibiae between sheep was marked, given the selection criteria for the sheep in the study. There were, however, no significant differences in the properties of sheep allocated to the different study time subgroups. This implies that the randomisation of the sheep into the allocated groups was successful.

4.5.2 Fractured Tibiae

4.5.2.1 Selection Bias

The results of all tested sheep have been presented. It should, however, be noted that the only tibiae tested from the 4 week group are the three (out of the original eight) which had regained sufficient strength to avoid refracture whilst being excised from the culled sheep. This indicates a selection bias in favour of the quicker healing tibiae and an artificial elevation of the mean values in the 4 week subgroups. No such selection bias is likely to exist in the 6, 8 or 10 week subgroups as the reasons for exclusion (accidental fracture remote to the osteotomy;

anaesthetic complications; and computer storage failure) are unlikely to be related to the mechanical properties of the healing tibial osteotomy.

4.5.2.2 Time-related changes

The marked variations in stiffness and strength of healing tibiae at each of the sampled healing times are important. They indicate that clinically applicable 'normal' time limits for fracture healing in terms or either stiffness or strength cannot be defined. This variability occurred despite the use of a standard fracture model in respect to population, mechanism of fracture, and of fixation. This emphasises the poor predictive value of the passage of time as an indicator of fracture healing.

Because of the marked variability in the degree of mechanical healing at any point in time, the only measurably significant change over a two week period was between weeks 6 and 8. Significant differences may have been found between weeks 4 and 6 if not for the selection bias in group 4, (as discussed in section 4.5.2.1), but were not demonstrated in these results. The addition of many more samples within each group may have resulted in statistically significant differences between the time subgroups but the marked overlap in values would severely restrict the sensitivity of mechanical monitoring in determining "normal" healing for a given time frame. The findings in this study of wide variability of both stiffness and strength during healing are therefore in keeping with the findings of Henry (1968). Whether there is a reduction in this variability with increasing time (and at what stage), cannot be answered from this study. Thus for the assessment of fracture healing by mechanical monitoring in the early stages of union, isolated measurements are insufficient; sequential monitoring is required to show progression towards a defined endpoint.

The pattern of fracture healing in this sheep model is for early return to prefracture stiffness values under low-loading conditions. These loads may be similar to those imposed on the tibia during the usual daily activities of the sheep. Strength is the slowest mechanical property to be restored in this model and is still much less than normal at the time of clinical healing. This is likely to be a reflection of the amount of strength reserve in the normal tibia.

Even though the absolute values of ML fail stiffness are greater than those of ML stiffness in the healing tibia, the healing *ratios* are less. This indicates that the non-linear behaviour of the bone to load is not fully restored until the later stages of fracture healing. Clinically, this means that 'high-load' stiffness is a more sensitive indicator of fracture healing.

4.5.2.3 Stiffness v Strength

In this group of fractured tibiae, the stronger correlation found between strength and ML fail stiffness (compared to the correlation with ML stiffness measured at the lower loads) was consistent with the findings in the control tibiae. Unlike the uniform correlation found in the control group, however, the relationship in the fractured group varied depending on the stage of healing. This 'biphasic' correlation found between stiffness and strength may represent two histo-mechanical phases of fracture healing. In the early stages both stiffness and strength result from the same healing process which is the formation of early woven bone callus with relatively uniform mechanical properties throughout. After this phase, the organisation and remodelling of callus with an increasing amount of lamellar bone may increase fracture strength with little or no effect on fracture stiffness. The large individual variation in bone composition in this phase may explain the latter part of the correlation.

From the data on healing ratios, it appears that the second phase may start when stiffness has reached approximately 65% of normal. Thus, stiffness increases can potentially monitor changes in fracture strength until stiffness reaches about two-thirds of normal. After this, stiffness can determine only a 'baseline' of fracture strength. Stiffness monitoring could only be used to determine an endpoint to fracture healing if the baseline were to indicate a strength that was sufficient for 'clinical healing'. Stiffness determinations under heavier loads reflect strength properties more accurately and have the advantage of indicating a higher baseline. Even if a baseline for clinical fracture healing could be assumed, there would be insufficient specificity from determinations of stiffness to indicate which bone had attained the greater strength characteristics required for an early return to strenuous labour or high-demand sport. Thus techniques of fracture assessment which rely on

stiffness monitoring alone are inherently limited. Richardson et al (1994) have provided clinical evidence that stiffness determinations alone can predict a safe return to independent weight bearing. They reported no refractures in 95 patients with tibial fractures when the decision to remove external fixation was made solely on the basis of a stiffness endpoint of 15 Nm/deg. None of these patients, however, was allowed to return to sports such as football for six months.

It is interesting to note that Richardson et al (1987) considered the stiffness of the normal unfractured tibiae to be 55-60 Nm/deg. This narrow range of values in the intact group contrasts with the large variation found in this sheep study. In addition, 15 Nm/degree corresponds to a 25% return of original stiffness. In this study, the weakest of the healing tibiae to have survived the careful excision from the culled sheep was that from sheep "@12". The fracture in this tibia was 4 weeks old and had regained 25 and 40 percent of its original bending stiffness in the ML plane at fail and low loads respectively. The strength regained was only 5 percent : one twentieth of the original strength! Thus, from these results, a 25% regaining of stiffness (as measured at *low loads)* was well short of being clinically healed. Although these discrepancies may be due to differences between the human and sheep models, it is also possible that they are due to fundamental differences in the measuring technique. Like Henry et al (1968), this study has used four-point bending tests which measure bending stiffness. Using the technique outlined by Richardson et al (1987), the bending at the fracture site in response to the distal load is as in a cantilever beam. This involves a combination of *both bending and shear*. Thus the discrepancies in the results may be explained by differences in regaining the ability to resist bending forces as compared to the ability to resist shearing forces. Resistance to shear might therefore show much less variability between different individuals both in the normal unfractured tibiae, and at comparable stages in normally healing fractured bones. Further studies aimed at determining the role of resistance to shear are therefore warranted.

The poor correlation shown between stiffness and strength may explain some cases of refractures in clinical practice. When there is clinical healing, patients with tibial fractures are pain-free and report a sense of 'stability' on full weight-bearing. Despite this, some will have refractures as the result of loads that would appear to

be trivial. It seems possible that the proprioceptive signals for fracture stability are related to stiffness. If this is so then the refractures may be in bones which have not achieved adequate strength in spite of 'normal' stiffness. This also implies that clinical healing occurs during the second phase of the stiffness-strength relationship, when there is marked variability in fracture strength for a given stiffness. This clinical experience of refracture may be an example of the shortcomings of stiffness monitoring for fracture healing in nature. A more sensitive clinical test for fracture strength may therefore be the patients' 'stability sensation' to controlled higher loads which are still short of failure.

Despite the limitations shown, stiffness monitoring remains of value in the early assessment of fracture healing. It can demonstrate progress towards union and thus identify potential delay or failure of union at an early stage. When clinical healing is suspected, stiffness measurements must take the loading conditions into account. This is not a problem in the early stages of healing when there is a good correlation between stiffness and strength which appears to be independent of the loading conditions.

The assessment of fracture healing by monitoring stiffness is inherently limited but a baseline for fracture healing may be predicted from the inter-relationship between stiffness, strength and minimum functional requirements.

CHAPTER FIVE

BONE RESONANCE ANALYSIS

5.1 INTRODUCTION

In chapter three, a reproducible in-vivo technique of BRA on sheep tibiae was presented. In chapter four, a sheep fracture healing model was described and the mechanical properties of the healing fractures were examined. In this chapter the in-vivo resonant frequency data from the healing fracture were examined and correlated with the mechanical properties determined in the previous chapter. The resonant frequency data were analysed both as a frequency index (FI) and as a stiffness index (SI). FI was calculated by dividing the resonant frequency of the fractured tibia by the resonant frequency of the same tibia which was measured immediately prior to fracture (control frequency):

$$FI = \frac{f_{fracture}}{f_{control}}$$

SI was calculated by squaring FI:

$$SI = FI^2$$

The rationale for squaring the frequency ratio to obtain a ratio to represent stiffness came from the Euler-Bernouilli beam theory model. In this model the bending stiffness of a uniform beam, EI, is proportional to the square of the resonant frequency (see section 1.5.3.2):

$$f^2 \propto EI$$

By comparing the correlations of these two indices with the mechanical properties of the healing fractures an assessment of the validity of this relationship was made.

5.2 AIMS

The aims of this study were:

1. To examine time-related in-vivo resonant frequency changes during fracture healing;
2. To determine to what extent these resonant frequency changes represent changes in the mechanical properties of the healing bone.

5.3 METHODS

In this study, in-vivo BRA was performed to determined the resonant frequency of the sheep tibiae both prior to fracture and immediately prior to culling. The ovine fracture model using an osteotomy to the midshaft of the left tibia was described in the previous chapter.

The sheep were anaesthetised and positioned for BRA testing as described in sections 3.3.2 and 3.3.3. Under anaesthesia and prior to insertion of the external fixator, the resonant frequency of the unfractured left tibiae were determined using the BRA technique described in sections 3.3.4 and 3.3.5. Four scans were taken and the average resonant frequency of these four scans was used as the control resonant frequency.

At the designated culling time (2, 4, 6, 8 or 10 weeks) the sheep were again anaesthetised and the external fixator was carefully removed from the healing fractured tibia. The resonant frequency of each of these fractured tibiae were then determined from the average of four scans and labelled as the fracture resonant frequency. This was then divided by the control resonant frequency to give the frequency index.

After BRA testing, the sheep were culled with phenobarbitone and the tibiae were excised and prepared for mechanical and histomorphometric testing (as detailed in chapters four and six).

The resonant frequency indices (FI and SI) were analysed as a function of healing time and then correlated with the mechanical properties of the healing fracture. Linear correlation analysis was performed on the data throughout the study as examination of power analyses failed to show any better modelling of the results.

5.4 RESULTS

The FI and SI values for each sheep are tabulated in Appendix F.

5.4.1 Study Exclusions

Six of the forty sheep were excluded from the study correlating BRA with time (Table 5.1). In three of the sheep from the 2 week group and one sheep from the 4 week group, it was not possible to determine a resonant frequency from the scan of the fractured tibia. The remaining two sheep could not be tested as their tibiae fractured through the external fixator pins prior to the scheduled culling.

Table 5.1 BRA exclusions

SHEEP	*GROUP*	*REASON*
@04	2	Unable to determine resonant frequency
@06	2	"
@26	2	"
@27	4	"
@35	6	Fracture through external fixator pin sites
@41	6	"

A total of fifteen sheep could not be included in the correlation of BRA with the mechanical properties of the healing fracture for the reasons outlined in chapter four (section 4.4.1).

5.4.2 BRA v Time

Both the FI and SI were examined as a function of healing time. The mean SI and FI values at each of the healing times were plotted with the standard deviations (Figures 5.1 & 5.2). After an initial rapid increase in the first 4 weeks, the BRA indices were found to peak at 8 weeks and then to plateau. After the fourth week considerable overlap was found between the individual time groups in both FI and SI.

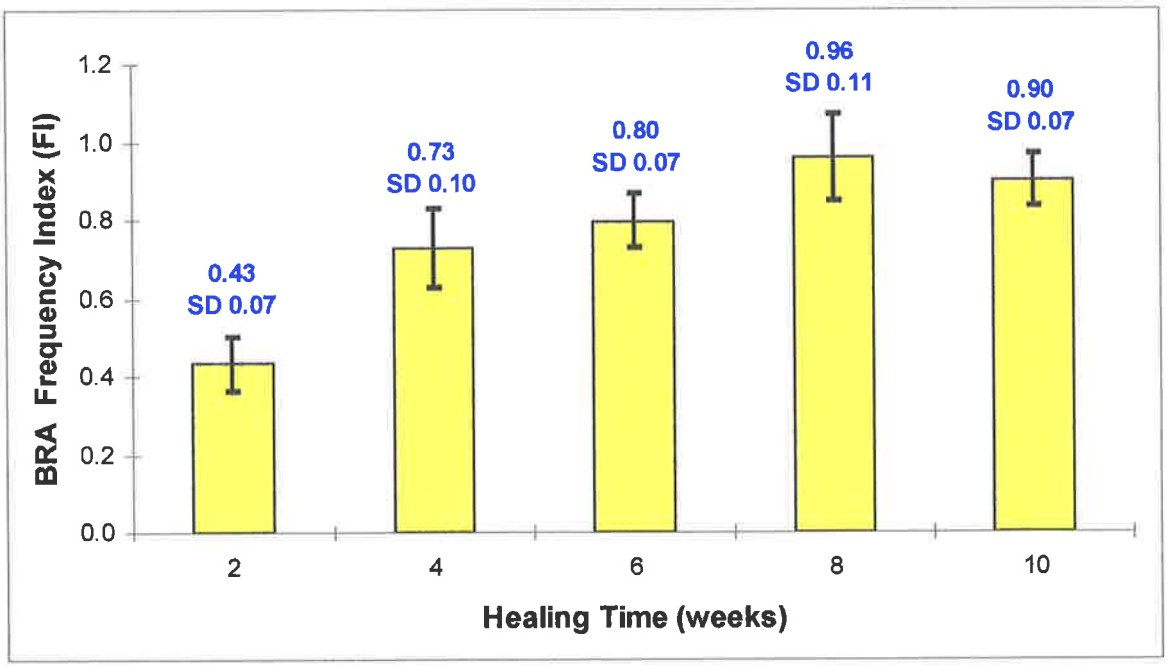

Figure 5.1 Changes in mean FI during fracture healing

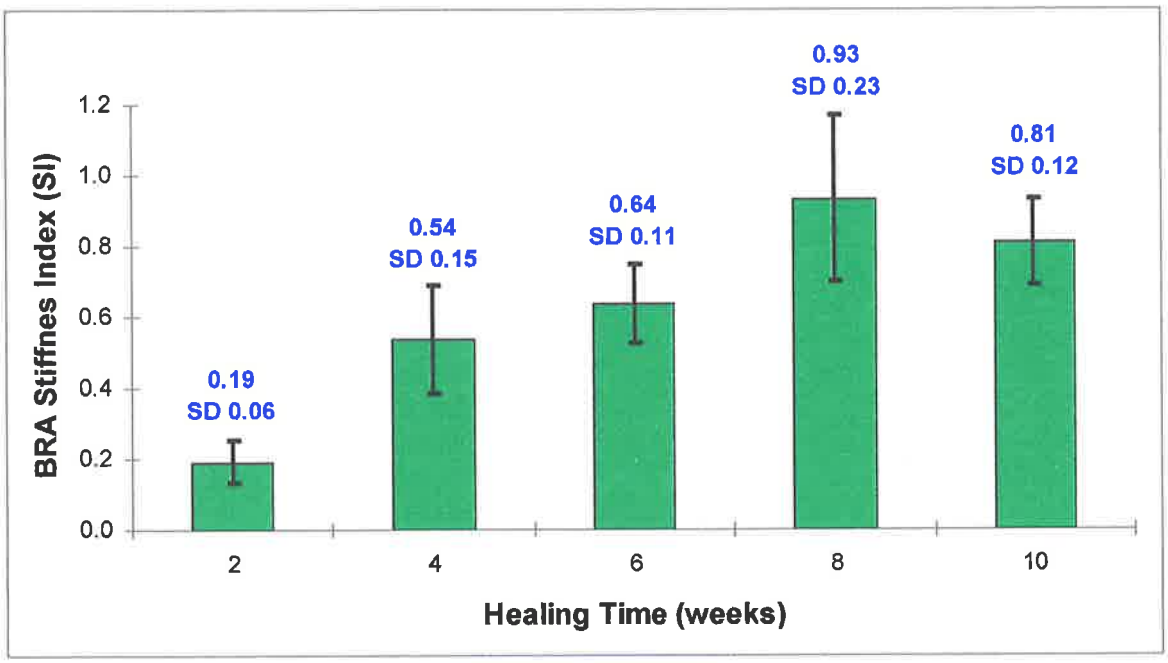

Figure 5.2 Changes in mean SI during fracture healing

An analysis of variance showed that there were significant differences between the healing time groups for both FI ($p = 4.8E-10$) and SI ($p = 7.9E-8$). There was a decrease in the mean FI and SI between weeks 8 and 10 (0.96 decreasing to 0.90 and 0.93 decreasing to 0.81 respectively). Subsequent t-tests showed that these differences were not statistically significant (Table 5.2). The only significant differences found between adjacent groups were between weeks 2 and 4 and weeks 6 and 8 (Table 5.2).

5.4.3 BRA v Mechanical Properties

As FI and SI are both ratios, they were correlated with the healing ratios of the mechanical properties. The coefficient of correlation (r) and the p value were determined from a linear regression analysis (Table 5.3). FI and SI only correlated significantly with bending stiffness in the ML plane. There were no significant correlations with AP bending stiffness, torsional stiffness or strength. The correlations with ML stiffness at low loads were slightly better than at the fail loads. The correlations of FI with the mechanical properties were better than those of SI.

Table 5.2 Student's t-tests between healing time groups of FI and SI using pooled variance from ANOVA test

Groups	*FI*	*SI*
2-4	< 0.001	< 0.001
4-6	> 0.1	> 0.1
6-8	< 0.01	< 0.01
8-10	> 0.1	> 0.1

Table 5.3 Correlation coefficients (r) and p values of BRA Frequency Index (FI) and Stiffness Index (SI) with mechanical healing ratios

Mechanical Property		*FI*	*SI*
ML Stiffness Ratio	r	0.56	0.51
	p	0.004	0.010
ML Fail Stiffness Ratio	r	0.50	0.45
	p	0.004	0.022
AP Stiffness Ratio	r	0.16	0.12
	p	0.44	0.57
Strength Ratio	r	0.31	0.28
	p	0.13	0.18
IR Torsional Stiffness Ratio	r	0.35	0.34
	p	0.09	0.11
ER Torsional Stiffness Ratio	r	0.19	0.18
	p	0.39	0.40

Graphs showing the relationships of ML stiffness, ML fail stiffness and strength with BRA are presented in this chapter (Figures 5.3 to 5.8). The remaining graphs are presented in Appendix G. The linear regression equations are shown on the graphs with the coefficient of determination (R^2) and are also summarised in Table 5.4. The regression line has been projected backward to demonstrate differences in the mathematical relationship with the ML stiffness ratios when FI is used (compared to SI).

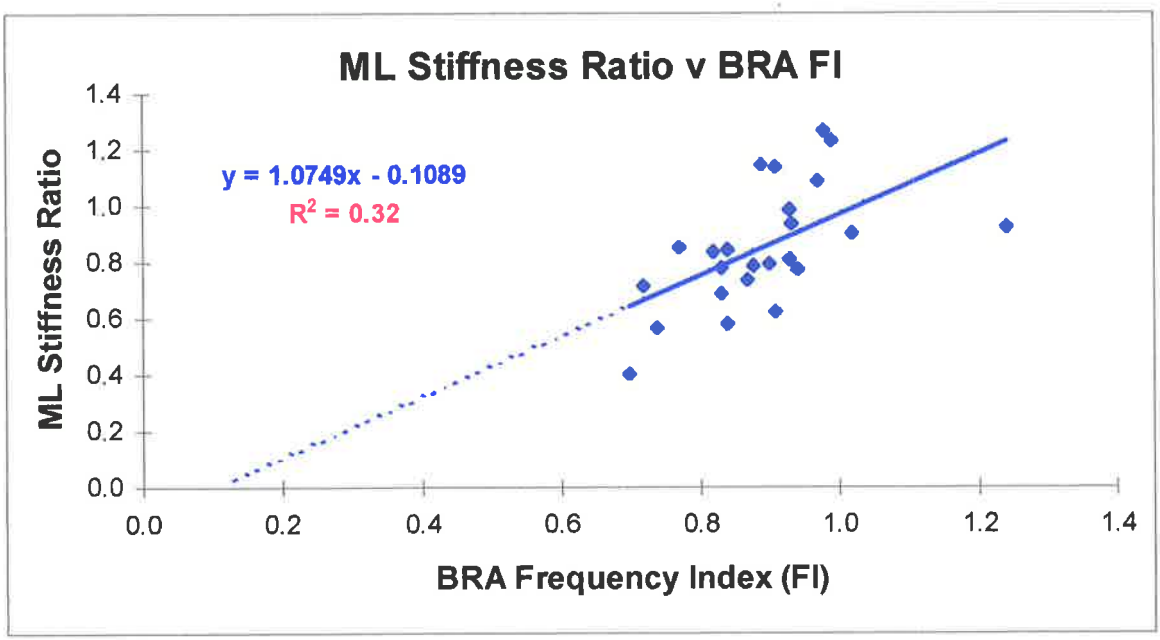

Figure 5.3 Relationship between ML stiffness ratio and BRA frequency index (FI)

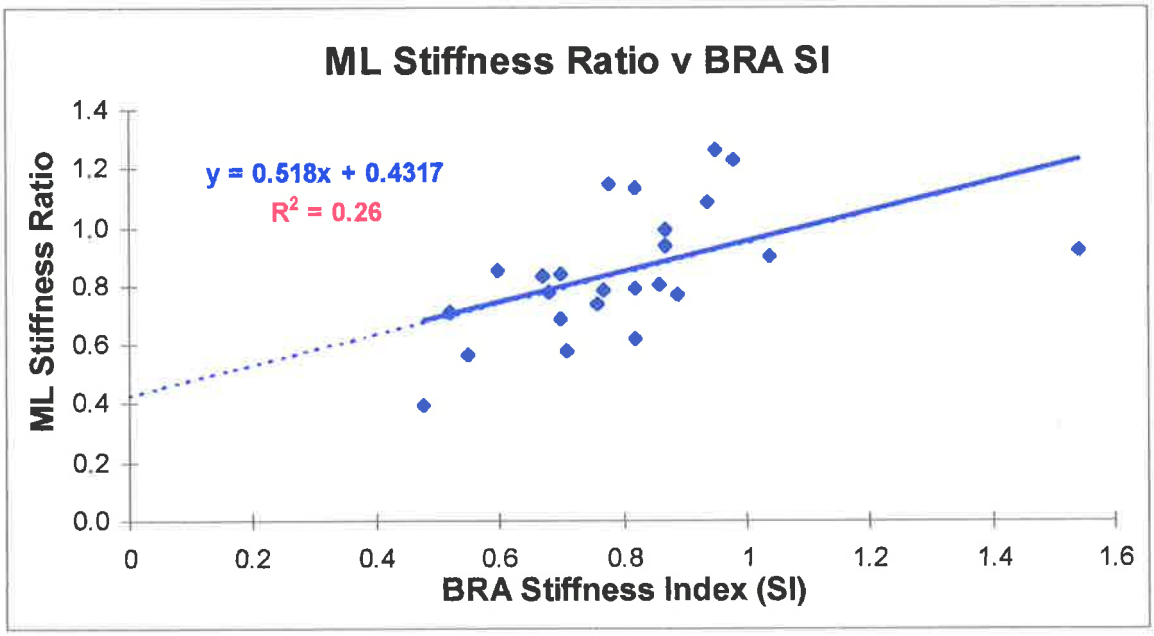

Figure 5.4 Relationship between ML stiffness ratio and BRA stiffness index (SI)

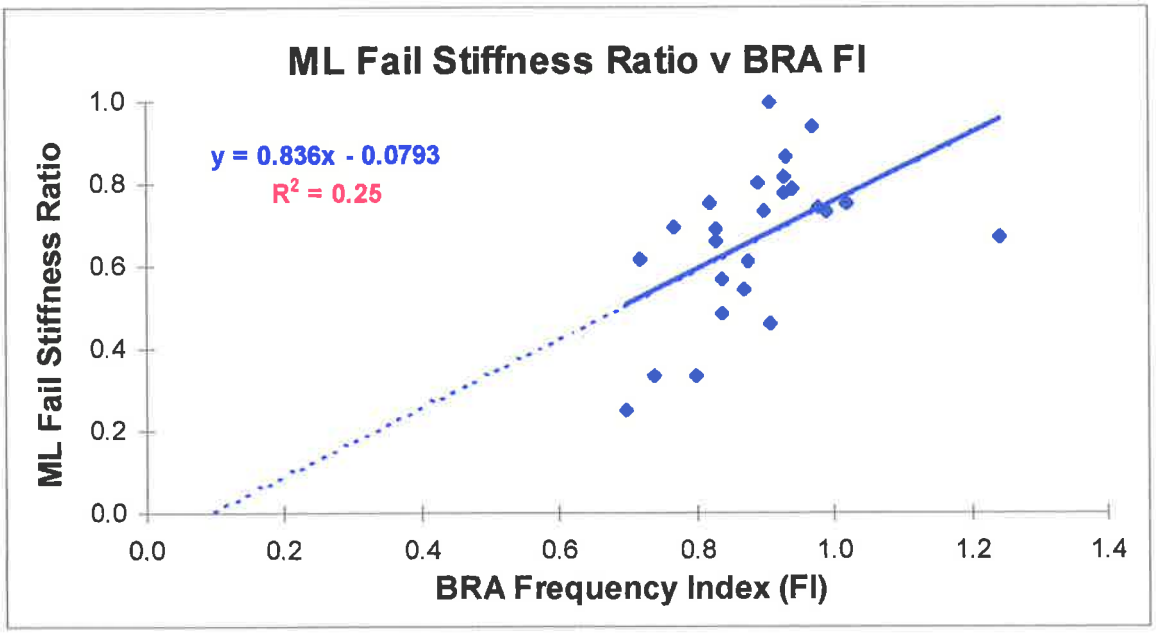

Figure 5.5 Relationship between ML fail stiffness ratio and BRA frequency index (FI)

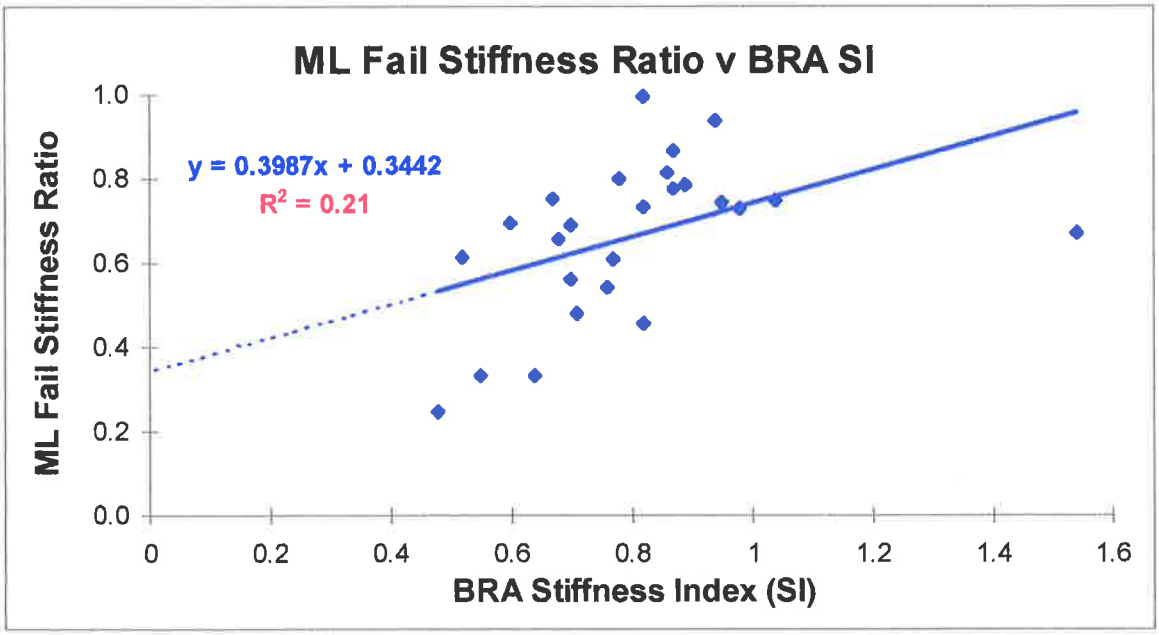

Figure 5.6 Relationship between ML fail stiffness ratio and BRA stiffness index (SI)

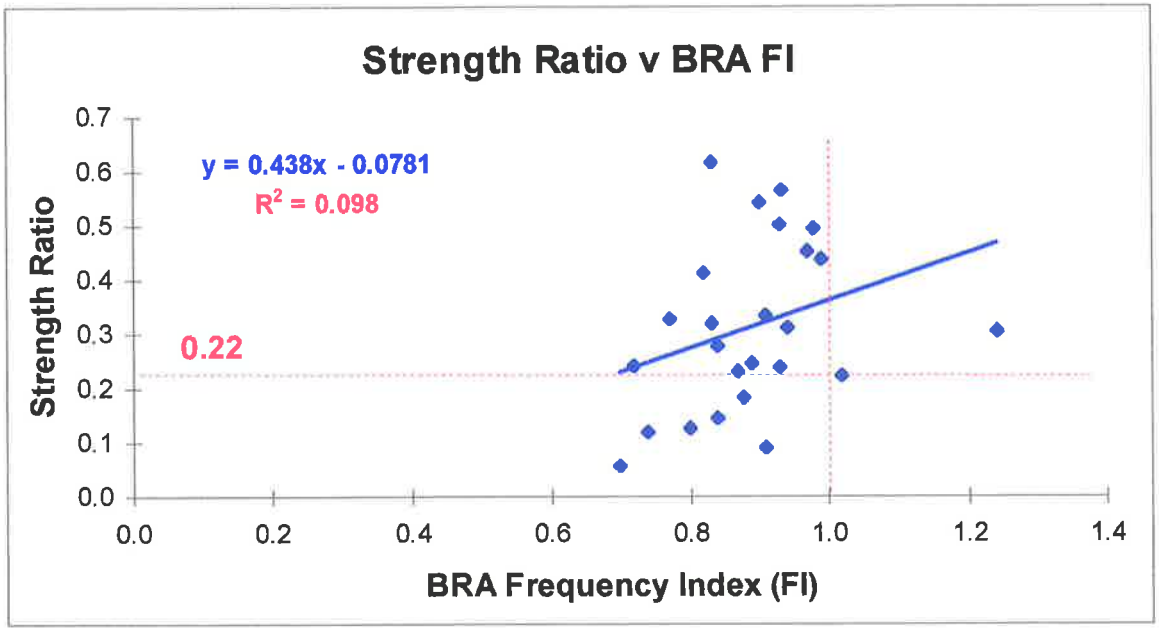

Figure 5.7 Relationship between strength ratio and BRA frequency index (FI)

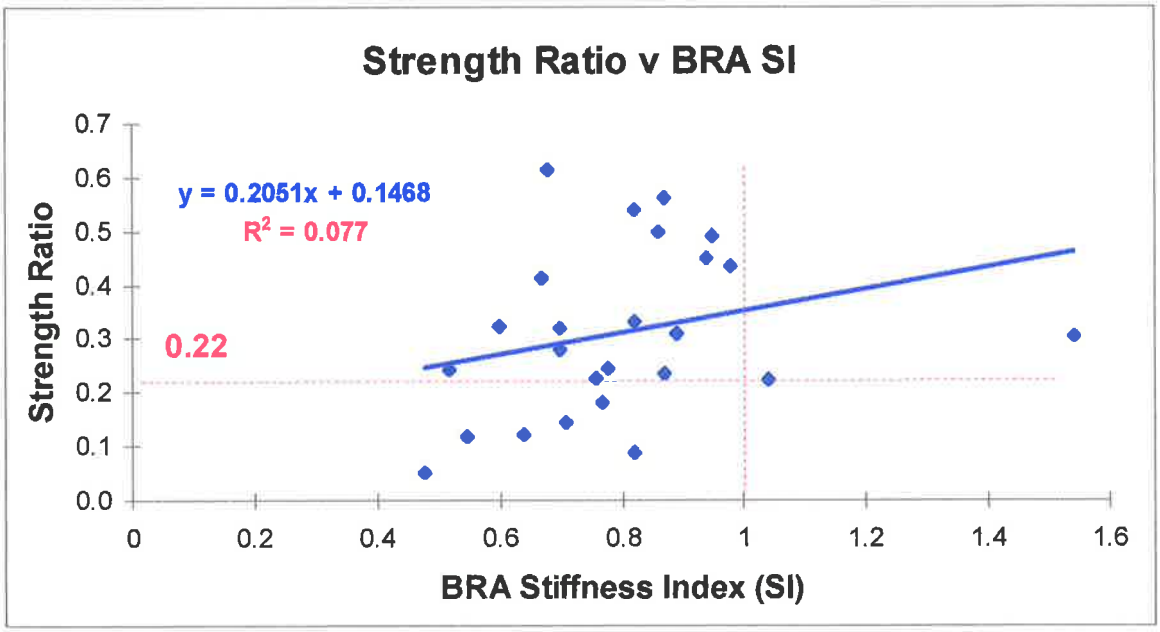

Figure 5.8 Relationship between strength ratio and BRA stiffness index (SI)

Table 5.4 Linear relationship between mechanical property (y) and FI or SI (x) and coefficient of determination (R^2)

Mechanical Property	*Frequency Index (FI)*	*Stiffness Index (SI)*
ML Stiffness Ratio	**y = 1.0749x - 0.1089** R^2 **= 0.32**	**y = 0.518x + 0.4317** R^2 = 0.26
ML Fail Stiffness Ratio	**y = 0.836x - 0.0793** R^2 = 0.25	**y = 0.3987x + 0.3442** R^2 = 0.21
AP Stiffness Ratio	**y = 0.2948x + 0.523** R^2 = 0.026	**y = 0.1136x + 0.6939** R^2 = 0.014
Strength Ratio	**y = 0.438x - 0.0781** R^2 = 0.098	**y = 0.2051x + 0.1468** R^2 = 0.077
IR Stiffness Ratio	**y = 0.7203x + 0.0716** R^2 = 0.12	**y = 0.37x + 0.4149** R^2 = 0.11
ER Stiffness Ratio	**y = 0.4295x + 0.4355** R^2 = 0.034	**y = 0.2206x + 0.6402** R^2 = 0.032

5.5 DISCUSSION

5.5.1 Study Exclusions

Only three sheep at 2 weeks and one sheep at 4 weeks posed difficulties in obtaining resonant frequency determinations using BRA. In addition to very low callus stiffness, post-fracture limb oedema with increased vibrational damping would have contributed to the difficulties. It is possible that the resonant frequency values obtained from the remaining sheep at weeks 2 and 4 were also significantly affected by these conditions. In the clinical situation, resonant frequency monitoring would ideally commence after the first four weeks. By this time a considerable reduction of the soft tissue oedema would be expected.

5.5.2 BRA v Time

The features of the resonant frequency changes occurring with time were qualitatively similar to the changes observed with the mechanically determined stiffness properties (Section 4.4.4; Figures 4.11 to 4.17). The intra-group variability and the overlap between groups seen in the mechanical properties was also evident with the BRA measurements. There was an increase in FI and SI which started to level off and possibly decrease after about 8 weeks. Quantitatively, the mean FI and SI values obtained at weeks 6, 8 and 10 were very similar to the stiffness values obtained from the mechanical testing at the lower loads. This was particularly so when BRA FI was compared with the ML stiffness ratio. The ML fail stiffness ratios, however, were considerably lower. As BRA was determined from the limb in an unloaded position, the closer quantitative association observed between the BRA and the mechanical properties tested under the lower loads is not surprising.

The most significant rise in the resonant frequency ratios occurred between weeks 2 and 4. With regard to the mechanical ratios, only three of the tibiae from the 4 week group and none from the 2 week group survived refracture at the time of collection to be included in the analysis. Therefore the proportion of this rise due to increasing bone stiffness as opposed to other factors (such as a decrease in limb mass secondary to resolution of oedema) could not be ascertained from this study. It may be possible to answer this question by using stiffness measurements obtained by instrumentation

instrumentation of external fixator pins after removal of the fixator body. The concern would still remain, however, that the callus would be disturbed if the fracture was destabilised at this early period. Another factor to be considered is that resonant frequency measurements theoretically relate to bending stiffness which may be quantitatively and qualitatively different to the stiffness measurements obtained through the angular deformation at the fracture site (see discussion section 4.5.2.3, paragraph 3).

5.5.3 BRA v Mechanical Properties

As the BRA was performed in the mediolateral plane of the sheep tibia, the better correlation found between the BRA indices and stiffness measured in that same plane, was expected. Although only moderate in size, the strongest and most significant correlations were of FI and SI with ML stiffness ($r = 0.56$ and 0.51 respectively). Even though a direct mathematical relationship existed between FI and SI, the correlation between FI and the stiffness ratios was better than those of SI. Of note was the effect that squaring FI had on the mathematical relationship between the resonant frequency and mechanical ratios. From the Euler-Bernouille beam model equation it was expected that, mathematically, SI would equate more directly with stiffness than FI. The converse, however, was found. The slope of the line relating FI with ML stiffness was very close to one (1.0749). This compared with a slope of 0.518 for SI. In addition, the y-intercept value was closer to zero with FI than with SI (-0.1089 versus 0.4317). The correlation of FI with ML fail stiffness was also better and more direct than that of SI. As discussed above, the better correlation and more direct relationship of the BRA indices with ML stiffness (when compared with ML fail stiffness) was in keeping with the unloaded condition of the tibia during testing. It is also noteworthy that for both ML fail stiffness and strength, the intercept of the linear equation with FI was also very close to zero (-0.0793 & -0.0781 respectively; Table 5.4). It was essentially only the slope which differed.

The distinct biphasic relationship found between stiffness and strength was not as evident between BRA and strength although less scatter was evident in the first part of the plots. Overall, however, there were no significant correlations between the

BRA indices and the strength ratio. This is also in keeping with the mechanical results (given that the resonant frequency is theoretically a measure of stiffness).

In attempting to define an endpoint to fracture healing from the resonant frequency data, a baseline strength ratio value was plotted on the strength ratio v FI and SI plots (Figure 5.7 & 5.8). From inspection of the graph, the FI value of 1.02 was the obvious value (from these results) to represent the strength 'baseline': the minimum expected strength value that would be obtained for a return to the control resonant frequency value. The corresponding strength ratio at this point was 0.22. This was very similar to the baseline level of 0.24 found from the plot of the strength ratio versus stiffness ratio as measured at low loads. It should also be noted that the strongest healing tibia had a strength ratio of 0.62 for a frequency index of only 0.83.

The coefficient of determination (R^2) for the linear relationship between FI and the ML stiffness ratio was 0.32. In other words, with this mathematical model, only 32% of the changes measured in the resonant frequency ratio were directly attributable to stiffness changes in the healing tibial fracture.

From the high reproducibility of the technique on normal tibiae (chapter three) it is unlikely that equipment inaccuracies contributed significantly to the results.

Other potential physical causes affecting the results are bone length, limb mass and boundary conditions. A change in the bone length was unlikely to have influenced the results as this was controlled with the external fixator and there was no evidence of fixator loosening throughout the study. Soft tissue oedema and increasing fracture callus may have increased tibial mass and reduced the expected resonant frequency. Boundary conditions may have also been affected by soft tissue changes influencing the constraint conditions at either end of the tibia. Slight alterations in the normal bending modal shape also may have occurred during healing which would have affected the healing ratio. It is also possible that the ML single bending mode was influenced by other modes of vibration resulting in modal coupling. If any of these factors had significantly affected the results, one would have expected a shift in the intercept and slope of the line equating the BRA indices with the ML stiffness ratio. This may partly explain why the direct relationship expected between stiffness and SI was not obtained. A modal analysis technique may have been able to ascertain the

influence of boundary conditions, modal shapes and damping conditions on these results. It is a much more involved procedure, however, and was outside the scope of this study in which the prime objective was to assess the technique of BRA.

Another potential source of error was the value assigned for the mechanical ratio. This used the contra-lateral tibia as the prefracture value. Earlier results showed that for the bending stiffness tests at low loads, the correlation between left and right was poor ($r = 0.39$ for ML stiffness; Figure 2.11; section 2.4.4). There was no significant difference, however, between their means. This suggests that a significant proportion of the scatter in the correlation between BRA and ML stiffness could be explained by inaccuracies created by using the contra-lateral tibia as a control for the mechanical properties. This might also explain why the linear equation describing the relationship between FI and ML stiffness ratio maintained a slope of approximately one. To prove this, in-vivo stiffness measurements of the tibia would need to be obtained prior to its fracture. None of the currently used in-vivo mechanical stiffness assessments, however, measure bending stiffness analogous to four-point bending tests. The validity of directly correlating stiffness measurements obtained using instrumented external fixator pins with vibrational analysis would therefore be questionable.

From the strong correlation between left and right resonant frequency data (section 2.4.3; Figure 2.8) it is unlikely that the frequency index would have significantly contributed to the scatter in the results. Similarly, the poor correlation of BRA with the strength ratio is not likely to be due to control inaccuracies given the very strong correlation found between left and right strength values in normal tibiae (Figure 2.13). However, the BRA measurements in-vivo would also include some inaccuracies due to the changed boundary and tissue conditions as described above.

In extrapolating these results to human studies it is important to recognise that this was an ovine model. The human tibia is bordered by a fibula which significantly stiffens the tibia in the ML plane and the presence or absence of a concomitant fibula fracture will influence results (Cornelissen et al 1986). There is no separate fibula in the ovine model to complicate the analysis.

Another limitation of this study was that the fracture was located at the tibial midshaft which is the optimal position to monitor stiffness changes (Cornelissen et al 1982). In clinical practice, of course, not all tibial fractures are midshaft fractures. In addition the amount of soft tissue trauma inflicted in performing this fracture was small compared to the many high-velocity clinical scenarios which result in fractures that are at an increased risk of delayed or non-union. Performing the tests under anaesthesia also had the advantage of controlling the influence of muscle tone on the resonant frequency.

This part of the study has shown that it was the frequency index obtained with BRA that gave an index of healing that most accurately equated with bending stiffness in the corresponding plane of vibration. This was not predicted from the Euler-Bernouille beam model equation and therefore raises questions about the validity of such a model when applied in-vivo. The correlation obtained between FI and stiffness was not strong enough to confidently allow accurate quantitative mechanical stiffness assessments to be made from isolated BRA assessments. Serial increases in the resonant frequency would be required to confidently indicate a progression in fracture stiffness.. If control stiffness asymmetry is in fact largely responsible for the scatter obtained in this study, it may be possible to more confidently quantify bending stiffness from BRA assessments. This hypothesis requires further evaluation.

Given the poor correlation found between BRA and strength, BRA measurements in isolation are likely to be inherently limited in predicting an endpoint to fracture healing. To what extent this will affect the clinical use of the technique also requires further evaluation. Using mechanical stiffness measurements, increasing the load improves the correlation with strength and 'raises the baseline' of predicted minimum strength for a given return to prefracture stiffness levels. Such a manoeuvre has not been attempted in BRA to date and would potentially be very difficult to achieve because of the effects of such loading on boundary conditions and on the reproducibility of testing. It is, however, a concept that should be pursued if BRA is to be considered for use in fracture research or clinical practice.

CHAPTER SIX

BONE HISTOMORPHOMETRY

6.1 INTRODUCTION

In the previous chapters, an ovine fracture healing model was studied with respect to the mechanical and vibrational attributes of the healing bone. In this chapter, the material properties of the callus and adjacent cortex were examined at the micro-structural level with the aim of better understanding the observed mechanical and vibrational changes.

6.2 AIMS

The specific aims of this study were:

1. To examine the histomorphometric and mechanical properties of the control group and determine the homogeneity of the study groups.
2. To describe callus microstructure and its changes during fracture healing.
3. To correlate callus microstructure with the mechanical properties of the healing fracture.
4. To correlate resonant frequency changes with healing callus histomorphometric data.

6.3 METHODS

6.3.1 Specimen Preparation

Following mechanical testing, specimens were X-rayed in the anteroposterior plane using a Faxitron X-Ray cabinet (Hewlett Packard Co., USA). The specimens were then cut on a band saw in the bone long axis in the anteroposterior plane, through the fracture site. Each specimen was then fixed in 10% neutral buffered formalin prior to infiltration and embedding in polymethyl methacrylate (PMMA) resin (Emmanual et al 1987).

6.3.1.1 Infiltration

Specimens were dehydrated through ascending grades of alcohol (70%, 95% and 100% x2 each for 24 hours) and then cleared in two changes of xylene (24 hours each). They were then infiltrated in PMMA resin using the schedule outlined in Table 6.1.

Table 6.1 Schedule for specimen infiltration with PMMA

PMMA solution I (PMMA:butyl pthalate = 75ml:20ml)		
3 days	Room temperature	Magnetic stirrer
PMMA solution II (PMMA:butyl pthalate:benzoyl peroxide = 75ml:20ml:1gm)		
5-7 days	4 C°	Vacuum
PMMA solution III (PMMA:butyl pthalate:benzoyl peroxide = 75ml:20ml:2.5gm)		
1 day	4 C°	Vacuum

6.3.1.2 Embedding

Approximately 1cm prepolymerised layers were previously prepared in 500ml polypropylene containers with screw-on lids. The infiltration specimen was placed on the prepolymerised layer and covered with PMMA solution III which was previously used for infiltration. This was then left in the fume cupboard until polymerisation occurred (approximately 3-5 days).

6.3.1.3 Section Preparation

Following polymerisation, the blocks were removed from the polypropylene containers and then gross sectioned on a band-saw to remove excess resin.

Approximately 1mm sections were then cut using the precision band-saw (EXAKT, Apparatebau, Germany) using a continuous diamond edged blade and water irrigation. These sections were ground using ascending grit paper (120, 240, 400, 800 and 1200 grit) and polished using a polishing cloth and 1μm alpha-alumina polish on a bench-top grinder (Buehler, Coventry, England).

The polished surface was adhered to flexible polycarbonate slides using 5 minute araldite (cure overnight). The sections were then ground to approximately 80 -100 microns thickness using the above technique.

The sections were surface stained with toluidine blue modified for ground section analysis (Dickson 1984) and then viewed using plain and polarised light microscopy.

6.3.2 Histoquantitation

Cortical and medullary width adjacent to the fracture site (5mm), were measured directly from the X-Ray using a HP 9874A digitiser (Hewlett Packard Co.,USA) (ie anterior and posterior surfaces).

Cortical porosity and callus histomorphometry were measured from ground sections at the sites shown in Figure 6.1. Using a Quantimet 520 image analyser (Leica Cambridge, UK), a total magnification of x32 was used (Appendix H). Cancellous Bone Volume / Total Tissue Volume (BV / TV); Cancellous Bone Surface / Total Tissue Volume (BS / TV); and Cancellous Bone Surface / Cancellous Bone Volume (BS / BV) were measured directly. These were referred to as 'Bone Volume', 'Bone Surface' and 'Specific Bone Surface' respectively (Parfitt et al 1987). The Trabecular Thickness (Tb.Th), Trabecular Separation (Tb.Sp) and Trabecular Number (Tb.N) were calculated using the parallel plate model (Parfitt et al 1987). Histology examples are given in Appendix H.

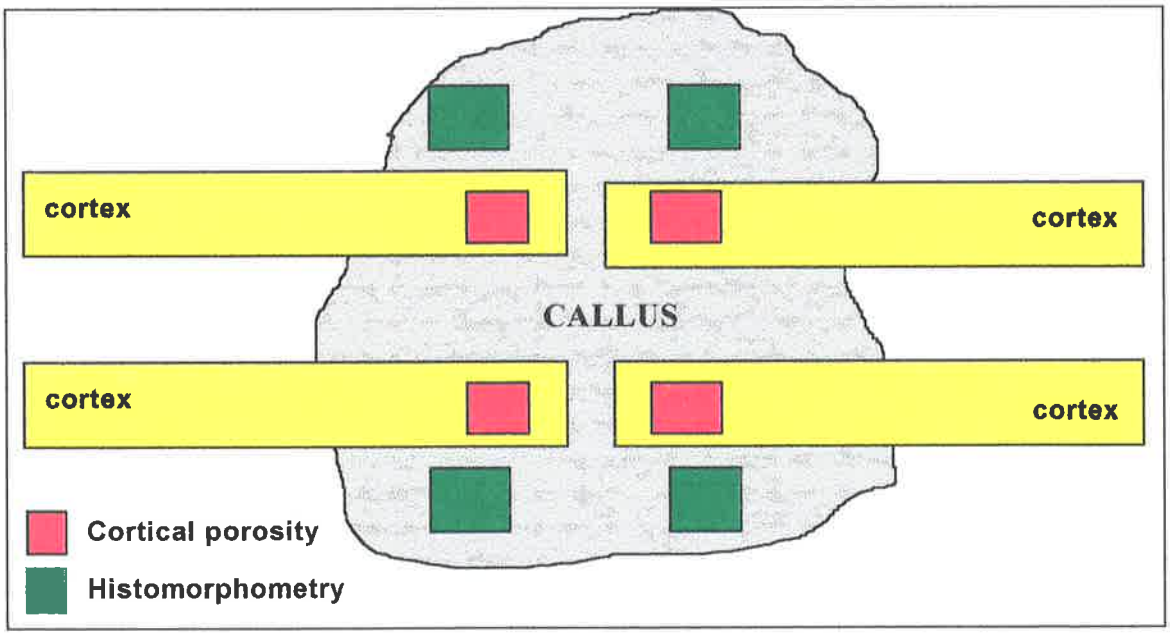

Figure 6.1 Sites used for analysis of cortical porosity and callus histomorphometry

6.4 RESULTS

Statistical analyses were performed using PC-SAS (SAS Inc. Cary, NC) and the graphic and linear analysis tools of Excel 5 (Microsoft Corporation, USA). Correlations were assessed using Pearson's correlation coefficient (r) and significance between groups was accepted at $p < 0.05$. Linear correlation analysis was performed on the data throughout the study as examination of power analyses failed to show any better modelling of the results except were shown.

6.4.1 Study Group

The data are tabulated in Appendix I. In all forty sheep, measurements were obtained of the cortical and medullary widths and of the cortical porosity. Histomorphometric data, however, were not obtainable from eight sheep because of insufficient callus. These same eight sheep had also been previously excluded from mechanical testing because of refracture during excision (Table 4.1).

SHEEP	GROUP	REASON
@04	2	Insufficient Callus
@06	2	"
@26	2	"
@43	2	"
@05	4	"
@27	4	"
@35	6	"
@41	6	"

Table 6.2 Exclusions from histomorphometric analysis

6.4.2 Baseline Studies

6.4.2.1 Cortical & Medullary Widths

Cortical and medullary widths were analysed as a guide to inter-group homogeneity, with respect to the gross morphological properties. The group distributions are shown in Figures 6.2 and 6.3. A single factor ANOVA failed to show any significant difference between the groups with $p = 0.14$ and $p = 0.50$ for cortical and medullary widths respectively.

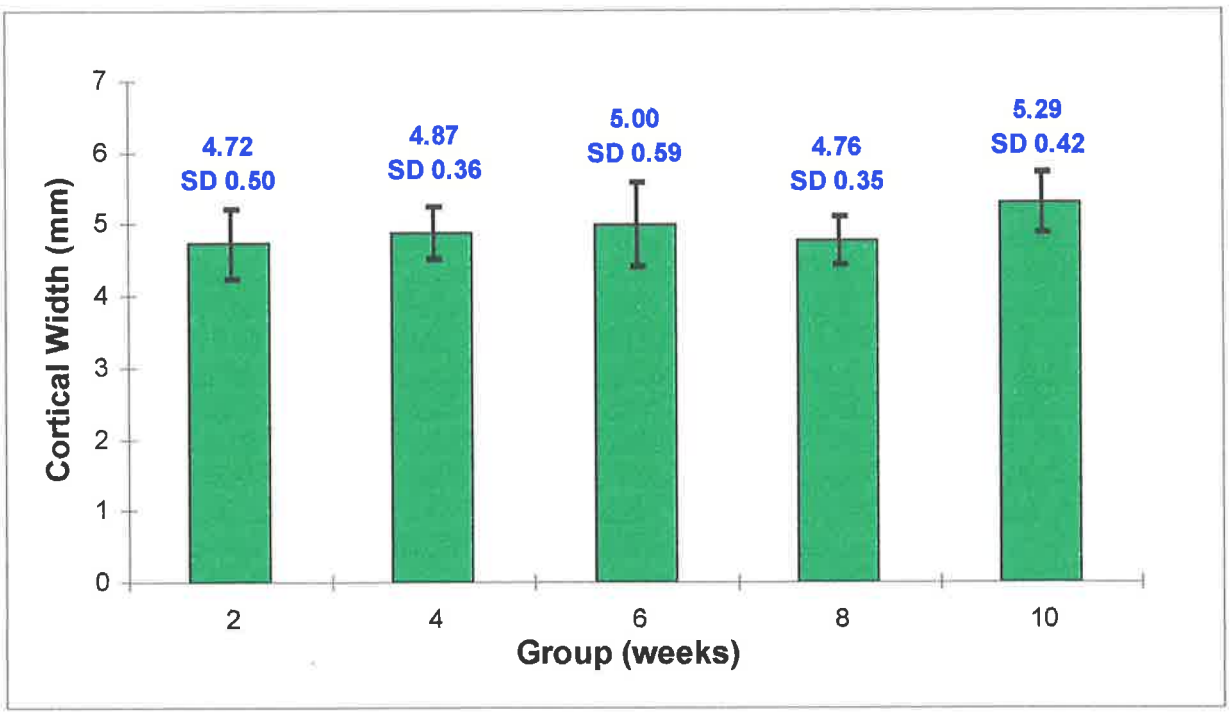

Figure 6.2 Group distribution of cortical widths (ANOVA p = 0.14)

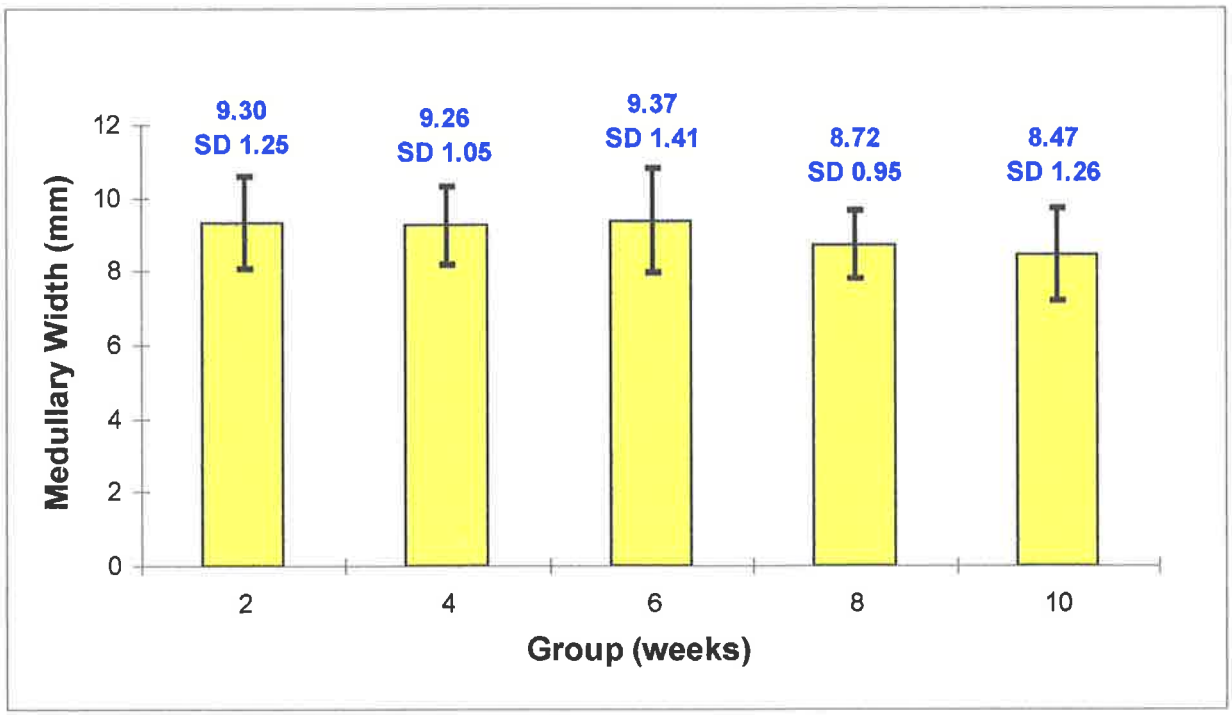

Figure 6.3 Group distribution of medullary widths (ANOVA p = 0.50)

6.4.2.2 Cortical Porosity

The porosity of the tibial midshaft cortex was measured from six randomly selected control sheep and the baseline cortical porosity was found to be 0.78% SD 0.44 (Table 6.3).

Table 6.3 Cortical porosity measurements from randomly selected control tibiae

Sheep	*Porosity (%)*
@11	1.6
@17	0.5
@25	0.4
@29	0.9
@32	0.8
@38	0.5
MEAN	**0.78**
SD	**0.44**

6.4.2.3 Callus Histomorphometry

The obvious prefracture value or "baseline" value for callus histomorphometry was no callus.

6.4.2.4 Mechanical Properties

As a baseline mechanical study of tibial morphometry, the cortical and medullary widths and the tibial diameter (mediolateral) were correlated with the measured mechanical properties (Table 6.4).

Table 6.4 Correlations between tibial morphometry and mechanical properties in controls

MORPHOMETRY		*IR*	*ER*	*AP*	*ML*	*MLF*	*STR*
Cortical Width	r	0.51	0.44	0.39	0.46	0.33	0.11
	p	0.01	0.03	0.06	0.02	0.11	0.61
Medullary Width	r	0.37	0.35	0.44	0.31	**0.74**	0.33
	p	0.08	0.10	0.03	0.14	**4.1E-05**	0.11
Tibial Diameter	r	0.51	0.58	0.55	0.50	**0.74**	0.31
	p	0.003	0.01	0.005	0.01	**3.8E-05**	0.14

The relationships of both medullary width and tibial diameter with ML fail stiffness were the only ones found to correlate strongly ($r=0.74$; $p<0.0001$; Figures 6.4 and 6.5). There was no significant correlation between cortical width and ML fail stiffness ($r=0.33$; $p=0.11$; Figure 6.6). Smaller, but significant, correlations were found with the tibial diameter and the other stiffness measurements but not with strength (Table 6.4; Figure 6.7).

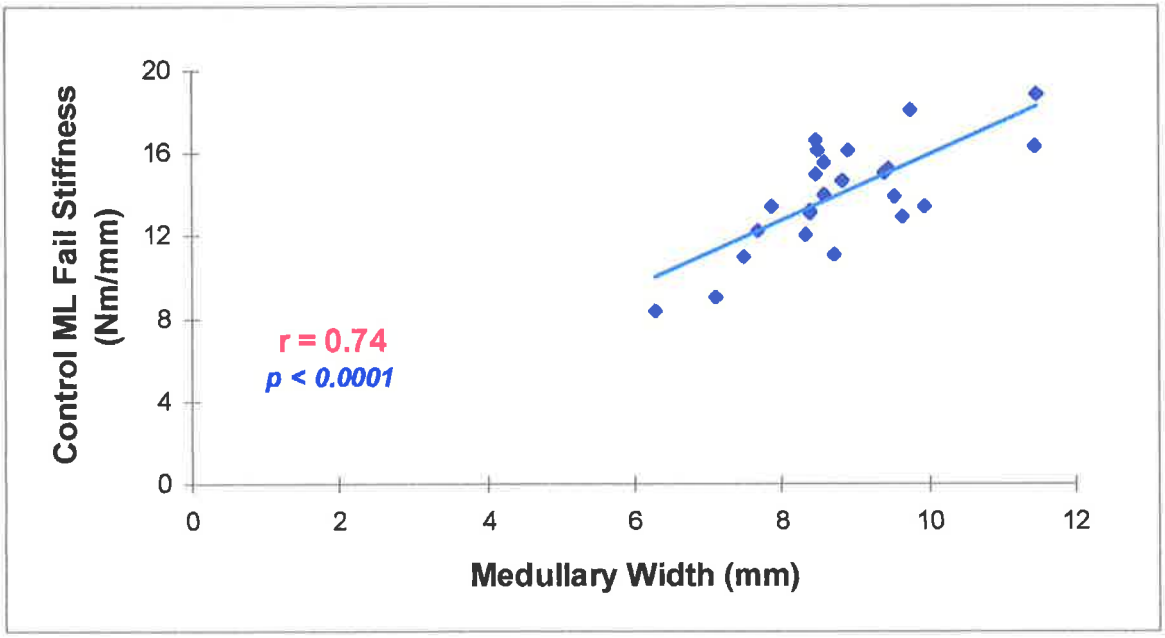

Figure 6.4 Correlation of ML fail stiffness in controls with medullary width

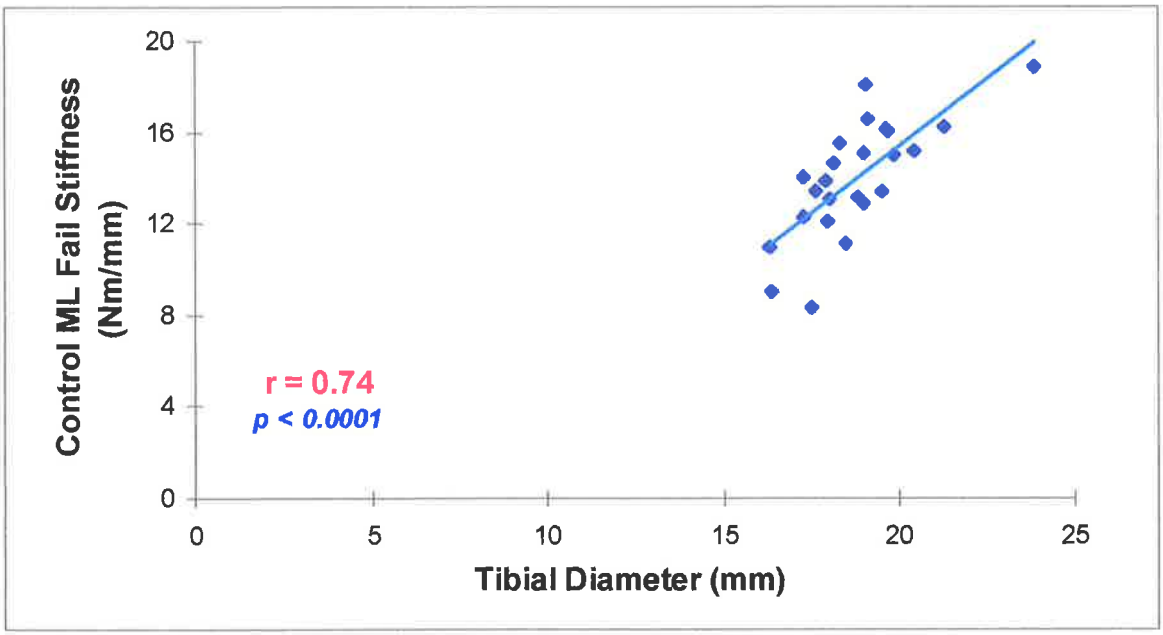

Figure 6.5 Correlation of ML fail stiffness in controls with tibial diameter

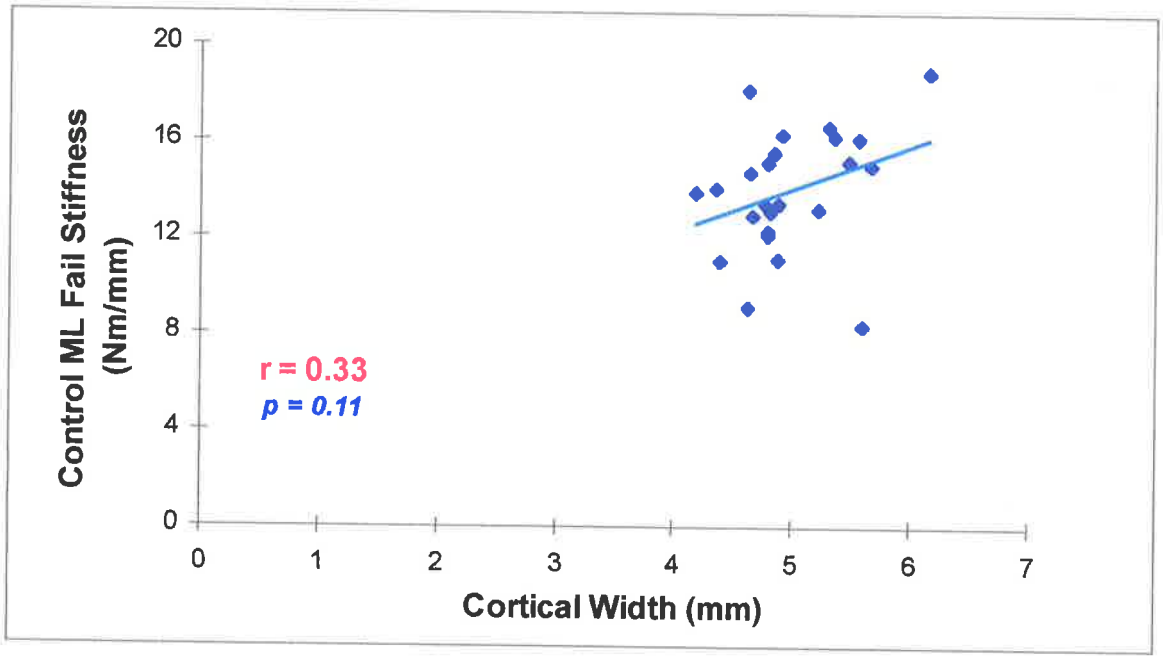

Figure 6.6 Correlation of ML fail stiffness in controls with cortical width

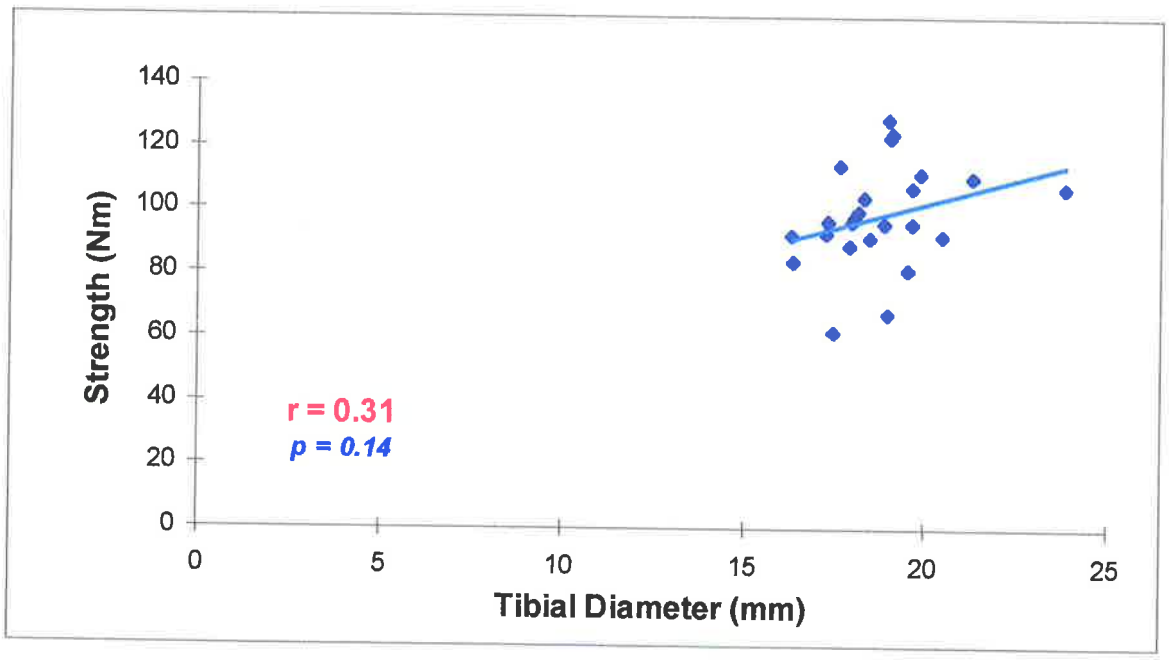

Figure 6.7 Correlation of strength in controls with tibial diameter

6.4.3 Fracture Histomorphometry

6.4.3.1 Cortical Porosity

Changes in the cortical porosity as a function of increasing healing time are shown in Figure 6.8. The baseline control values have been included in the analysis as "week 0". A progressive increase was found in the mean cortical porosity (0.78% and 8.22% at 0 and 10 weeks respectively). The intra-group heterogeneity also increased (SD 0.44% at 0 weeks and 6.98% at 10 weeks). Student's t-testing showed that the only statistically significant increase (between adjacent groups over a two week interval) was between weeks 6 and 8 (Appendix J).

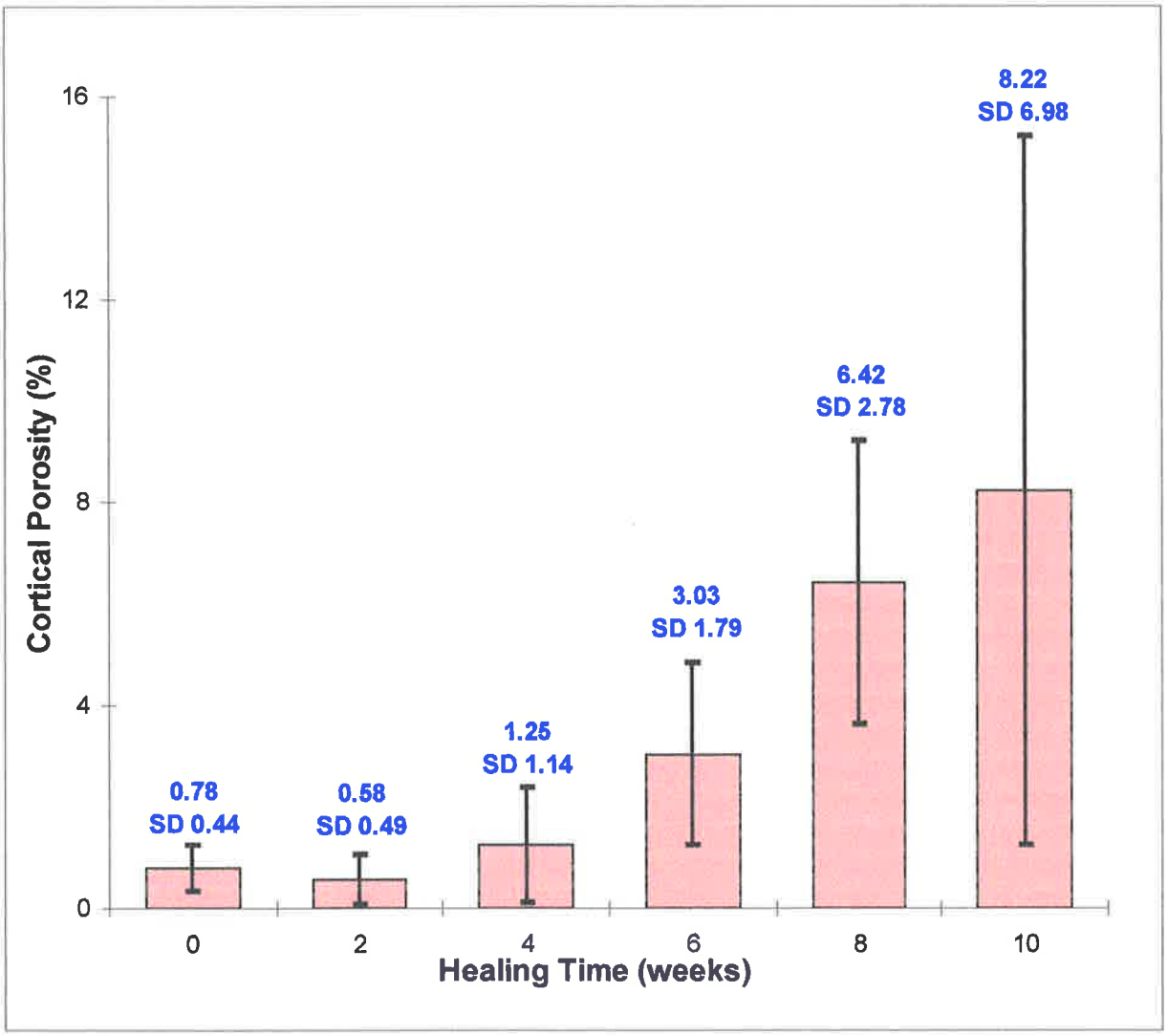

Figure 6.8 Changes in mean cortical porosity (adjacent fracture site) with healing time

6.4.3.2 Bone Volume

There were significant increases in callus bone volume up to 4 weeks (Figure 6.9). Increases thereafter were not statistically significant (Appendix J).

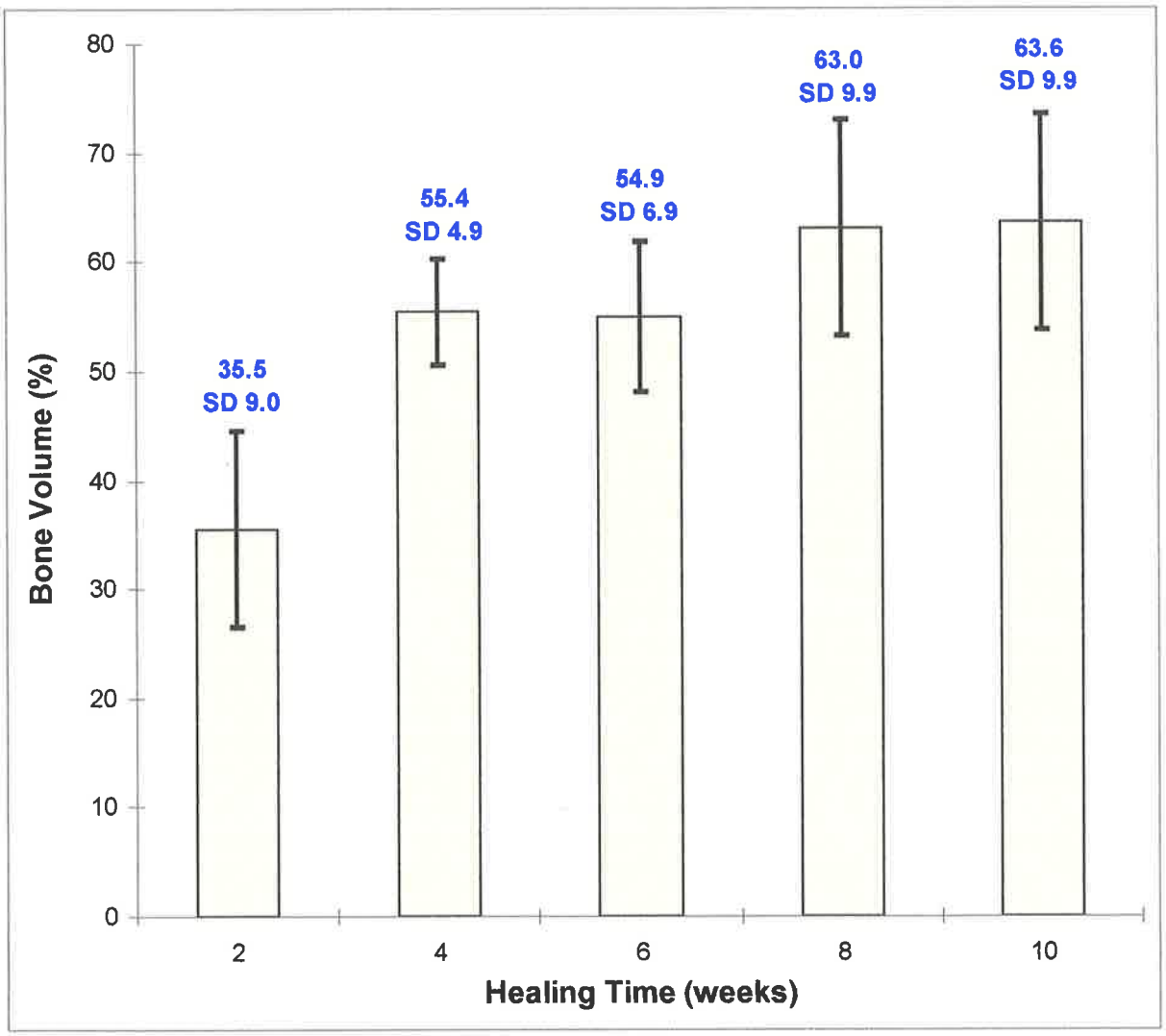

Figure 6.9 Changes in mean callus bone volume with healing time

6.4.3.3 Bone Surface

The mean callus bone surface was found to be maximal at 2 weeks (Figure 6.10). Thereafter there was a decrease in bone surface which was most marked and was statistically significant between weeks 4 and 6 (Appendix J).

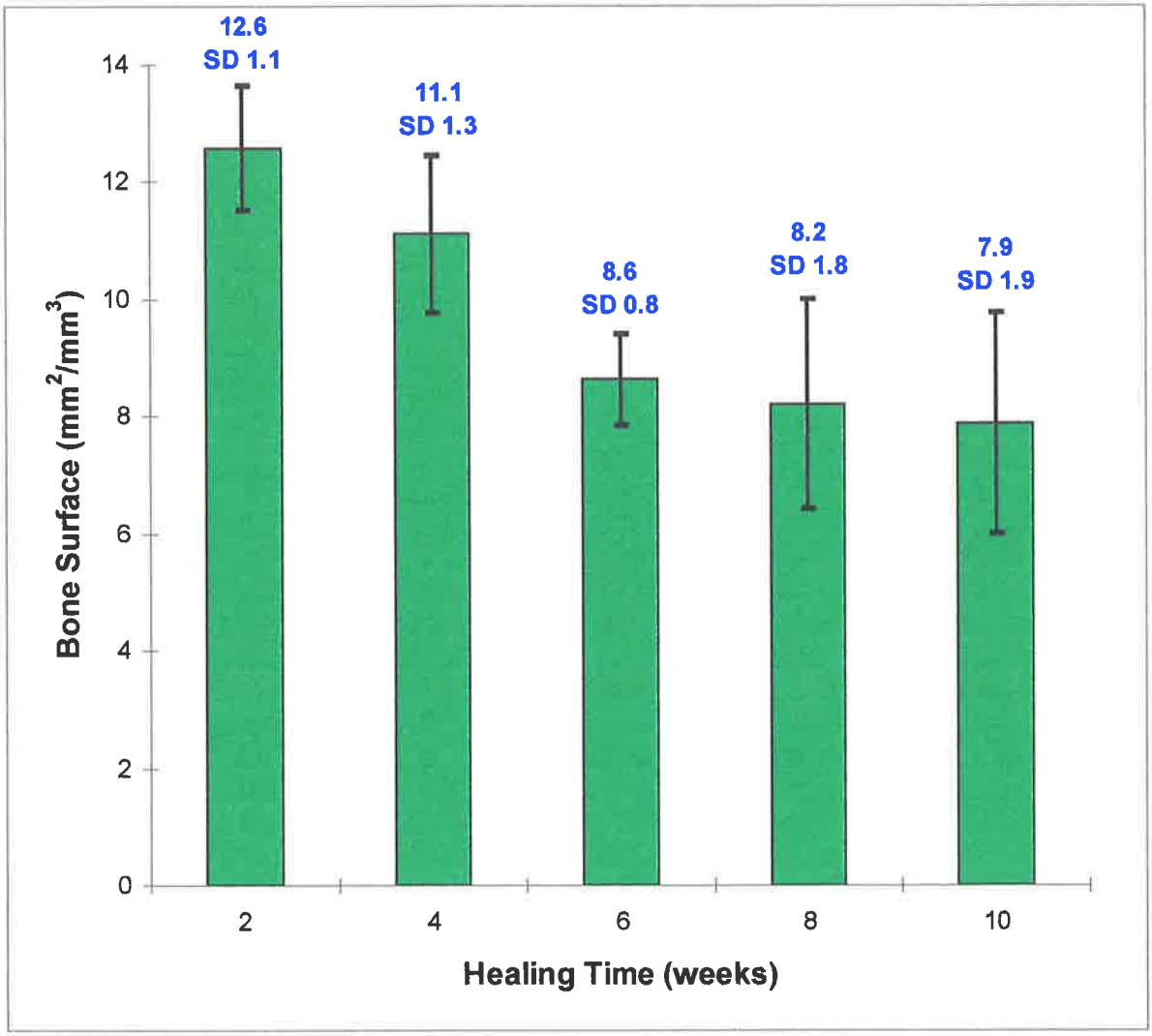

Figure 6.10 Changes in mean callus bone surface with healing time

6.4.3.4 Specific Bone Surface

The changes in specific bone surface (Figure 6.11) were similar to those seen in bone surface (Figure 6.10) except that the most significant decrease was between weeks 2 and 4 (Appendix J). The change was also more pronounced.

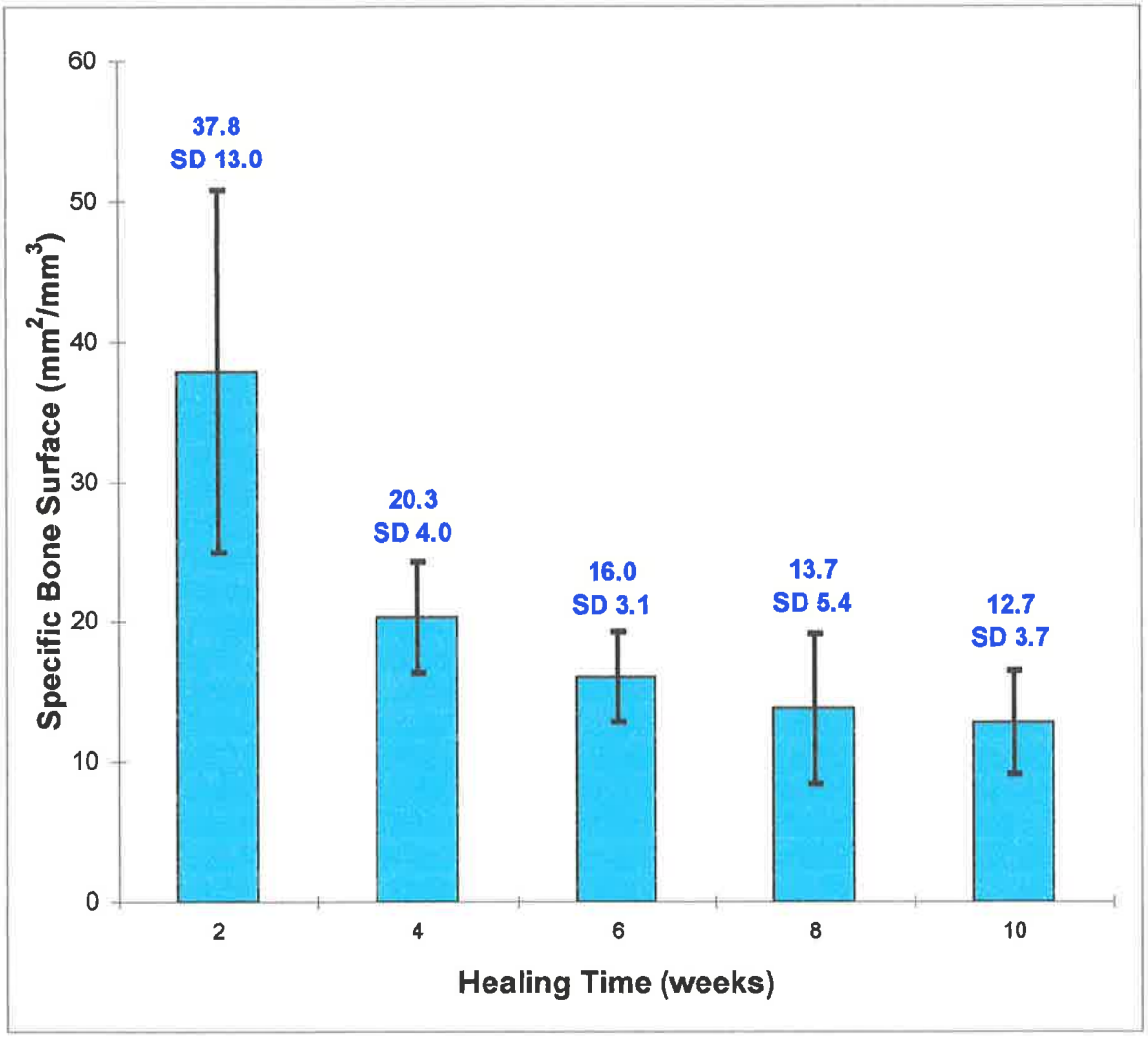

Figure 6.11 Changes in mean callus specific bone surface with healing time

6.4.3.5 Trabecular Thickness

Callus trabecular thickness increased significantly until week 8 (Figure 6.12; Appendix J). There was also marked intra-group heterogeneity noted in weeks 8 and 10.

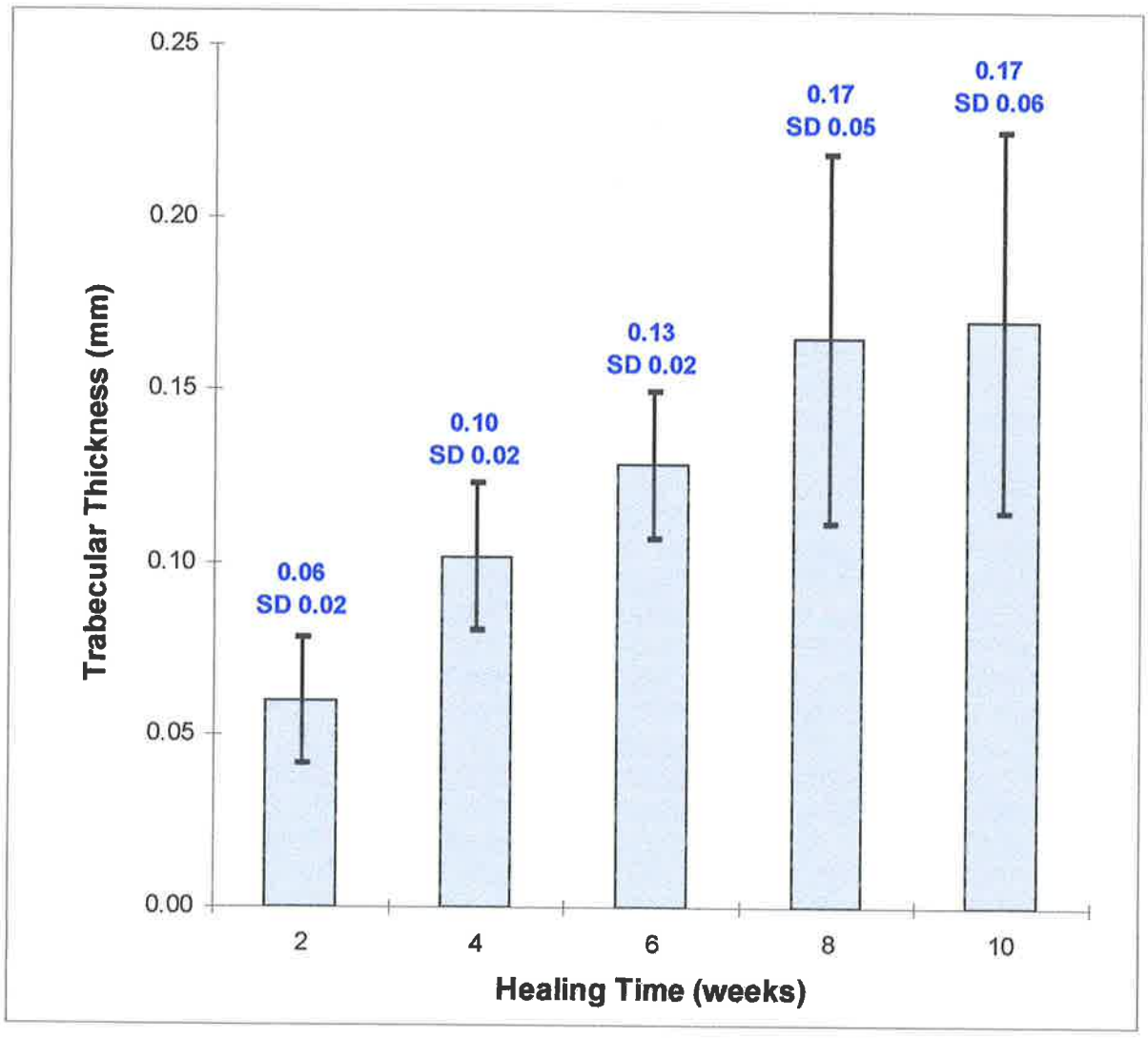

Figure 6.12 Changes in mean callus trabecular thickness with healing time

6.4.3.6 Trabecular Separation

There was no significant change found in the mean trabecular separation after week 2 (Figure 6.13, Appendix J).

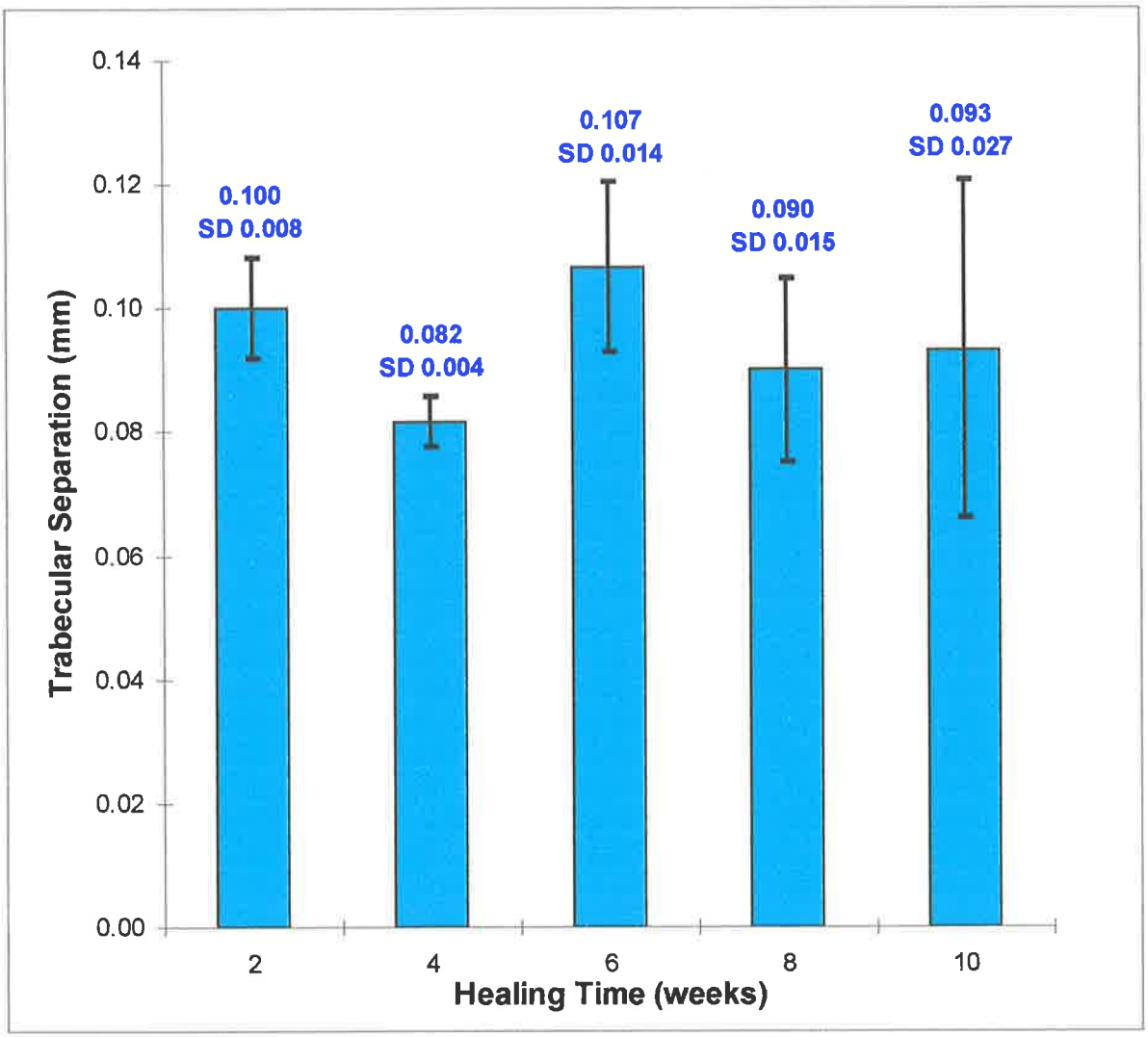

Figure 6.13 Changes in mean callus trabecular separation with healing time

6.4.3.7 Trabecular Number

The number of callus trabeculae was found to decrease after week 2 (Figure 6.14). This was most significant between weeks 4 and 6 (Appendix J).

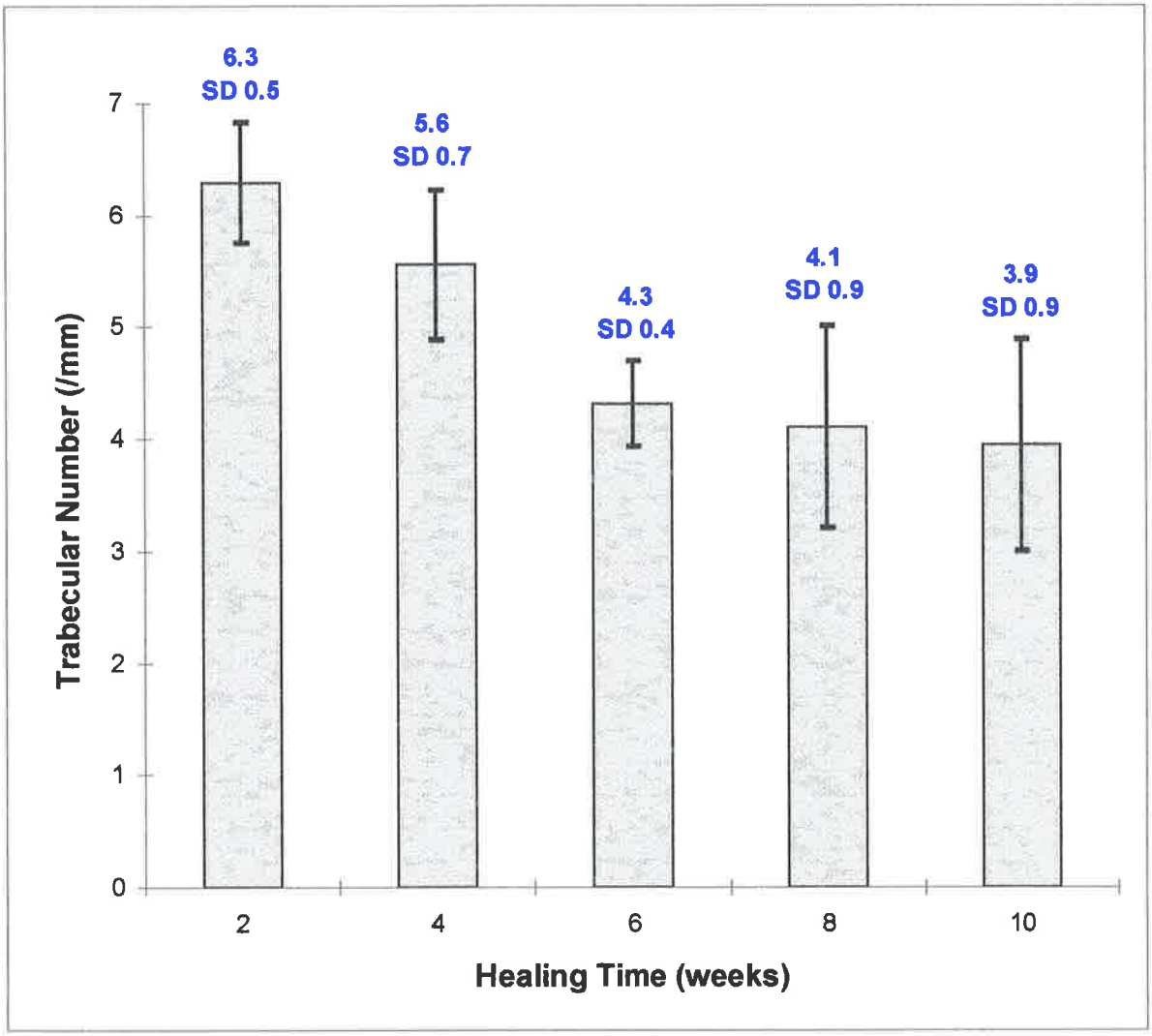

Figure 6.14 Changes in mean callus trabecular number with healing time

6.4.4 Mechanical Analysis Of Histomorphometry

In the following section, results of the correlations between the histomorphometric analyses and mechanical properties are tabled. The significant correlations are also presented in graphical form.

6.4.4.1 Bone Volume

No significant correlations were found between callus bone volume and any of the measured callus mechanical properties (Table 6.5).

Table 6.5 Correlations of callus bone volume with mechanical properties

Bone Volume	*ER*	*IR*	*AP*	*ML*	*FLS*	*STR*
r	0.05	0.08	0.10	0.09	0.05	0.24
p	0.81	0.70	0.65	0.69	0.82	0.25

6.4.4.2 Bone Surface

Significant negative correlations were found between callus bone surface and ER stiffness, IR stifffness, and ML stiffness (Table 6.6; Figures 6.15 to 6.17).

Table 6.6 Correlations of callus bone surface with mechanical properties

Bone Surface	*ER*	*IR*	*AP*	*ML*	*FLS*	*STR*
r	-0.41	-0.46	-0.02	-0.48	-0.35	-0.37
p	0.04	0.02	0.93	0.02	0.08	0.07

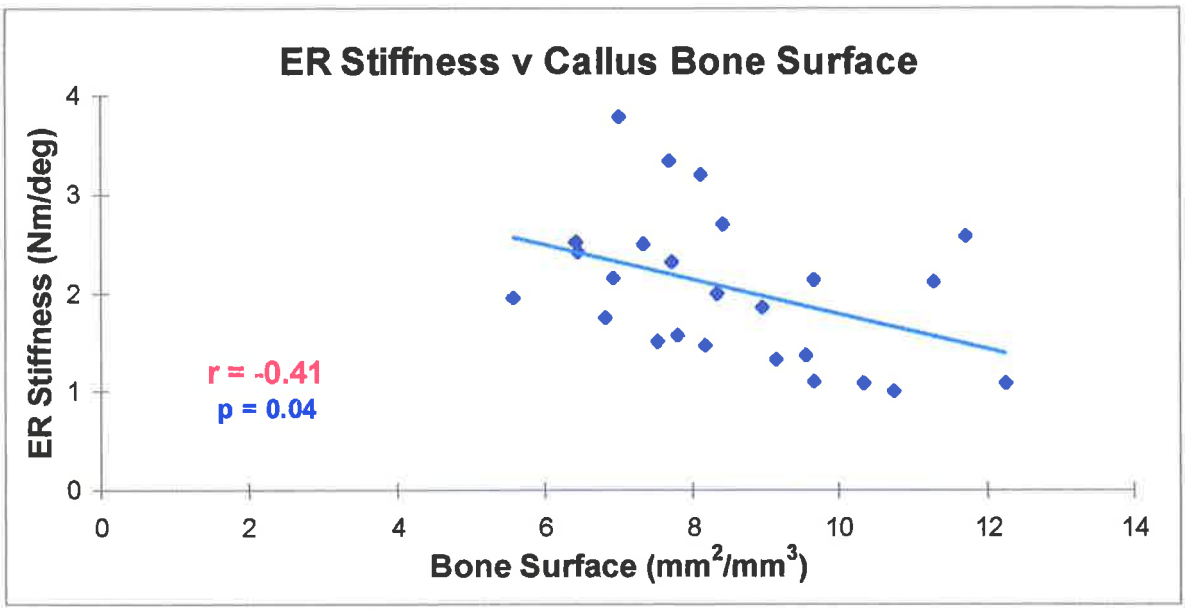

Figure 6.15 Relationship of ER stiffness to callus bone surface

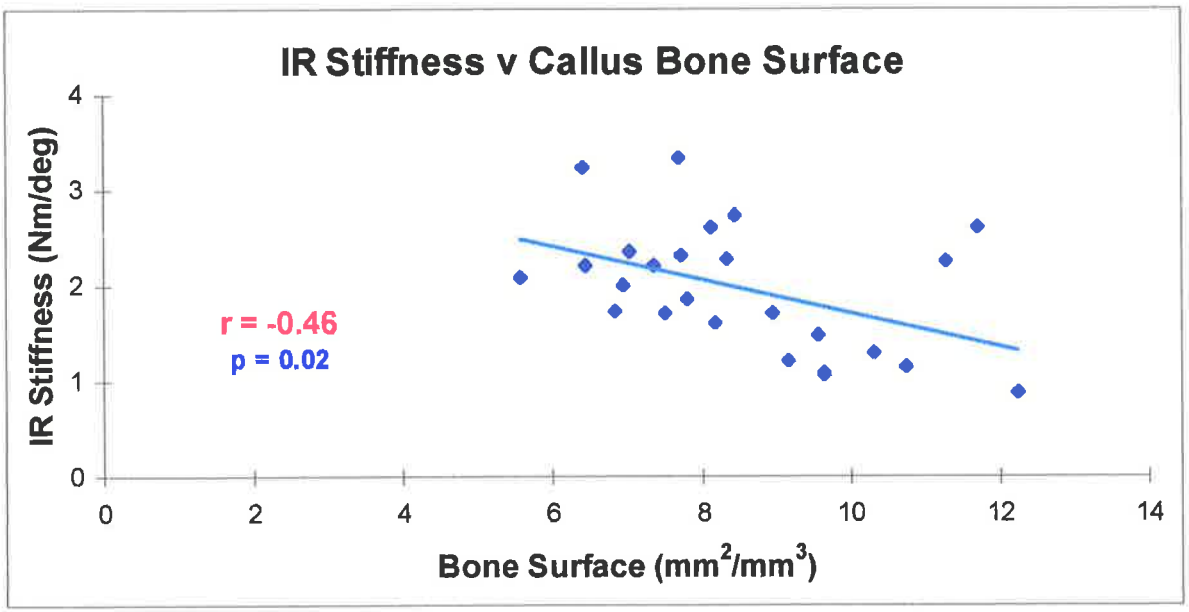

Figure 6.16 Relationship of IR stiffness to callus bone surface

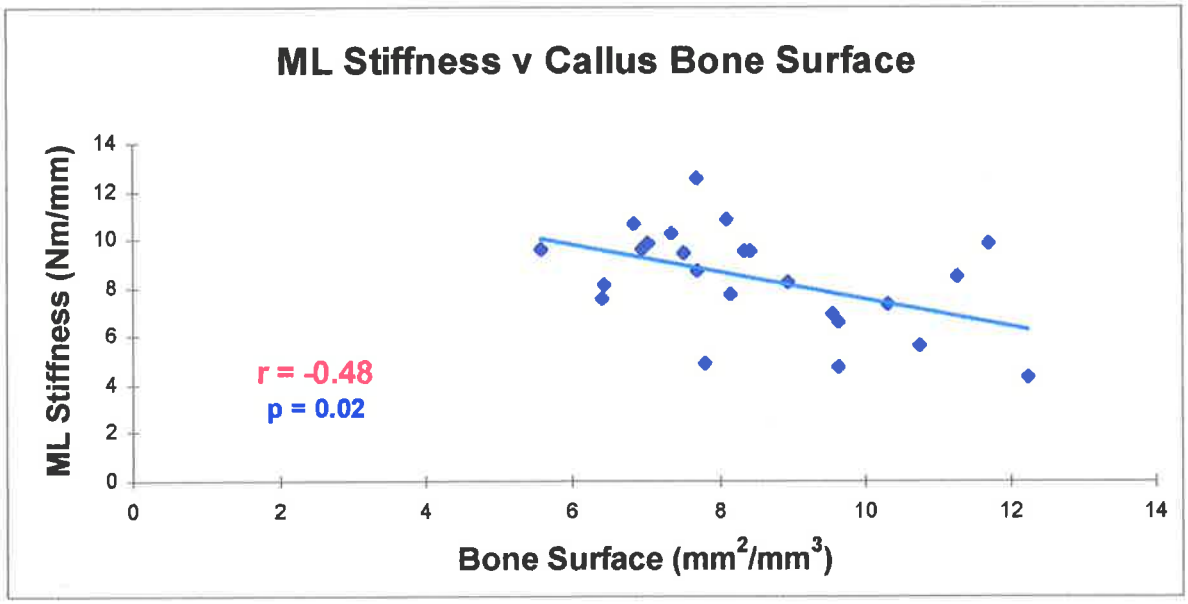

Figure 6.17 Relationship of ML stiffness to callus bone surface

6.4.4.3 Specific Bone Surface

Negative correlations were found between specific bone surface and the mechanical properties but none were statistically significant (Table 6.7).

Table 6.7 Correlations of callus specific bone surface with mechanical properties

Specific Bone Surface	*ER*	*IR*	*AP*	*ML*	*FLS*	*STR*
r	-0.28	-0.32	-0.07	-0.34	-0.22	-0.35
p	0.17	0.13	0.74	0.11	0.29	0.08

6.4.4.4 Trabecular Thickness

Weak, positive correlations were found between trabecular thickness and the mechanical properties but none were significant (Table 6.8).

Table 6.8 Correlations of callus trabecular thickness with mechanical properties

Trabecular Thickness	*ER*	*IR*	*AP*	*ML*	*FLS*	*STR*
r	0.26	0.32	0.01	0.31	0.26	0.13
p	0.21	0.12	0.98	0.14	0.20	0.08

6.4.4.5 Trabecular Separation

No significant correlations were found between callus trabecular separation and the mechanical properties of the healing fracture (Table 6.9).

Table 6.9 Correlations of callus trabecular separation with mechanical properties

Trabecular Separation	*ER*	*IR*	*AP*	*ML*	*FLS*	*STR*
r	0.31	0.31	0.13	0.33	0.23	0.01
p	0.13	0.14	0.53	0.12	0.26	0.97

6.4.4.6 Trabecular Number

Significant negative correlations were found between callus trabecular number and ER stiffness, IR stifffness, and ML stiffness (Table 6.10; Figures 6.18 to 6.20).

Table 6.10 Correlations of callus trabecular number with mechanical properties

Trabecular Number	*ER*	*IR*	*AP*	*ML*	*FLS*	*STR*
r	-0.41	-0.46	-0.02	-0.48	-0.35	-0.37
p	0.04	0.02	0.92	0.02	0.08	0.07

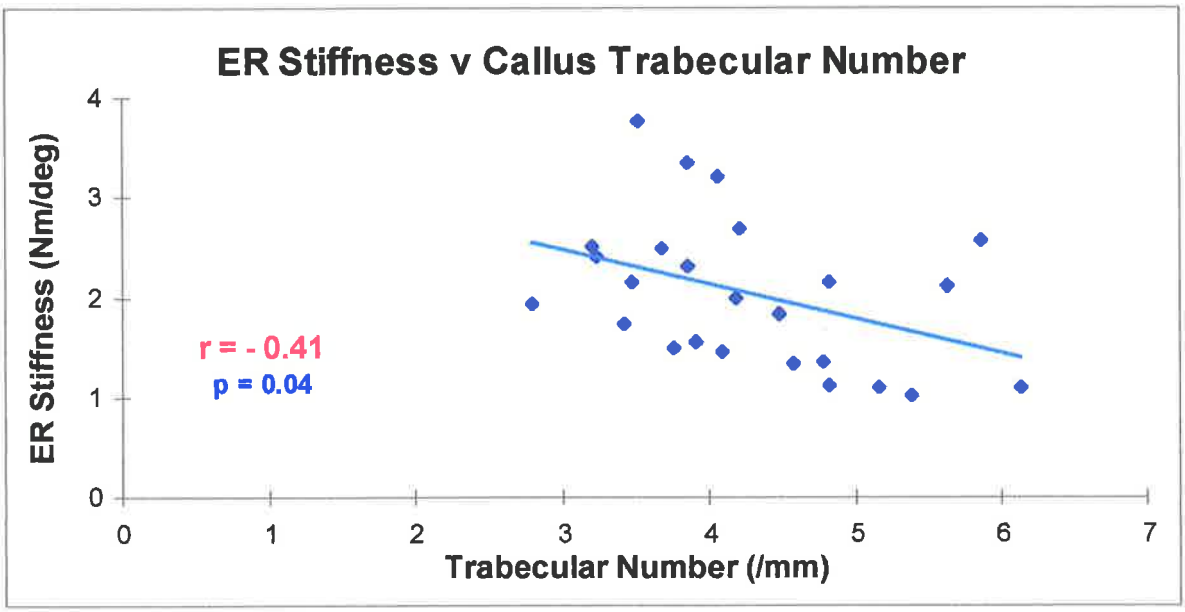

Figure 6.18 Relationship of ER stiffness to callus trabecular number

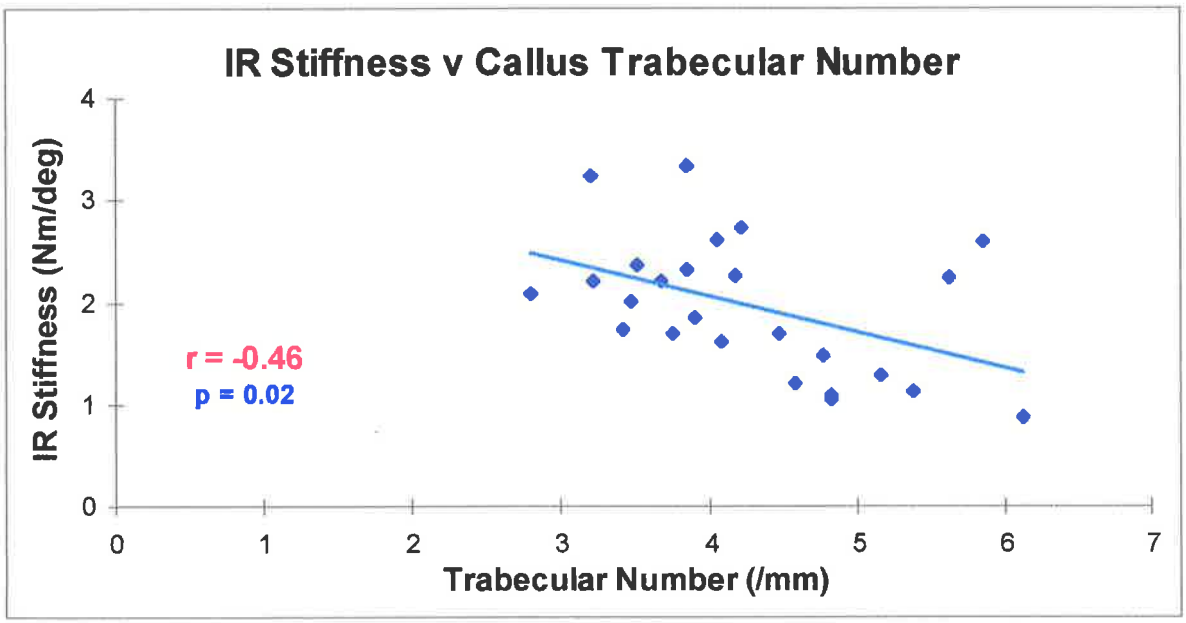

Figure 6.19 Relationship of IR stiffness to callus trabecular number

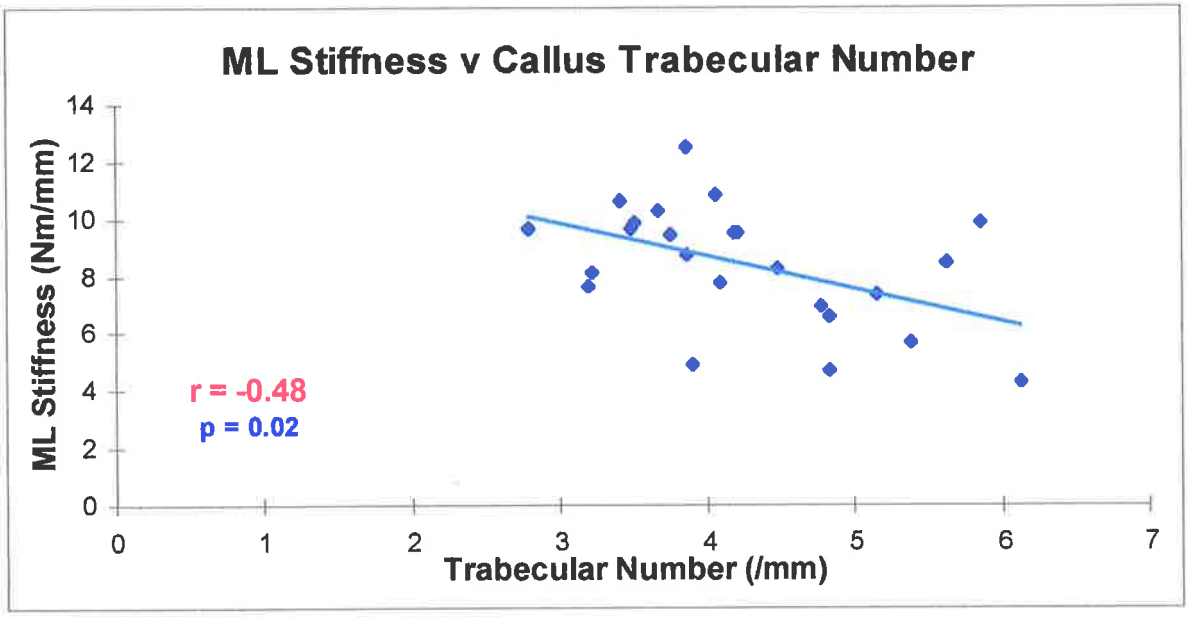

Figure 6.20 Relationship of ML stiffness to callus trabecular number

6.4.4.7 Cortical Porosity

When cortical porosity was correlated with the mechanical properties, a moderately strong and significant linear correlation was found with callus strength ($r = 0.64$, $p = 0.0005$; Table 6.11). A significant moderate correlation was found with FLS and a weak, but significant, correlation was found with AP stiffness (Table 6.11). A power regression was also performed between cortical porosity and strength which gave a much better mathematical correlation ($R^2 = 0.62$ compared with 0.42; Figure 6.21). The power of the logarithmic relation (0.5024) suggested that a better linear relationship could be obtained between strength and the square root of the cortical porosity. An improvement was found in the correlations with all mechanical properties when the square root of cortical porosity was used. In particular, the correlation with strength increased to $r = 0.70$ (Table 6.11; Figure 6.22). Graphs of the remaining significant correlations are located in Appendix K.

Table 6.11 Correlations of cortical porosity and √cortical porosity with mechanical properties

		ER	*IR*	*AP*	*ML*	*FLS*	*STR*
Cortical Porosity	*r*	0.25	0.36	0.42	0.40	0.57	**0.64**
	p	0.24	0.08	0.04	0.051	0.003	**0.0005**
√Cortical Porosity	*r*	0.34	0.47	0.47	0.54	0.65	**0.70**
	p	0.09	0.02	0.02	0.006	0.0004	**9E-05**

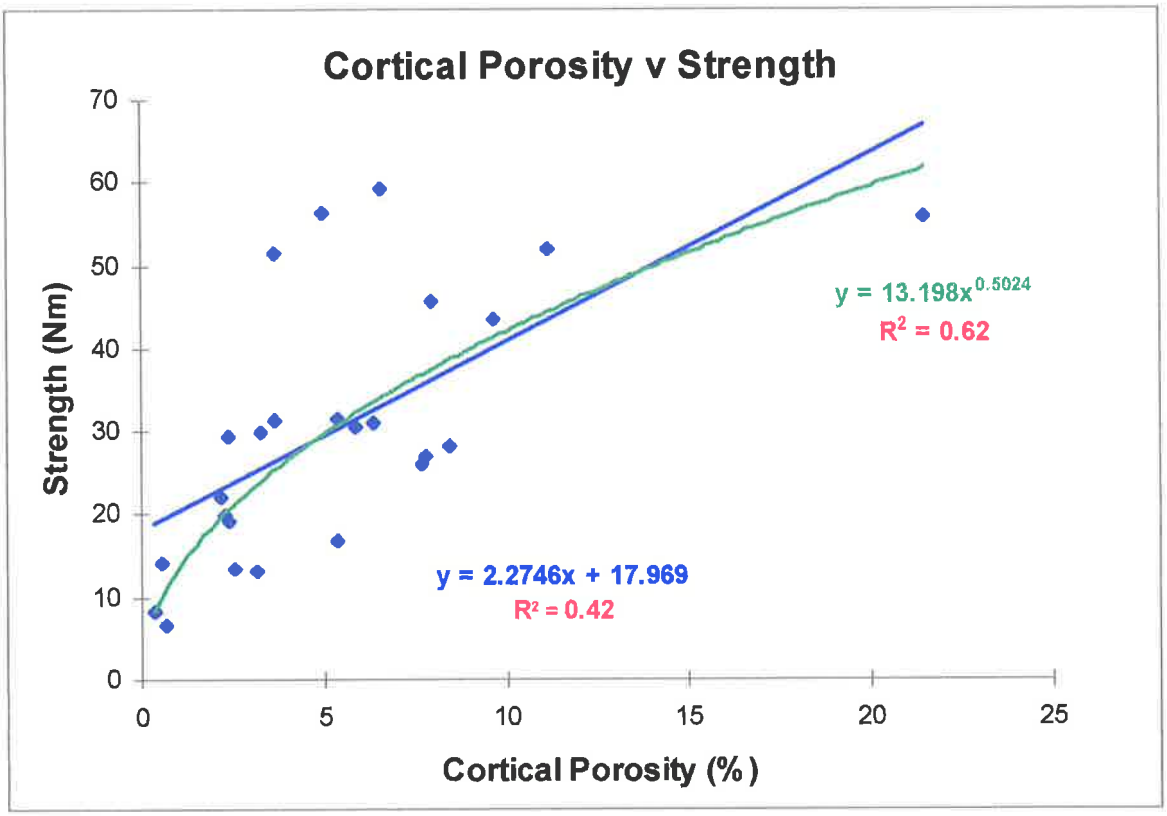

Figure 6.21 Linear and power regression analyses of relationship between strength and cortical porosity

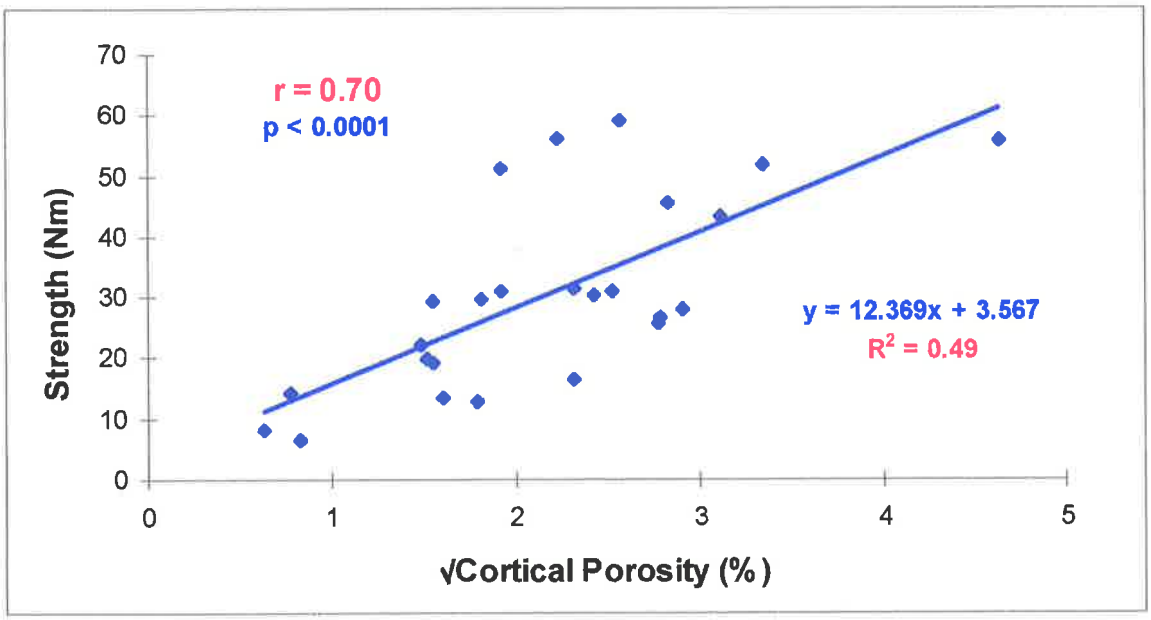

Figure 6.22 Linear relationship between strength and √cortical porosity

6.4.5 Histomorphometry v BRA

Both the BRA Frequency Index (BRA FI) and Stiffness Index (BRA SI) were correlated with the fracture histomorphometry (Table 6.12). Overall, there were slightly better correlations found with FI (when compared to SI) which was, therefore, used for the linear regression plots.

Table 6.12 Correlations of BRA SI and FI with histomorphometry

		CP	√CP	BV/TV	BS/TV	BS/BV	TbTh	TbSp	TbN
BRA FI	r	0.45	0.58	0.78	-0.70	-0.74	0.74	0.25	-0.70
	p	0.010	0.0003	1.8E-07	7.0E-06	1.1E-06	1.0E-06	0.16	7.1E-06
BRA SI	r	0.43	0.54	0.77	-0.68	-0.70	0.76	0.31	-0.68
	p	0.011	0.001	3.3E-07	1.7E-05	8.5E-06	5.5E-07	0.089	1.7E-05

6.4.5.1 Cortical Porosity

BRA was found to correlate better with cortical porosity when the square root of cortical porosity (√CP) was used. This gave a moderately strong positive correlation (Table 6.12; Figure 6.23).

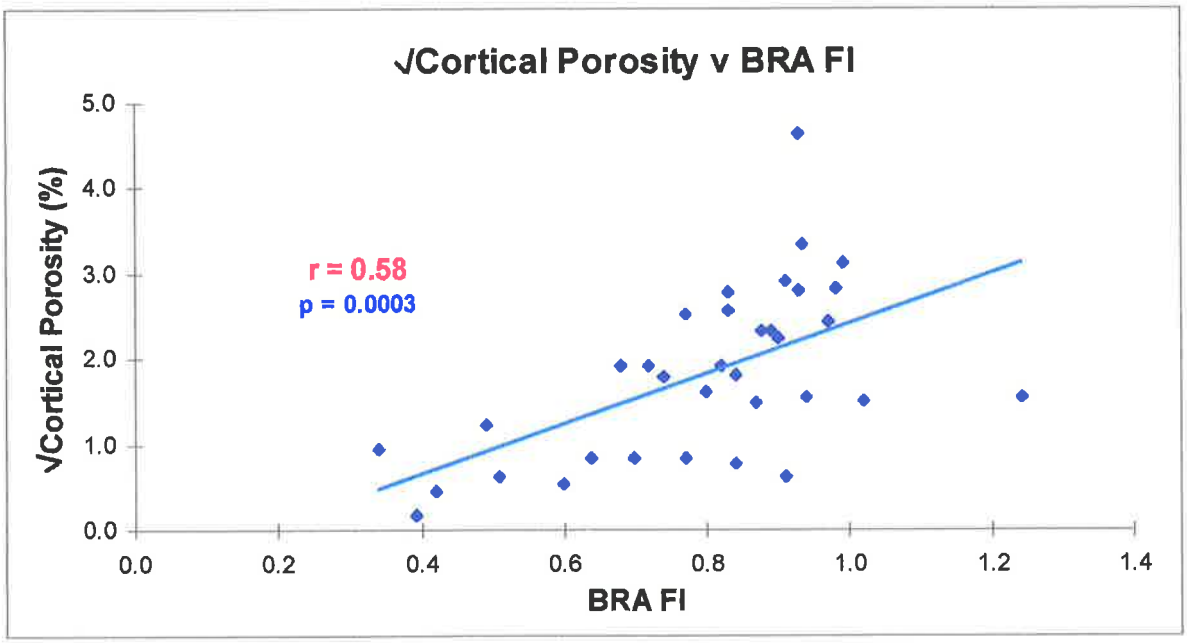

Figure 6.23 Correlation of √cortical porosity with BRA frequency index (FI)

6.4.5.2 Bone Volume

A strong and highly significant linear correlation was found between the bone volume and BRA (Table 6.12; Figure 6.24).

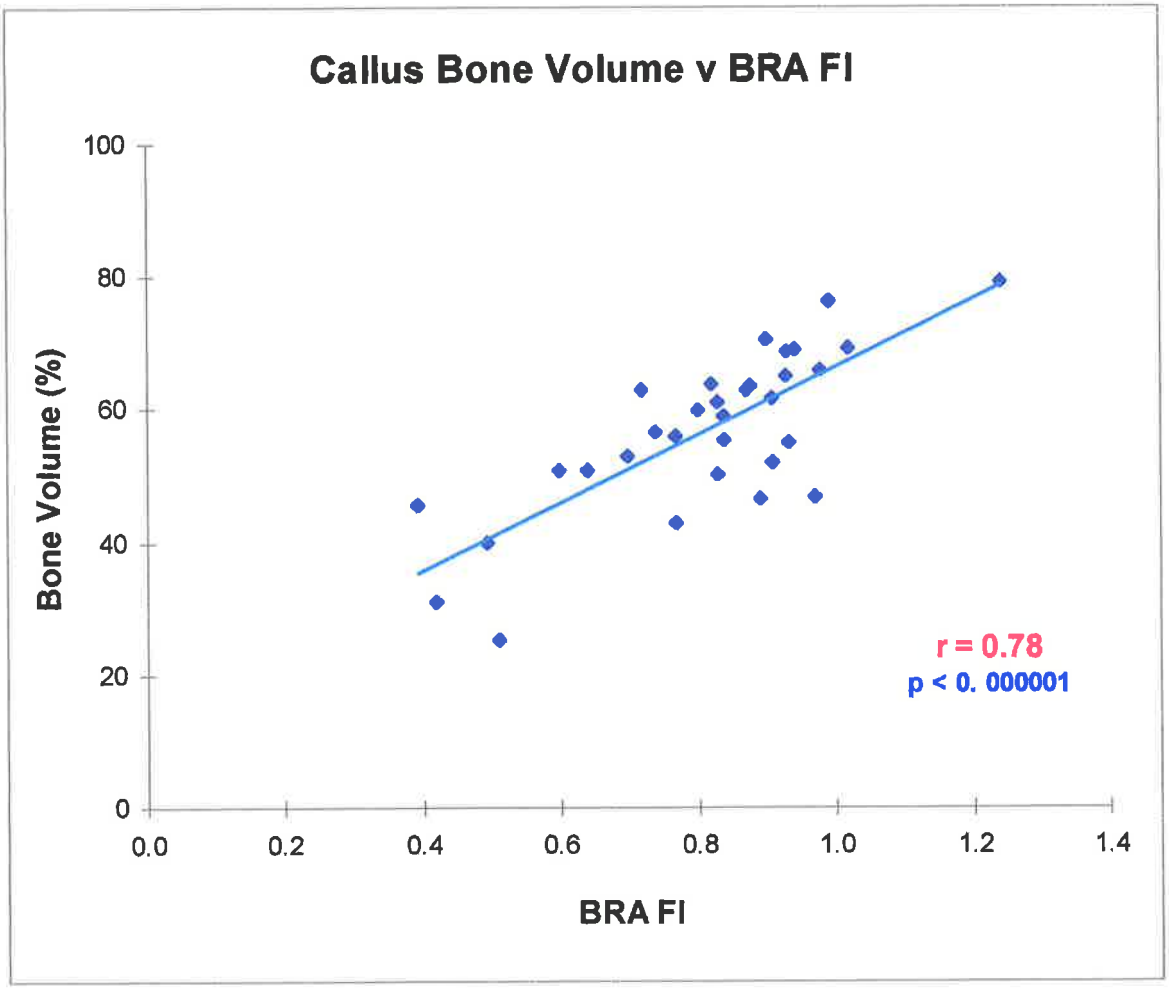

Figure 6.24 Relationship between callus bone volume and BRA frequency index (FI)

6.4.5.3 Bone Surface

A strong and highly significant negative correlation was found between BRA and the callus bone surface (Table 6.12; Figure 6.25).

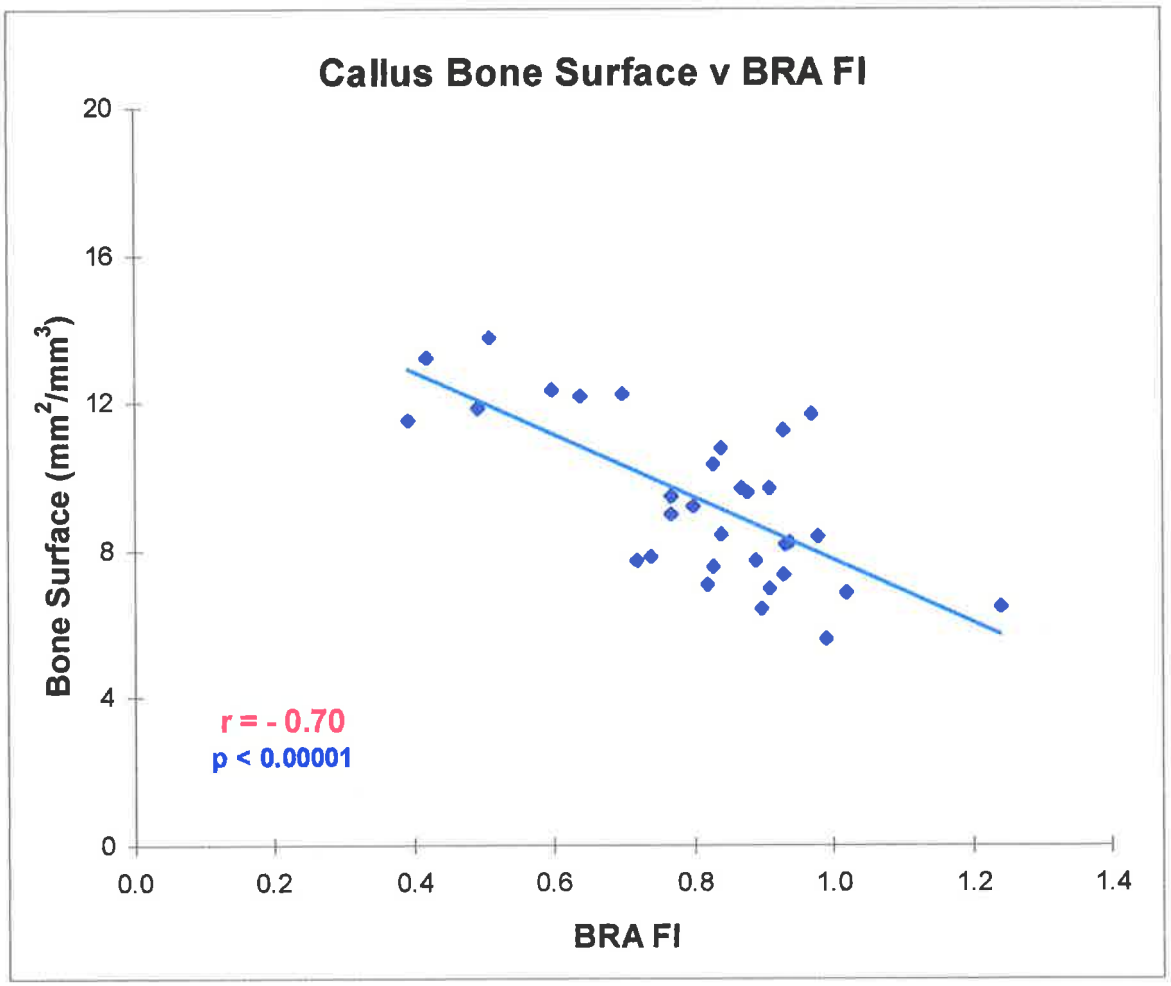

Figure 6.25 Relationship between callus bone surface and BRA frequency index (FI)

6.4.5.4 Specific Bone Surface

A strong and highly significant negative correlation was found between FI and specific bone surface (Table 6.12; Figure 6.26).

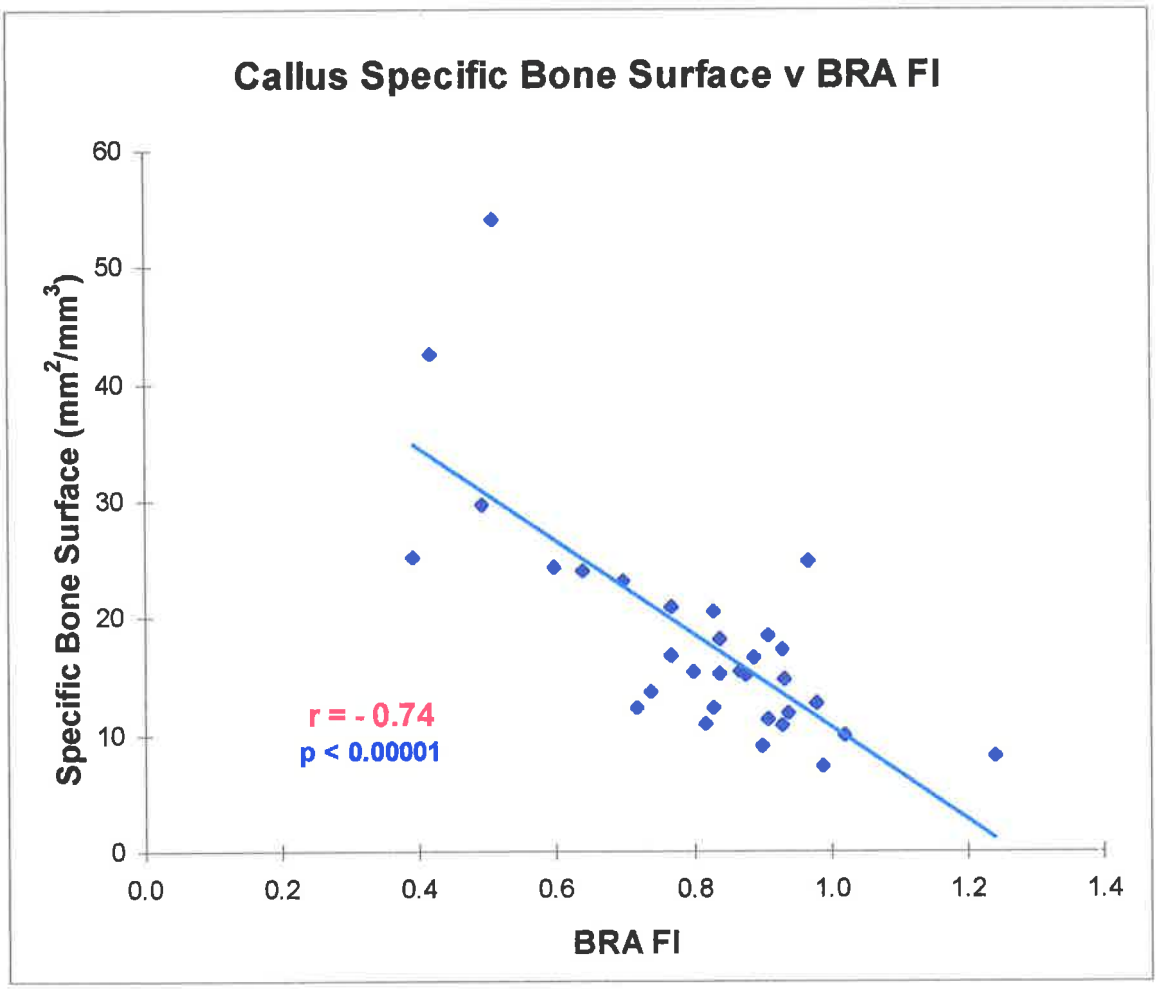

Figure 6.26 Relationship between callus specific bone surface and BRA frequency index (FI)

6.4.5.5 Trabecular Thickness

Resonant frequency increases were shown to correlate strongly with increases in the thickness of the callus trabeculae (Table 6.12; Figure 6.27).

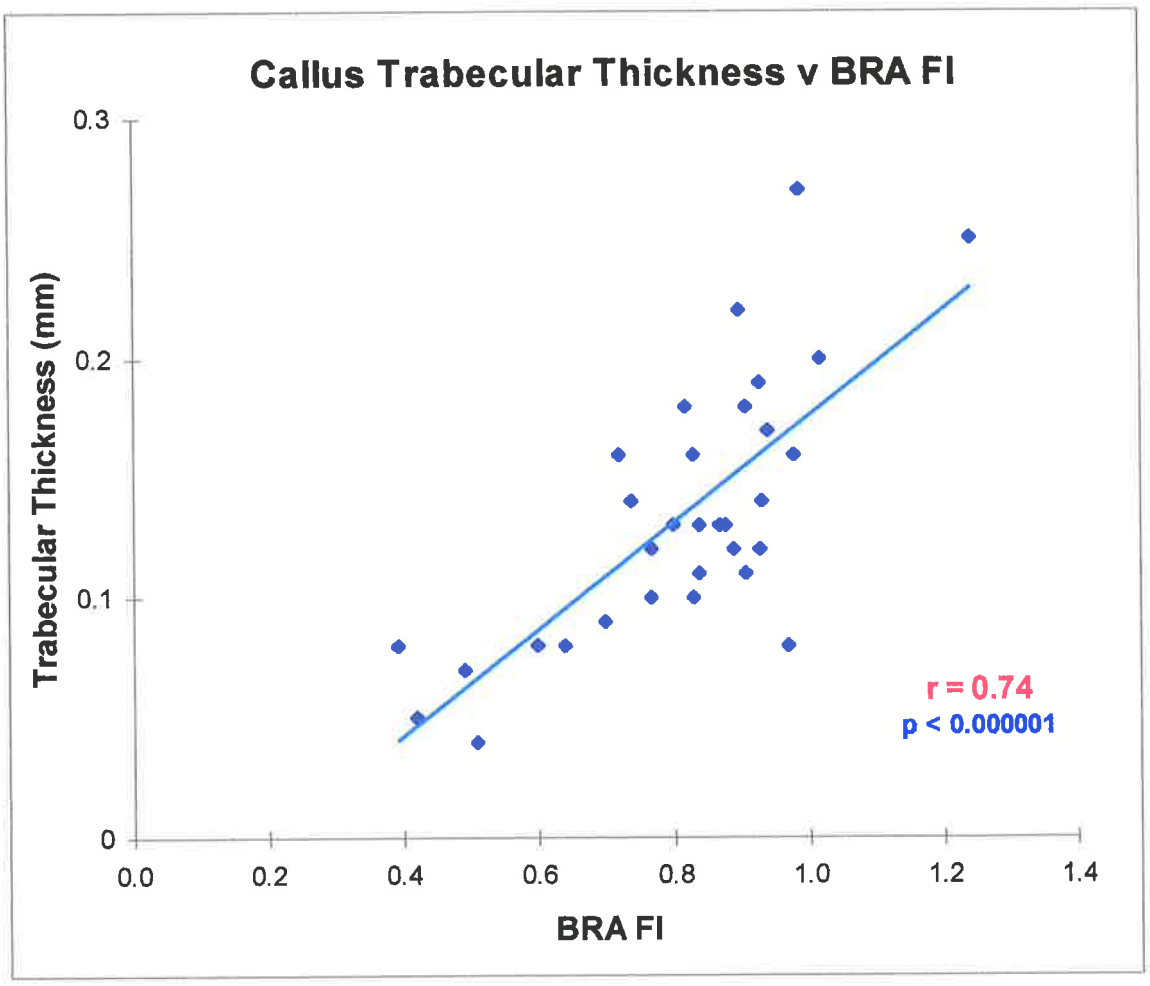

Figure 6.27 Relationship between callus trabecular thickness and BRA frequency index (FI)

6.4.5.6 Trabecular Separation

No significant correlation was found between BRA and trabecular separation (Table 6.12).

6.4.5.7 Trabecular Number

A strong and highly significant negative correlation was found between BRA and trabecular number (Table 6.12; Figure 6.28).

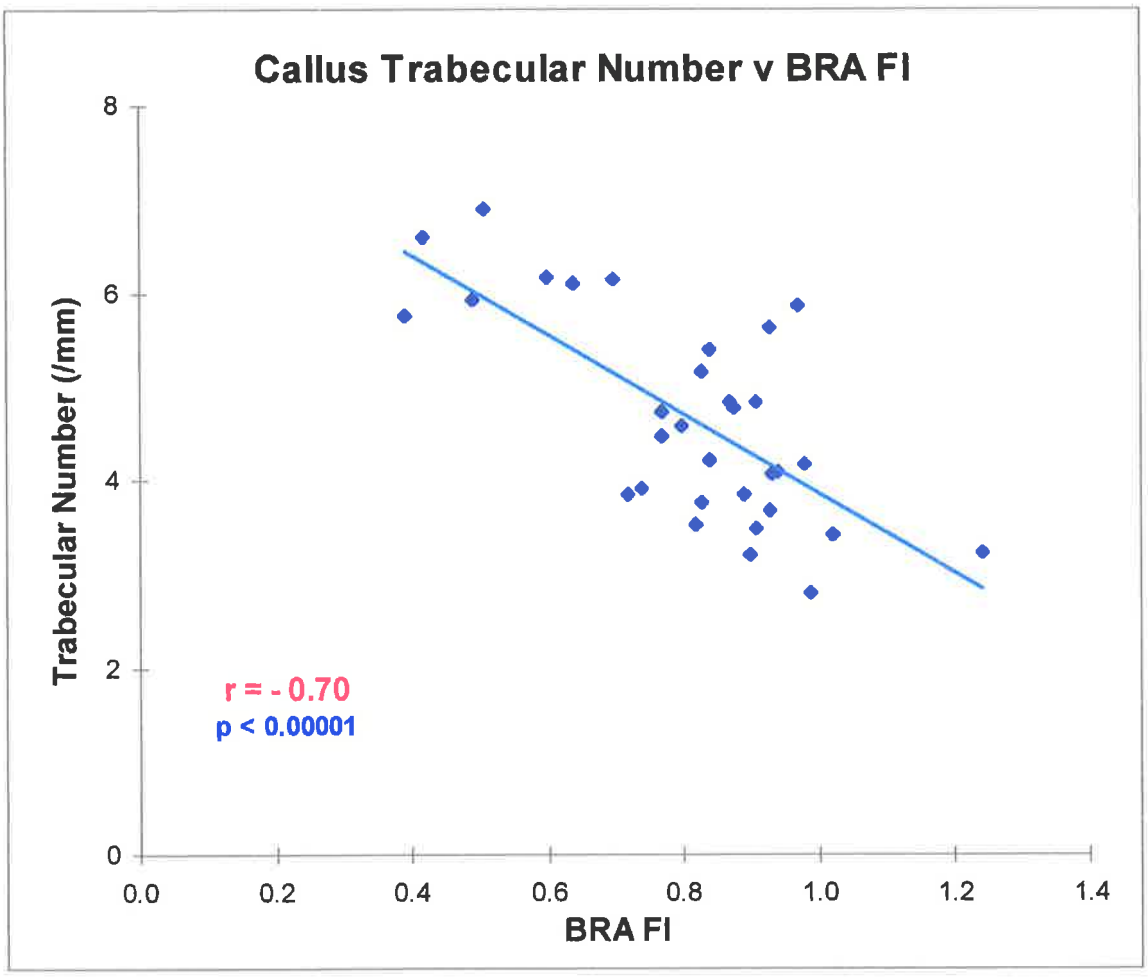

Figure 6.28 Relationship between callus trabecular number and BRA frequency index (FI)

6.5 DISCUSSION

6.5.1 Baseline Studies

In looking at the medullary and cortical widths, the means and standard deviations were found to be similar in each of the allocated time groups. This implies that, for the purpose of this study, the groups were comparable in terms of their gross morphological characteristics.

The much higher correlation between the bending stiffness and the tibial diameter, when compared with the cortical width, is consistent with basic mechanical principles and the effect of the moment of inertia, I, on bending stiffness. In this regard, the stronger correlation of bending stiffness with the medullary width (when compared with the cortical width) was probably because the medullary width was a reflection of the overall tibial diameter. It was not a 'mechanical property' per se. The tibial diameter also correlated better with all of the stiffness measurements than did the medullary width. These results, therefore, add credence to the overall accuracy of the study data. The fact that the correlation only existed with ML Fail Stiffness and not ML Stiffness, further supports the importance of the loading conditions in the assessment of bending stiffness in long bones.

6.5.2 Fracture Histomorphometry

Considering the callus histomorphometry and the cortical porosity changes together, several conclusions can be drawn. The mineralised callus formed very quickly in this sheep fracture model, having attained its maximal overall volume by about 4 weeks. The bone trabeculae were initially relatively thin and numerous. This was followed by a simultaneous increase in trabecular thickness and a reduction in trabecular number (most obvious between weeks 2 and 6). There was no significant change in the mean trabecular separation. This occurred in conjunction with the reduction in callus specific bone surface. Figure 6.29 graphically summarises these changes.

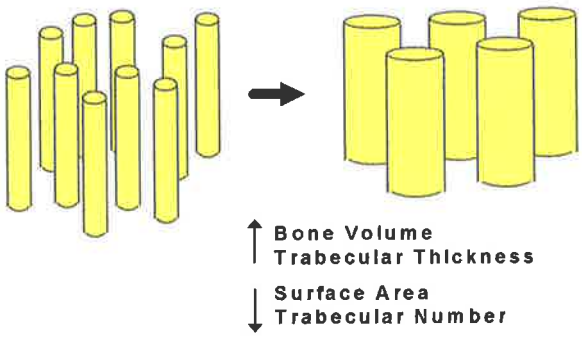

Figure 6.29 Changes in callus microstructure with progressive healing

This scenario suggests either consolidation of adjacent trabeculae or, alternatively, a remodelling phenomenon in which there is resorption of the finer trabeculae and formation of new, thicker trabeculae. In this early stage of fracture healing (first 4-6 weeks), when there is marked cellular proliferation, differentiation and organisation, one could argue for the consolidation explanation. After this period, callus remodelling may play an increasingly significant role. The greater variability in trabecular morphology noted from 6 weeks onwards would tend to support the remodelling explanation if we assume that the *rate* of remodelling is subject to greater individual variability than the *rate* of callus formation. Further support can be gained from the cortical porosity data where it can be seen that there was little change in the first 4 weeks. Thereafter there was a marked increase in porosity of the cortex in some of the fractures. This was presumably from increased resorption as part of the fracture callus remodelling process. This concept is further discussed below.

6.5.3 Mechanical Analysis

Only the callus Bone Surface and Trabecular Number showed any significant correlations with the measured mechanical properties of the healing fracture. That these correlations were almost identical is because the surface area of the trabeculae was clearly dependant on the number of trabeculae. It is interesting that the correlations were only found with torsional stiffness and ML stiffness. Why such low correlations were found with AP stiffness is not clear from this study. The external fixator may have imparted greater rigidity in the AP plane leading to callus formation and maturation in a manner which was more specifically aimed at

increasing stiffness in the mediolateral plane. That the AP plane is normally the plane of minimum stiffness in sheep tibiae is unlikely to be a significant factor when one considers that the difference is normally relatively small (Table 2.4) and also that the fracture healing occurred in the presence of an external fixator.

The weak and insignificant correlations of callus histomorphometry with ML fail stiffness and strength may indicate that these properties were being determined by histomorphometric factors not measured in this study. The type and orientation of the callus trabeculae could be important in this regard as is discussed below.

The positive nature of the correlations found between the cortical porosity and the mechanical properties are very interesting and surprising; in particular, the correlations with ML fail stiffness and strength. The stronger correlations with these factors (when compared to the stiffness determinations made under low loading conditions) suggest that the cortical porosity is acting as an index of important 'maturational' features of the healing callus. Of particular importance was that the correlations of $\sqrt{CP}$ with the mechanical properties (Section 6.4.4.7; Table 6.11) were generally stronger than those of BRA (Table 5.3). The exception was correlations of BRA FI with ML stiffness which was only very slightly better ($r = 0.56$ v 0.54). No definite conclusions, however, can be drawn from this comparison because BRA was compared with the mechanical *ratios* which are inherently inaccurate because of symmetry variance (Section 5.5.3). The true correlation of BRA with the mechanical properties is, therefore, likely to be better than this study has been able to show. The cortical porosity was correlated with the mechanical properties directly and was not subjected to the same potential errors. In an attempt to understand processes underlying the cortical porosity changes, the following argument is presented:

Increases in cortical porosity are the result of increased bone resorption relative to new bone formation. Fundamental to this action is the Basic Multicellular Unit (BMU) which is responsible for the normal bone remodelling process. For a BMU to function it must first be made active. Then, through the action of osteoclasts, the bone on which it acts is resorbed. This is followed by the formation of new bone to replace the resorbed bone. The key to explaining the cortical porosity changes may

be in the understanding of the mechanisms involved in the initial activation and control of the BMU.

One possible explanation is that "disuse" was the stimulus for the increased porosity observed in this study. A change in the normal mechanical environment of the cortex adjacent the fracture may have been the stimulus, which, by acting through other mediator mechanisms, resulted in the activation of the BMU and the subsequent increase in cortical resorption. If so, it could be assumed that in this model (in the earlier stages of fracture healing) greater "disuse" was associated with the development of greater strength. There are, however, several factors in this study which would tend to dispel this theory:

Firstly, the sheep in this study were treated with rigid external fixation. Initially, in all sheep, the cortices between the inner pins of the fractures are totally "stress - shielded". As fracture healing advanced and the fracture gap was bridged, progressively greater loads were assumedly transmitted through the fracture site and a decreasing load was taken by the external fixator. It would therefore stand to reason that, in this model, increased fracture strength would result in less "disuse". This is based on the assumption that there is no decrease in the load taken by the sheeps' fractured tibiae during ambulation. This assumption is supported by the fact that by two weeks, all sheep in this study were ambulating without any obvious "limp". This implied that the fractured tibiae were being fully loaded.

Another argument against this disuse theory is the work of other investigators (Sarmiento et al 1977; Rubin and Lanyon 1984; Goodship and Kenwright 1985; Kenwright and Goodship 1989; Kenwright et al 1991) who have found that intermittent loads across the fracture site can enhance fracture healing when compared to unloaded fractures.

An alternative theory to explain the increased cortical porosity occurring with healing, and its association with increased fracture strength, is the regional acceleratory phenomenon (RAP) reported by Frost (1983). The RAP is described as a process initiated at the time of injury, (in this case the osteotomy), and which can accelerate each phase of fracture healing by 2 to 10 fold (Section 1.4.1.6). Included in its action is its effect on the BMU mediated remodelling of the mineralised callus. In this process, the weaker mineralised cartilage and woven bone are

removed and replaced with the stronger, lamellar bone with the appropriate trabecular alignment for the biomechanical demands. Thus RAP, while acting on the callus, may be having an equivalent effect on activating the BMUs in the adjacent normal cortex. In this way, both the presence of the increased cortical porosity, and its association with the mechanical integrity of the healing fracture, might be explained.

Whatever the explanation, these findings have important potential clinical applications and warrant further research. It might even be shown that, in the early stages of fracture healing, an assessment of fracture strength may be possible by indirectly assessing the cortical porosity. This could potentially be done by radiographic means such as Dual Energy Xray Absorptiometry (DEXA). A failure of these cortical porosity changes to occur within some early time frame might also be used to predict abnormal healing. A delayed or non-union model would be required to test this hypothesis.

6.5.4 Vibrational Analysis

Apart from the weak and insignificant correlation with trabecular separation, BRA showed highly significant correlations with all of the measured histomorphometric parameters. These were particularly strong with Bone Volume and Trabecular Thickness. As these factors could be logically expected to relate to stiffness, these finding are consistent with the expectations of resonant frequency analysis. An explanation, however, is required for why the callus histomorphometry should correlate strongly with BRA yet correlate so weakly with the mechanical properties measured in this study.

In correlating histomorphometry with stiffness, a comparison was made between structural material properties on the one hand, and a combination of both material and geometric properties under the influence of load, on the other hand. BRA, by comparison, utilises very small amplitude vibrations with negligible forces compared with the 4 point bending tests utilised in this study. Even the 'low-load' tests were 'high-load' by comparison. In addition to the geometrical and material properties, the resonant frequency is also influenced by factors other than those relating directly to bone stiffness (e.g. soft tissue and boundary conditions). For such a strong correlation to exist between BRA and the histomorphometry, the

influence of such other 'non-bony factors' must be less than might have been deduced on the basis of the relatively poor correlation of BRA with stiffness alone. This further supports the assumption that the measured relationship between BRA and ML bending stiffness was largely affected by experimental error resulting from left/right variance.

Another possible influencing factor to be considered is the callus geometry. It could be hypothesised that a failure to fully account for the geometrical configuration of the callus was the reason BRA did not reflect stiffness more accurately. In other words, the BRA was reflecting the callus material properties without adequately accounting for the geometrical properties. When it is considered that the resonant frequency is related to the material and geometrical properties of the entire bone, not just the fracture site, callus geometry alone was not likely to have been the major influencing factor.

The results of this part of the study, however, have conclusively demonstrated a strong relationship between the callus microstructure and the resonant frequency using this BRA technique.

CHAPTER SEVEN

SUMMARY AND CONCLUDING REMARKS

The principal aim of this thesis was to determine the role of bone resonance analysis (BRA) in the assessment of fracture healing. In doing so, mechanical and histomorphometric properties of fracture healing were considered.

From the literature review it was evident that an absolute "endpoint" to fracture healing could not be satisfactorily defined and that any practical assessment of healing would need to be made with regard to the mechanical demands of the bone. To assess refracture risk, ultimately, an assessment of strength is required. Direct strength assessments necessitate destructive testing which are not clinically applicable. Stiffness measurements have therefore been used to assess fracture healing. Using stiffness to define an endpoint to fracture healing in terms of refracture risk assumed a workable relationship between stiffness and strength but this relationship had never been adequately assessed.

Resonant frequency analysis is an approach that has been used to assess the mechanical properties of healing fractures. Theoretically, it is an indirect measure of stiffness. No studies, however, had previously correlated in-vivo resonant frequency monitoring of healing fractures with accurately determined mechanical properties nor with fracture histomorphometry.

The details of the histomorphometric features of healing fractures in general and the relationship of histomorphometry to healing fracture mechanical properties was not clearly established in the literature and required further study.

The contra-lateral unfractured limb had frequently been used as a control for fracture healing assessment. This assumed left/right symmetry which had also not been adequately established for the vibrational or mechanical properties of long bone pairs.

Whereas an ovine model had been successfully employed in many fracture healing studies, no techniques for in-vivo vibrational analysis of sheep tibiae had previously been described.

The first part of this thesis addressed the issue of symmetry. The physical and vibrational properties of left and right sheep tibiae correlated strongly indicating that the contra-lateral limb could be used as reference of normality for these

parameters. Of the mechanical properties, the strength of left and right tibiae also correlated strongly. Bending stiffness, however, showed wide left/right variations in individual pairs making their correlations poor: even though there was no asymmetry as a population. This variability was influenced by load. Confidence in the use of the contra-lateral limb as a reference of normality for mechanical bending stiffness was therefore shown to be restricted.

This thesis also identified non linear bending stiffness properties in the sheep tibiae. In normal, unfractured tibiae, stiffness increased with load. In fracture healing, however, the non linear behaviour was not restored until more advanced healing had occurred. The stiffness of a fracture measured at low loads was quick to be restored to (or beyond) pre-fracture levels. When measured at high loads, however, the restoration of stiffness was much slower and better reflected advancing strength. This thesis, therefore, clearly showed that, because of non-linear stiffness properties, the loading conditions must be considered in any assessment of long bone stiffness.

The relationship between bending stiffness and strength was studied and a biphasic relationship was found: in the early stages of fracture healing stiffness and strength correlated strongly, but the correlation broke down with more advanced healing. In this later part of fracture healing, strength correlated much better with stiffness when the stiffness was measured at higher loads, further emphasising the importance of the non-linear properties of stiffness. These findings are important in fracture assessment because they imply inherent limitations in stiffness monitoring techniques (particularly using small loads) when the ultimate goal is an assessment of fracture strength.

A reproducible technique of in-vivo tibial resonant frequency determination in sheep was demonstrated using the non invasive BRA technique in which constant amplitude, sine swept sound waves were applied with a hand held shaker using a controlled static preload. Changes in the resonant frequency ratios during fracture healing were analogous to corresponding stiffness ratio changes: marked variations were found between sheep at each healing time. When directly related, however, only a moderate correlation was found between BRA and stiffness healing ratios. That a stronger correlation was not demonstrated was conceivably due to a

limitation in the study design: the stiffness ratio with which BRA was compared was unreliable due to the relatively poor correlation found between the bending stiffness of normal left and right tibiae. This study also showed that BRA did not correlate significantly with strength, a finding consistent with the poor correlation found between stiffness (low load) and strength in the mechanical tests.

The histomorphometry of callus in early fracture healing was described: while there was an increase in the bone volume and the thickness of the trabeculae there was a corresponding decrease in the number of trabeculae and their surface area. The separation between trabeculae did not alter significantly. The increases in bone volume and trabecular thickness correlated strongly with increases in the resonant frequency.

The porosity of the cortex adjacent the fracture site increased with fracture healing and correlated strongly with callus *strength*. This finding was best explained by a regional acceleratory phenomenon (Frost 1983) rather than a disuse osteoporosis process. This relationship between cortical porosity and strength has exciting clinical implications as it indicates a potential method of strength assessment in fracture healing.

Allowing for the limitations of an ovine model, this thesis supports the use of BRA in the assessment of fracture healing - but with limitations. The strong correlation with healing callus microstructure and, to a lesser degree, the correlation with stiffness, suggest that the principal role of BRA is in the assessment of early fracture healing: increases in the resonant frequency indicate progressive healing. Because of the poor correlation of BRA with fracture strength, the ability to determine an endpoint to fracture healing based on mechanical properties is limited using BRA. A 'baseline' for fracture strength may be predicted from a return to the prefracture resonant frequency but whether this 'baseline' is sufficient to indicate 'clinical healing' requires further study.

APPENDICES

APPENDIX A

Apparatus for vibrational symmetry testing

1. 10 sheep tibial pairs
2. Dual channel spectrum analyser — Brüel & Kjær, Type 2032
3. Preamplifier — Brüel & Kjær, Type 2635
4. Impact trigger hammer — Brüel & Kjær, Type 8202
5. Piezoelectric accelerometer — Brüel & Kjær, Type 4382
6. Computer software — Modal Analysis Package, PC-Modal
7. IBM compatible 486 personal computer equipped with a GPIB interface card
8. Metal frame
9. Fishing line

APPENDIX B

Sheep BRA reproducibility data

Resonant Frequency - Sheep 1					
Day	*Test*	*Observer 1*	*Observer 2*	*Observer 1-2*	*%Var*
1	1	592	584	8	1.4
	2	598	580	18	3.1
	3	593	588	5	0.8
2	1	584	591	7	1.2
	2	579	594	15	2.6
	3	588	588	0	0.0
3	1	595	579	16	2.7
	2	590	596	6	1.0
	3	588	593	5	0.8
Mean		590	588	9	1.5
STDev		5.8	6.1	6.1	1.0
CV		1.0	1.0		

Resonant Frequency - Sheep 2					
Day	*Test*	*Observer 1*	*Observer 2*	*Observer 1-2*	*%Var*
1	1	563	558	5	0.9
	2	558	567	9	1.6
	3	560	558	2	0.4
2	1	572	554	18	3.2
	2	555	571	16	2.8
	3	562	566	4	0.7
3	1	578	562	16	2.8
	2	577	570	7	1.2
	3	564	574	10	1.8
Mean		565	564	10	1.7
STDev		8.3	6.8	5.8	1.0
CV		1.5	1.2		

Resonant Frequency - Sheep 3					
Day	*Test*	*Observer 1*	*Observer 2*	*Observer 1-2*	*%Var*
1	1	578	567	11	1.9
	2	572	576	4	0.7
	3	584	579	5	0.9
2	1	574	558	16	2.8
	2	577	558	19	3.3
	3	580	566	14	2.4
3	1	573	569	4	0.7
	2	582	578	4	0.7
	3	568	576	8	1.4
Mean		576	570	9	1.7
STDev		5.2	8.1	5.8	1.0
CV		0.9	1.4		

Resonant Frequency - Sheep 4					
Day	*Test*	*Observer 1*	*Observer 2*	*Observer 1-2*	*%Var*
1	1	518	519	1	0.2
	2	502	514	12	2.4
	3	516	518	2	0.4
2	1	506	509	3	0.6
	2	512	506	6	1.2
	3	518	510	8	1.6
3	1	510	519	9	1.7
	2	514	518	4	0.8
	3	510	527	17	3.3
Mean		512	516	7	1.3
STDev		5.4	6.5	5.2	1.0
CV		1.1	1.3		

Resonant Frequency - Sheep 5					
Day	*Test*	*Observer 1*	*Observer 2*	*Observer 1-2*	*%Var*
1	1	612	619	7	1.1
	2	634	625	9	1.4
	3	628	628	0	0.0
2	1	625	617	8	1.3
	2	641	629	12	1.9
	3	630	624	6	1.0
3	1	633	633	0	0.0
	2	617	614	3	0.5
	3	624	618	6	1.0
Mean		627	623	6	0.9
STDev		8.9	6.4	4.0	0.6
CV		1.4	1.0		

Resonant Frequency - Sheep 6					
Day	*Test*	*Observer 1*	*Observer 2*	*Observer 1-2*	*%Var*
1	1	551	570	19	3.4
	2	570	555	15	2.7
	3	568	565	3	0.5
2	1	563	559	4	0.7
	2	579	574	5	0.9
	3	576	570	6	1.0
3	1	566	567	1	0.2
	2	566	562	4	0.7
	3	571	569	2	0.4
Mean		568	566	7	1.2
STDev		8.1	6.0	6.2	1.1
CV		1.4	1.1		

APPENDIX C

Original allocation of sheep into study groups

Sheep Identification Number	*Group Allocation*
@03	10
@04	2
@05	4
@06	2
@07	10
@08	4
@09	6
@11	8
@12	4
@13	10
@14	2
@15	8
@16	8
@17	6
@18	10
@19	8
@20	4
@21	6
@22	6
@23	4
@24	8
@25	8
@26	2
@27	4
@28	4
@29	10
@30	4
@31	2
@32	10
@33	10
@35	6
@36	8
@38	6
@39	2
@40	6
@41	6
@42	2
@43	2
@44	8
@45	10

APPENDIX D

Mechanical test results

(* denotes missing data; *C* denotes control data from right tibiae)

NAME	GROUP	IR	IRC	ER	ERC	AP	APC	ML	MLC	FLS	FLSC	STR	STRC
		Nm/deg				Nm/mm						Nm	
@03	8	1	2.6	1.4	2.58	5.9	7.63	6.9	8.84	6.77	11.1	16.6	91.13
@04	2												
@05	4												
@06	2												
@07	10	2	2.1	1.9	2.06	7.8	7.96	9.6	7.82	10.7	14.67	43.4	99.63
@08	4												
@09	6	2	3	1.6	2.71	5.2	9.37	4.9	8.66	5.39	16.27	13	110.25
@11	8	2	2.7	1.7	2.5	10	10.09	11	11.8	10.4	13.87	19.9	89
@12	4	1	2.3	1.1	2.08	5.4	7.48	4.3	10.8	4.46	18.06	6.63	123.13
@13	8	1	1.7	1.1	1.7	7.8	10.24	7.3	10.7	9.24	13.42	25.9	81.25
@14	2												
@15	8	2	2.7	2.4	2.56	4.7	8.73	8.1	8.8	9.4	14.02	29.3	96.38
@16	8	3	2.6	2.5	2.15	8.3	8.89	7.6	9.56	11.4	15.54	56.3	104
@17	6	1	2.3	1.3	1.51	4.4	8.99	*	11.1	5.38	16.15	13.4	107.5
@18	10	2	1.9	1.5	1.92	6.8	9.29	7.7	10	6.57	8.37	19.1	61.75
@19	8	2	1.7	2	1.97	6.8	8.56	9.5	7.5	9.1	12.26	45.5	92.5
@20	4	1	2.2	2.1	2.05	5.8	8.96	6.6	8.91	6.53	12.08	22	96.55
@21	6	1	1.8	1.1	1.73	3.2	6.75	4.7	7.57	5	10.96	8.13	92
@22	6	2	2.4	1.8	2.48	7	6.84	8.3	9.69	9.12	13.16	31	95.63
@23	4	1	1.9	1	1.95	7	11	5.7	9.79	6.29	13.06	14.1	97.75
@24	8	2	2.1	2.2	2.11	6	6.89	9.6	8.48	9	9.05	28	84.13
@25	8	3	4.4	2.6	3.47	11	11.29	9.8	9.03	12.1	12.92	30.5	67.5
@26	2												
@27	4												
@28	4												
@29	10	2	4.3	1.5	3.88	7.5	10.29	9.4	12.1	10.6	16.09	59	95.75
@30	4												
@31	2												
@32	10	2	4.3	2.1	3.46	8.7	8.89	8.5	10.5	12.2	15	55.8	111.75
@33	10	2	4	3.8	2.34	7.1	12	9.8	11.8	12.5	16.6	51.3	124.38
@35	6												
@36	8	3	3.7	3.2	3.11	8.7	10.83	11	11.6	13.1	15.2	51.9	92.25
@38	6	3	4.2	2.7	3.4	7.3	11.51	9.5	11.3	10.6	18.86	29.9	107.38
@39	2												
@40	6	2	2.7	2.3	2.5	6.3	9.17	8.8	12.3	9.23	15.07	31.1	128.5
@41	6												
@42	2												
@43	2												
@44	8	2	3.5	2.5	2.85	6.8	7.21	10	10.4	10.4	13.4	26.9	114.25
@45	10	3	*	3.3	*	8.9	6.78	13	10.9	13.3	16.6	31.5	128.13

APPENDIX E

ANOVA of distribution of mechanical properties in controls

Anova: Single Factor **IR STIFFNESS**

SUMMARY

Groups	Count	Sum	Average	Variance
4	3	6.34	2.11	0.03
6	6	16.39	2.73	0.66
8	10	27.7	2.77	0.73
10	5	16.52	3.30	1.55

ANOVA

Source of Variation	SS	df	MS	F	P-value	F crit
Between Groups	2.72	3	0.91	1.13	**0.36**	3.10
Within Groups	16.10	20	0.80			
Total	18.82	23				

Anova: Single Factor **ER STIFFNESS**

SUMMARY

Groups	Count	Sum	Average	Variance
4	3	6.08	2.03	0.00
6	6	14.33	2.39	0.47
8	10	25	2.50	0.29
10	5	13.66	2.73	0.78

ANOVA

Source of Variation	SS	df	MS	F	P-value	F crit
Between Groups	0.98	3	0.33	0.81	**0.51**	3.10
Within Groups	8.12	20	0.41			
Total	9.10	23				

Anova: Single Factor **AP STIFFNESS**

SUMMARY

Groups	*Count*	*Sum*	*Average*	*Variance*
4	3	27.44	9.15	3.12
6	6	52.63	8.77	3.18
8	10	90.36	9.04	2.35
10	6	55.21	9.20	3.31

ANOVA

Source of Variation	*SS*	*df*	*MS*	*F*	*P-value*	*F crit*
Between Groups	0.62	3	0.21	0.07	**0.97**	3.07
Within Groups	59.77	21	2.85			
Total	60.39	24				

Anova: Single Factor **ML STIFFNESS**

SUMMARY

Groups	*Count*	*Sum*	*Average*	*Variance*
4	3	29.46	9.82	0.86
6	6	60.53	10.09	3.13
8	10	96.62	9.66	1.96
10	6	63.23	10.54	2.41

ANOVA

Source of Variation	*SS*	*df*	*MS*	*F*	*P-value*	*F crit*
Between Groups	3.02	3	1.01	0.45	**0.72**	3.07
Within Groups	47.04	21	2.24			
Total	50.06	24				

Anova: Single Factor **ML FAIL STIFFNESS**

SUMMARY

Groups	*Count*	*Sum*	*Average*	*Variance*
4	3	43.2	14.40	10.29
6	6	90.47	15.08	7.50
8	10	130.78	13.08	3.68
10	6	87.33	14.56	9.84

ANOVA

Source of Variation	*SS*	*df*	*MS*	*F*	*P-value*	*F crit*
Between Groups	17.68	3	5.89	0.88	**0.47**	3.07
Within Groups	140.40	21	6.69			
Total	158.08	24				

Anova: Single Factor **CONTROL STRENGTH**

SUMMARY

Groups	Count	Sum	Average	Variance
4	3	317.43	105.81	225.35
6	6	641.26	106.88	165.48
8	10	912.39	91.24	160.03
10	6	621.39	103.57	585.75

ANOVA

Source of Variation	SS	df	MS	F	P-value	F crit
Between Groups	1226.54	3	408.85	1.52	**0.24**	3.07
Within Groups	5647.11	21	268.91			
Total	6873.65	24				

APPENDIX F

Fracture study BRA data

SHEEP	*GROUP*	*FI*	*SI*
@14	2	0.39	0.16
@31	2	0.51	0.26
@39	2	0.42	0.18
@42	2	0.49	0.24
@43	2	0.34	0.12
@05	4	0.68	0.46
@08	4	0.64	0.41
@12	4	0.70	0.48
@20	4	0.87	0.76
@23	4	0.84	0.71
@28	4	0.60	0.36
@30	4	0.77	0.59
@09	6	0.74	0.55
@17	6	0.80	0.64
@21	6	0.91	0.82
@22	6	0.77	0.6
@38	6	0.84	0.7
@40	6	0.72	0.52
@03	8	0.88	0.77
@11	8	1.02	1.04
@13	8	0.83	0.7
@15	8	1.24	1.54
@16	8	0.90	0.82
@19	8	0.98	0.95
@24	8	0.91	0.82
@25	8	0.97	0.94
@36	8	0.93	0.87
@44	8	0.93	0.87
@07	10	0.99	0.98
@18	10	0.94	0.89
@29	10	0.83	0.68
@32	10	0.93	0.86
@33	10	0.82	0.67
@45	10	0.89	0.78

APPENDIX G

Linear regression analysis of AP stiffness ratio with BRA FI and SI

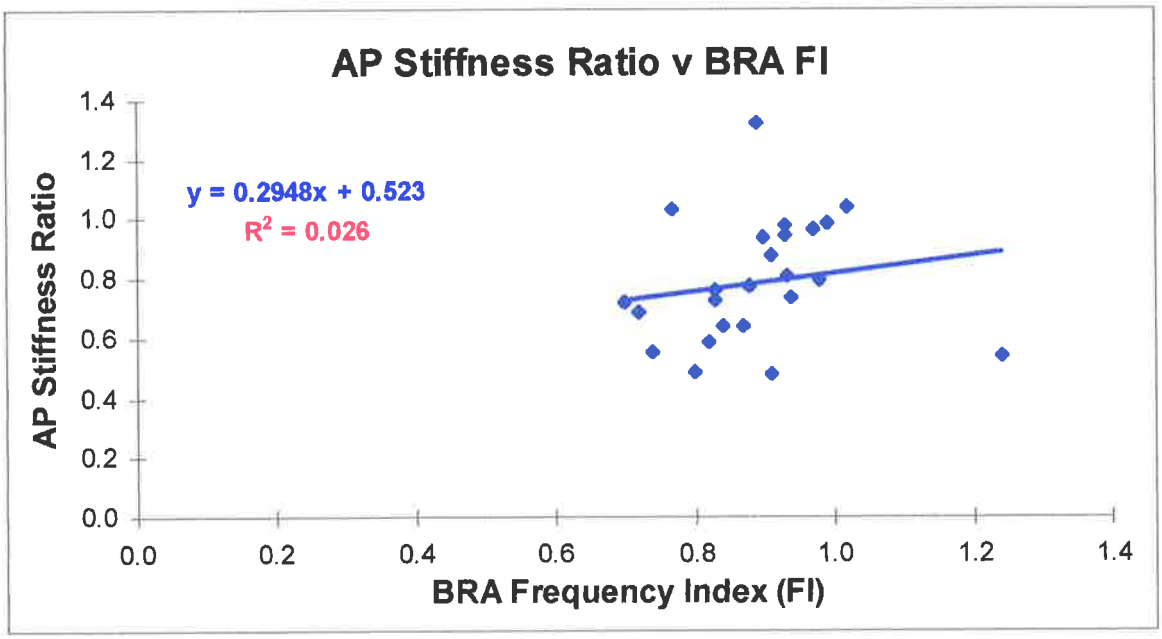

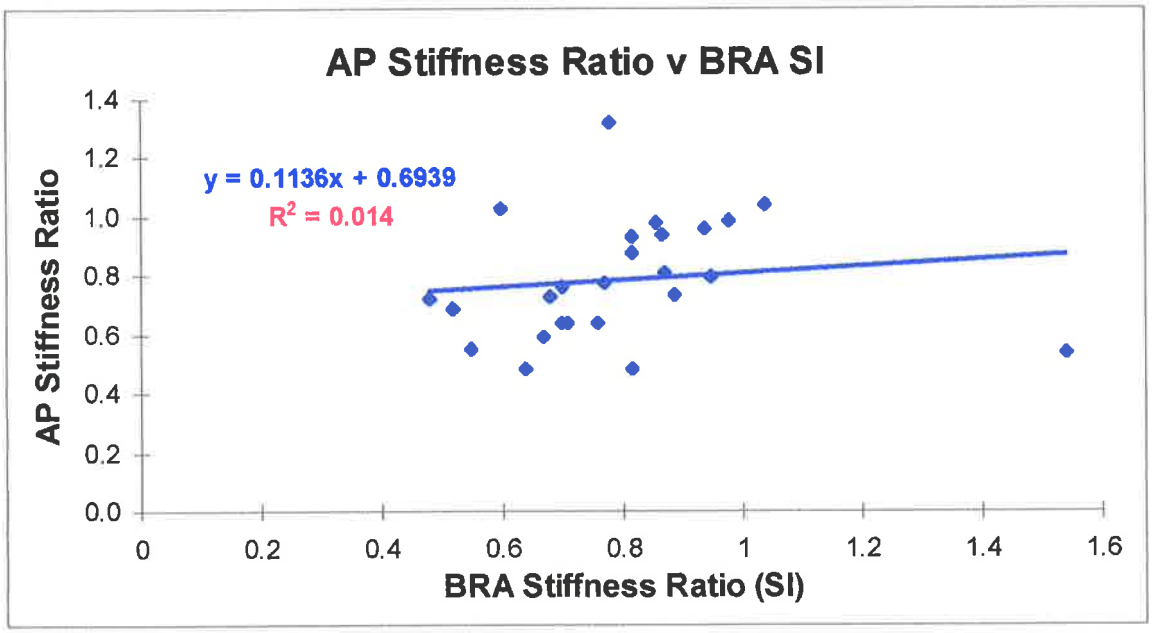

Linear regression analysis of ER stiffness ratio with BRA FI and SI

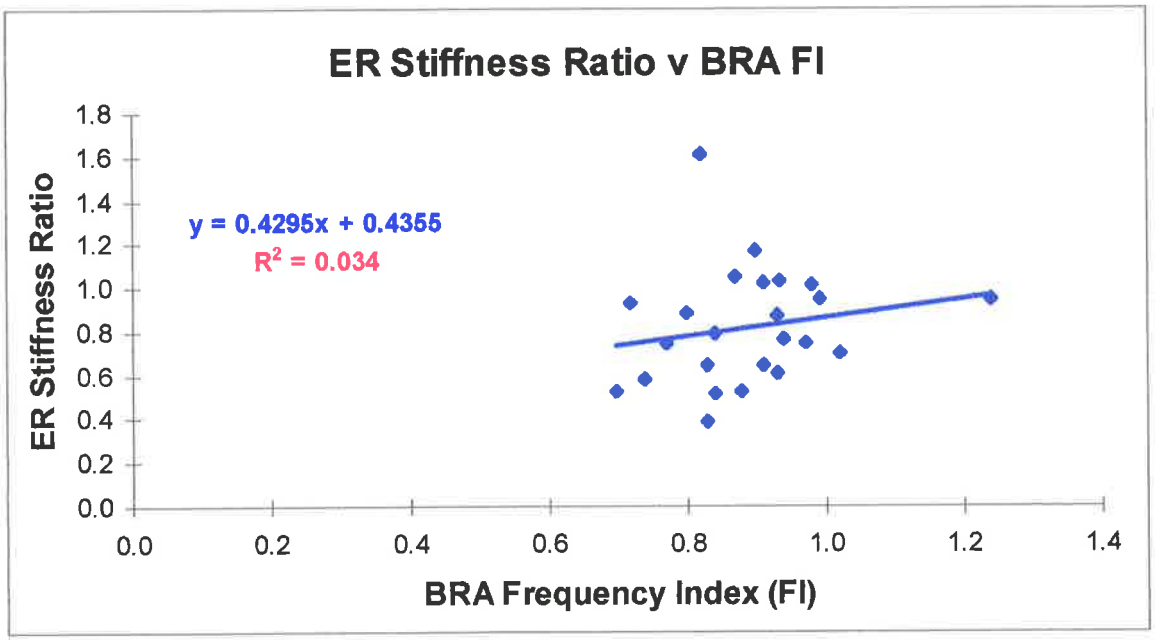

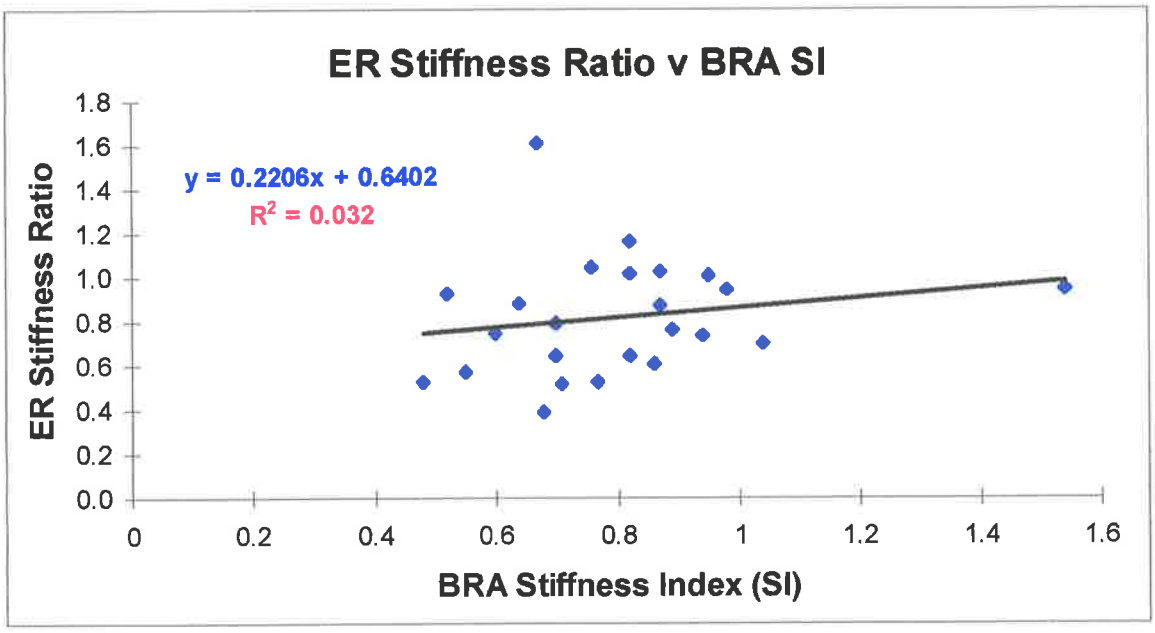

Linear regression analysis of IR stiffness ratio with BRA FI and SI

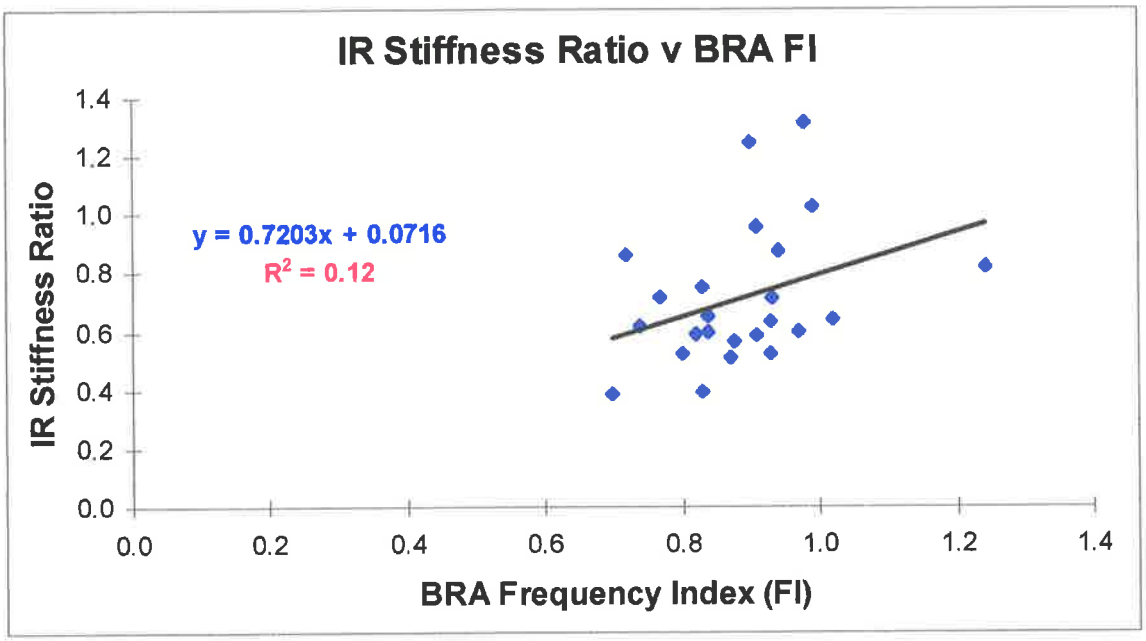

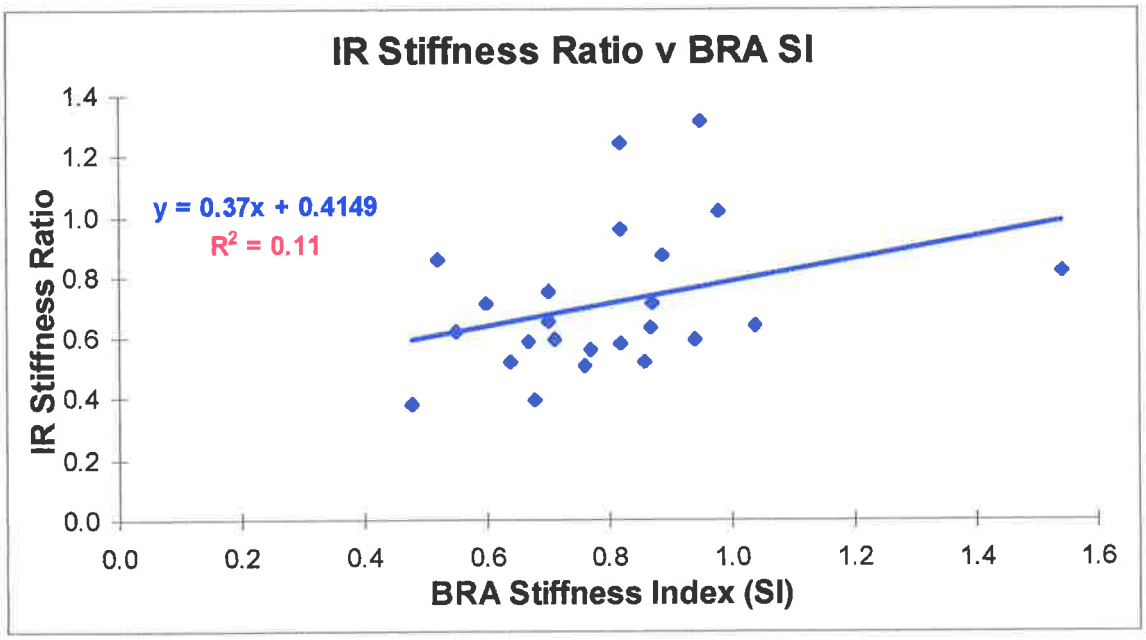

APPENDIX H

Histoquantitation setup: microscope and computer with a Quantimet 520 image analyser

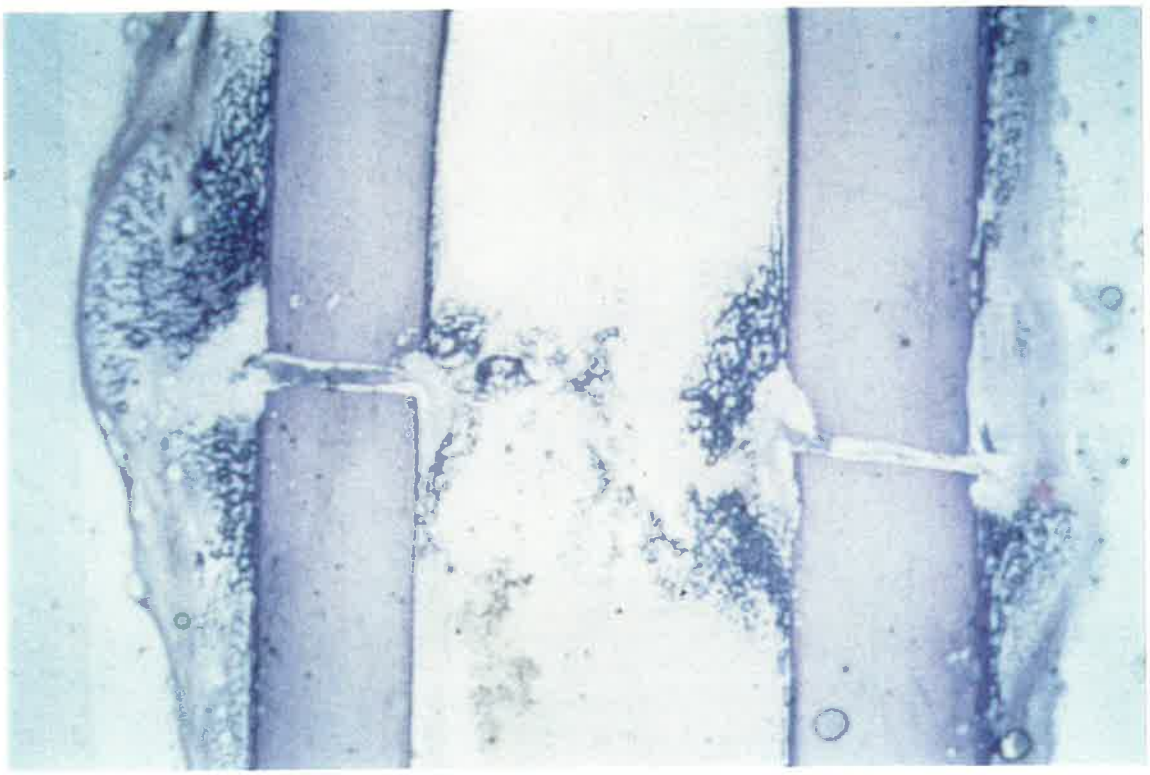

Fracture at 4 weeks

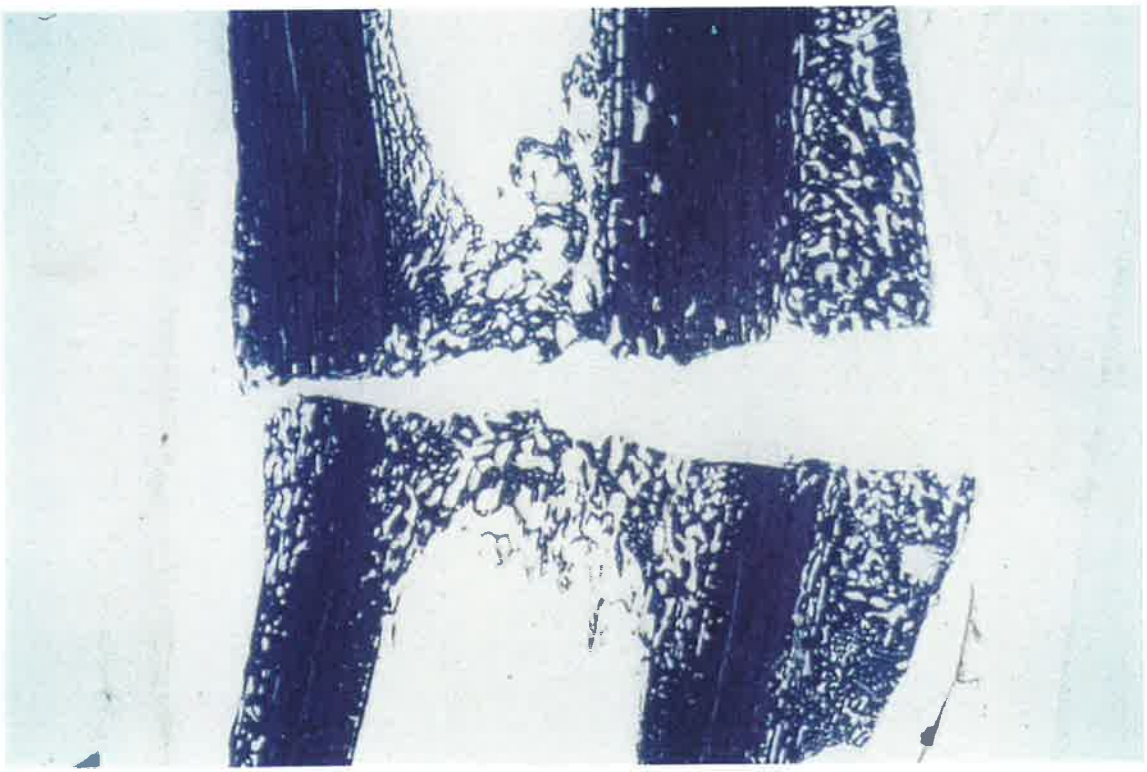

Fracture at 8 weeks

Note the porosity of the cortex compared with the fracture at four weeks.

APPENDIX I

Data on cortical and medullary widths and cortical porosity

Sheep	Group	Cortical Width (mm)	Medullary Width (mm)	Cortical Porosity (%)
@04	2	5.2	11.2	0.5
@06	2	4.6	8.6	0.2
@14	2	3.7	9.5	0.0
@26	2	5.1	9.8	0.9
@31	2	4.6	9.9	0.4
@39	2	4.8	10.2	0.2
@42	2	5.1	7.8	1.5
@43	2	4.6	7.5	0.9
@05	4	5.2	11.6	3.7
@08	4	4.6	9.0	0.7
@12	4	4.6	9.8	0.7
@20	4	4.8	8.4	2.2
@23	4	4.8	8.4	0.6
@27	4	4.3	9.2	1.1
@28	4	5.3	8.5	0.3
@30	4	5.4	9.2	0.7
@09	6	4.9	11.5	3.2
@17	6	5.4	8.9	2.6
@21	6	4.4	7.5	0.4
@22	6	5.2	8.4	6.4
@35	6	4.5	8.8	1.2
@38	6	6.2	11.5	3.3
@40	6	4.8	9.4	3.7
@41	6	4.6	9.1	3.4
@03	8	4.9	8.7	5.4
@11	8	4.2	9.6	2.3
@13	8	4.8	10.0	7.7
@15	8	4.4	8.6	2.4
@16	8	4.9	8.6	5.0
@19	8	4.8	7.7	8.0
@24	8	4.6	7.1	8.5
@25	8	4.7	9.7	5.9
@36	8	5.5	9.5	11.2
@44	8	4.9	7.9	7.8
@07	10	4.7	8.8	9.7
@18	10	5.6	6.3	2.4
@29	10	5.6	8.5	6.6
@32	10	5.7	8.5	21.5
@33	10	5.3	8.5	3.7
@45	10	4.9	10.2	5.4

Data on callus bone volume, bone surface and specific bone surface

Sheep	Group	Bone Volume BV/TV (%)	Bone Surface BS/TV (mm^2/mm^3)	Specific Bone Surface BS/BV (mm^2/mm^3)
@04	2			
@06	2			
@14	2	45.65	11.53	25.25
@26	2			
@31	2	25.52	13.77	53.96
@39	2	31.04	13.18	42.44
@42	2	39.89	11.86	29.74
@43	2			
@05	4			
@08	4	50.67	12.2	24.08
@12	4	53.02	12.25	23.11
@20	4	62.92	9.66	15.35
@23	4	59	10.75	18.22
@27	4			
@28	4	50.84	12.33	24.26
@30	4	56.02	9.45	16.87
@09	6	56.61	7.81	13.8
@17	6	59.67	9.16	15.36
@21	6	51.98	9.66	18.58
@22	6	42.99	8.96	20.83
@35	6			
@38	6	55.42	8.44	15.22
@40	6	62.7	7.72	12.31
@41	6			
@03	8	63.43	9.57	15.08
@11	8	69.14	6.84	9.9
@13	8	50.18	10.33	20.58
@15	8	79.15	6.46	8.16
@16	8	70.38	6.43	9.13
@19	8	65.96	8.35	12.66
@24	8	61.68	6.95	11.27
@25	8	46.97	11.71	24.93
@36	8	55.06	8.13	14.76
@44	8	68.45	7.36	10.75
@07	10	76.25	5.59	7.34
@18	10	68.91	8.18	11.88
@29	10	60.94	7.53	12.35
@32	10	65.1	11.27	17.3
@33	10	63.8	7.04	11.04
@45	10	46.54	7.71	16.57

Data on callus trabecular thickness, separation and number

Sheep	*Group*	*Trabecular Thickness Tb.Th (mm)*	*Trabecular Separation Tb.Sp (mm)*	*Trabecular Number Tb.N (/mm)*
@04	2			
@06	2			
@14	2	0.08	0.09	5.76
@26	2			
@31	2	0.04	0.11	6.89
@39	2	0.05	0.10	6.59
@42	2	0.07	0.10	5.93
@43	2			
@05	4			
@08	4	0.08	0.08	6.10
@12	4	0.09	0.08	6.13
@20	4	0.13	0.08	4.83
@23	4	0.11	0.08	5.38
@27	4			
@28	4	0.08	0.08	6.17
@30	4	0.12	0.09	4.73
@09	6	0.14	0.11	3.91
@17	6	0.13	0.09	4.58
@21	6	0.11	0.10	4.83
@22	6	0.10	0.13	4.48
@35	6			
@38	6	0.13	0.11	4.22
@40	6	0.16	0.10	3.86
@41	6			
@03	8	0.13	0.08	4.78
@11	8	0.20	0.09	3.42
@13	8	0.10	0.10	5.16
@15	8	0.25	0.06	3.23
@16	8	0.22	0.09	3.21
@19	8	0.16	0.08	4.18
@24	8	0.18	0.11	3.48
@25	8	0.08	0.09	5.86
@36	8	0.14	0.11	4.06
@44	8	0.19	0.09	3.68
@07	10	0.27	0.08	2.80
@18	10	0.17	0.08	4.09
@29	10	0.16	0.10	3.76
@32	10	0.12	0.06	5.63
@33	10	0.18	0.10	3.52
@45	10	0.12	0.14	3.86

APPENDIX J

Statistical analyses of cortical porosity and callus bone volume

Dependent variable: Cortical Porosity

Source	*DF*	*Sum of Squares*	*Mean Square*	*F Value*	*Pr > F*
Model	4	325.5195	81.3799	8.22	0.0001
Error	35	346.4406	9.8983		
Corrected Total	39	671.9601			

T tests:

Alpha = 0.05 Confidence = 0.95 df = 35 MSE =9.8983

Critical Value of T = 2.03011

Comparisons significant at the 0.05 level indicated by ***

Group Comparison

(2 week interval)		(4 week interval)	
2-4		2-6	
4-6		4-8	***
6-8	***	6-10	***
8-10			

Dependent variable: Bone Volume

Source	*DF*	*Sum of Squares*	*Mean Square*	*F Value*	*Pr > F*
Model	4	2509.75	627.43	8.63	0.0001
Error	27	1964.02	72.74		
Corrected Total	31	4473.77			

T tests:

Alpha = 0.05 Confidence = 0.95 df = 27 MSE = 72.74

Critical Value of T = 2.05183

Comparisons significant at the 0.05 level indicated by ***

Group Comparison

(2 week interval)		(4 week interval)	
2-4	***	2-6	***
4-6		4-8	
6-8		6-10	
8-10			

Statistical analyses of callus bone surface and specific bone surface

Dependent variable: Bone Surface

Source	*DF*	*Sum of Squares*	*Mean Square*	*F Value*	*Pr > F*
Model	4	89.27	22.31	9.71	0.0001
Error	27	62.07	2.30		
Corrected Total	31	151.34			

T tests:

Alpha = 0.05 Confidence = 0.95 df = 27 MSE = 2.30

Critical Value of T = 2.05183

Comparisons significant at the 0.05 level indicated by

Group Comparison

(2 week interval)		(4 week interval)	
2-4		2-6	***
4-6	***	4-8	
6-8		6-10	
8-10			

Dependent variable: Specific Bone Surface

Source	*DF*	*Sum of Squares*	*Mean Square*	*F Value*	*Pr > F*
Model	4	1978.48	494.62	13.92	0.0001
Error	27	959.63	35.54		
Corrected Total	31	2938.11			

T tests:

Alpha = 0.05 Confidence = 0.95 df = 27 MSE = 35.54

Critical Value of T = 2.05183

Comparisons significant at the 0.05 level indicated by ***

Group Comparison

(2 week interval)		(4 week interval)	
2-4	***	2-6	***
4-6		4-8	***
6-8		6-10	
8-10			

Statistical analyses of trabecular thickness, separation and number

Dependent variable: Trabecular Thickness

Source	*DF*	*Sum of Squares*	*Mean Square*	*F Value*	*Pr > F*
Model	4	0.04576	0.011439	6.65	0.0007
Error	27	0.04642	0.001719		
Corrected Total	31	0.09217			

T tests:

Alpha = 0.05 Confidence = 0.95 df = 27 MSE = 0.001719

Critical Value of T = 2.05183

Comparisons significant at the 0.05 level indicated by ***

Group Comparison			
(2 week interval)		(4 week interval)	
2-4		2-6	***
4-6		4-8	***
6-8		6-10	
8-10			

Dependent variable: Trabecular Separation

Source	*DF*	*Sum of Squares*	*Mean Square*	*F Value*	*Pr > F*
Model	4	0.00217	0.00054	2.11	0.1072
Error	27	0.00695	0.00026		
Corrected Total	31	0.00912			

Dependent variable: Trabecular Number

Source	*DF*	*Sum of Squares*	*Mean Square*	*F Value*	*Pr > F*
Model	4	22.3562	5.5890	9.73	0.0001
Error	27	15.5027	0.5742		
Corrected Total	31	37.8589			

T tests:

Alpha = 0.05 Confidence = 0.95 df = 27 MSE = 0.5742

Critical Value of T = 2.05183

Comparisons significant at the 0.05 level indicated by ***

Group Comparison			
(2 week interval)		(4 week interval)	
2-4		2-6	***
4-6	***	4-8	***
6-8		6-10	
8-10			

APPENDIX K

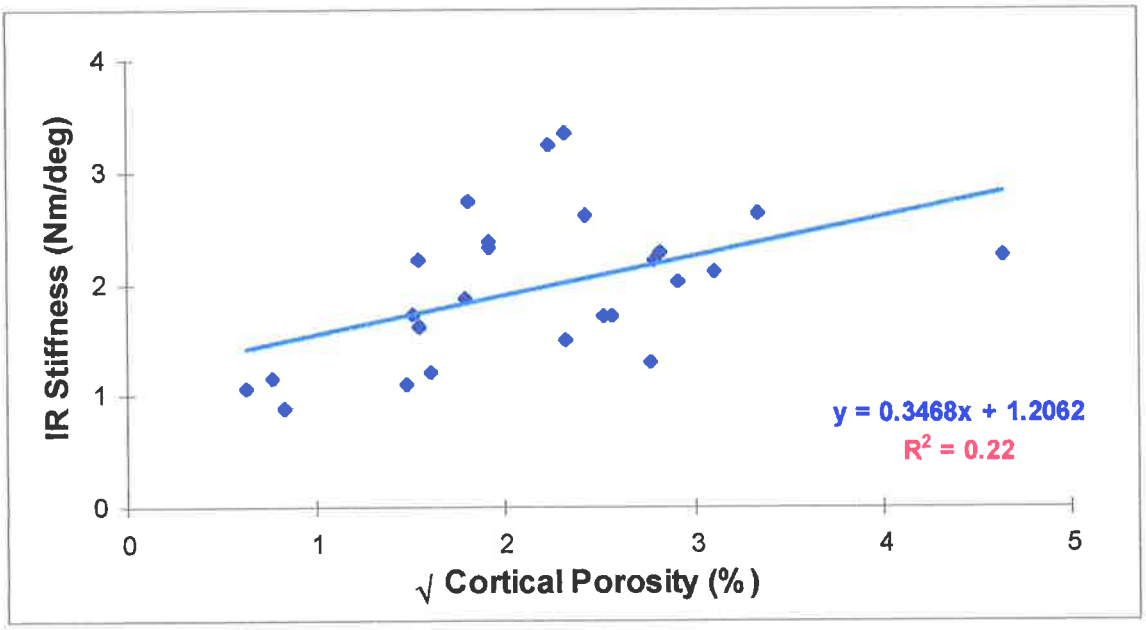

Linear correlation of IR stiffness with √cortical porosity

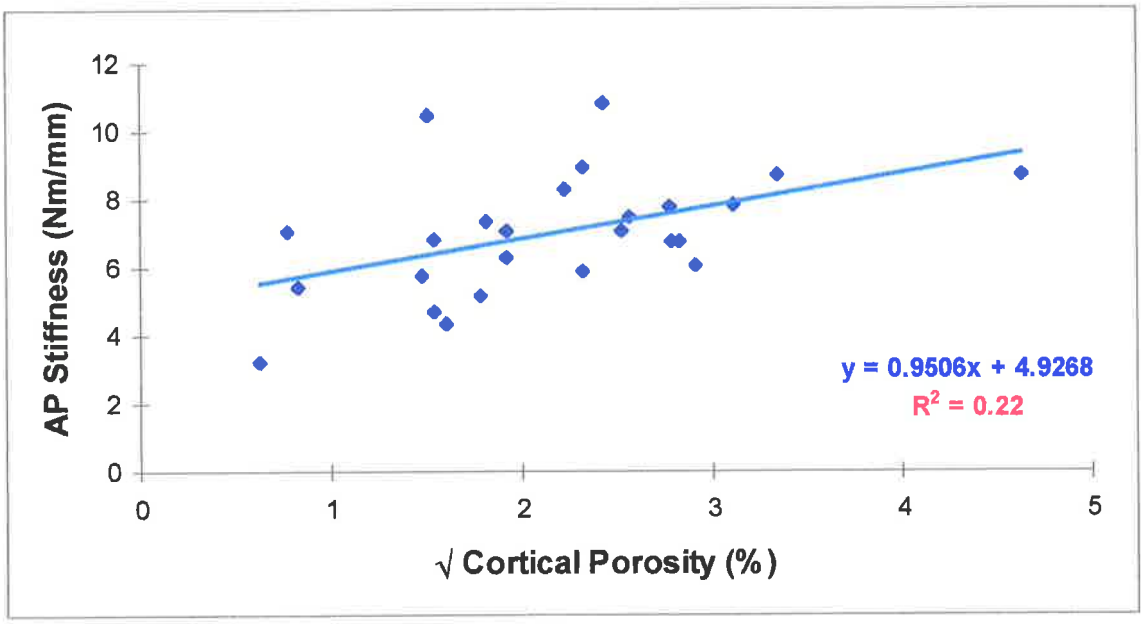

Linear correlation of AP stiffness with √cortical porosity

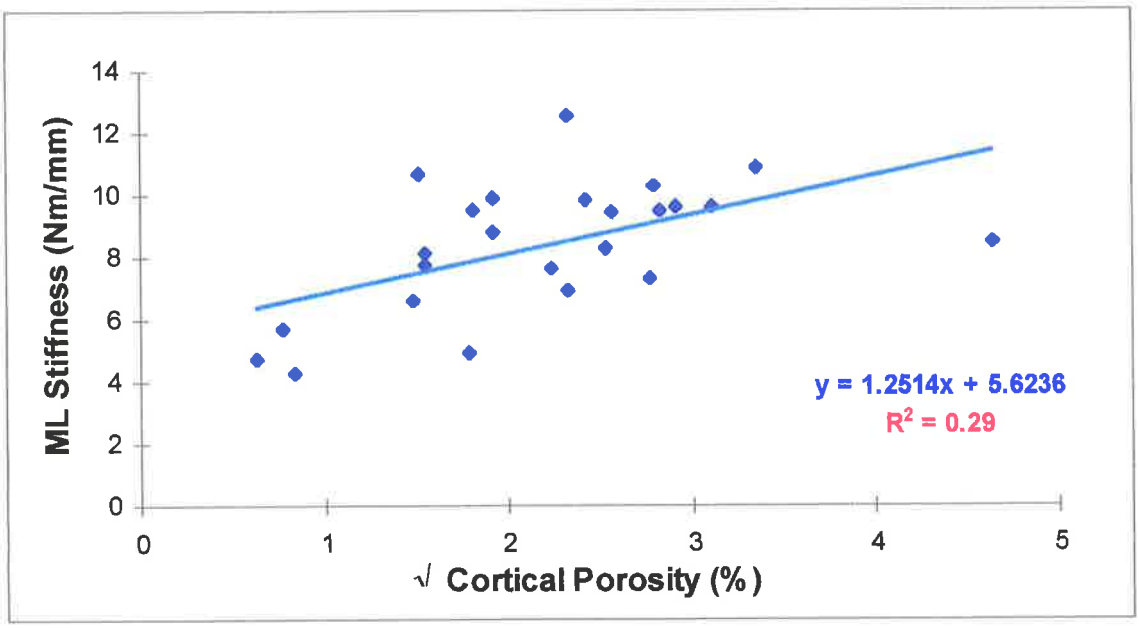

Linear correlation of ML stiffness with √cortical porosity

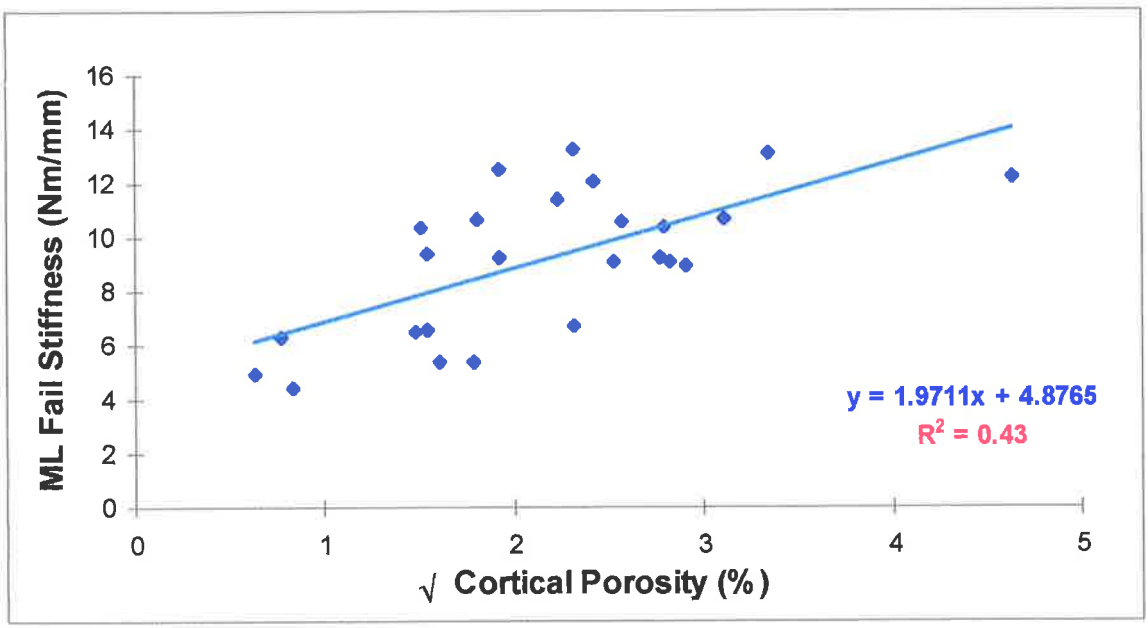

Linear correlation of ML fail stiffness with √cortical porosity

BIBLIOGRAPHY

Ammitzboll F, Borgwardt A, Dyrbye C. First clinical results with BRA supports and soft splint. In: Van Der Perre G, Borgwardt Christensen A, editors. Monitoring of Fracture Healing by Vibration Analysis and other Mechanical Methods. Leuven: K.U. Leuven, 1985:113-120.

An KN, Kasman RA, Chao EY. Theoretical analysis of fracture healing monitoring with external fixators. *Eng Med* 1988; 17:11-15.

Aro HT, Wippermann BW, Hodgson SF, Chao EY. Internal remodeling of periosteal new bone during fracture healing. *J Orthop Res* 1990; 8:238-246.

Benirschke SK, Mirels H, Jones D, Tencer AF. The use of resonant frequency measurements for the noninvasive assessment of mechanical stiffness of the healing tibia. *J Orthop Trauma* 1993; 7:64-71.

Borgwardt Christensen A, Tougaard L, Dyrbye C, Vibe Hansen H. Resonance of the human tibia. Method, reproducibility and effect of transection. *Acta Orthop Scand* 1982; 53:867-874.

Brandon JA, Richards J. A conjecture on the interface mechanics in fractures based on the interpretation of impulse vests. *Proc Inst Mech Eng H* 1989; 203:203-205.

Braunstein EM, Goldstein SA, Ku J, Smith P, Matthews LS. Computed tomography and plain radiography in experimental fracture healing. *Skeletal Radiol* 1986; 15:27-31.

Briggs T, King J, Collier RJ. A Comparison between the measurement of resonant frequency of the human tibia within and without plaster support. In: Cornelissen M, Borgwardt A, Van Der Perre G, editors. Monitoring of Bone Condition by Vibration Testing. 1988:59-60.

Buckwalter JA, Einhorn TA, Bolander ME, Cruess RL. Healing of musculoskeletal tissues. In: Rockwood CA, Green DP, Bucholz RW, Heckman JD, editors. Fractures in Adults. 3rd ed. Philadelphia . New York: Lippincott-Raven, 1991:

Burny F. Etude par jauges de deformation de deformation de la consolidation des fractures en clinique. *Acta Orthop Belg* 1968; 34:917-927.

Burny F, Donkerwolcke M, Bourgois R, Domb M, Saric O. Twenty Years Experience in Fracture Healing with Strain Gauges. *Orthopedics* 1984; 7:1823-1826.

Burny F, Donkerwolcke M, Bourgois R, Hinsenkamp M. Twenty years experience of clinical measurement of bone implants deformation with strain gauges. In: Van Der Perre G, Borgwardt Christensen A, editors. Monitoring of Fracture Healing by Vibration Analysis and other Mechanical Methods. Leuven: K.U.Leuven, 1985:145-162.

Burny F, Donkerwolcke M, Bourgois R, Saric O. Nail Plates Instrumented with Strain Gauges: Review of the First 100 Cases of Fractures of the Upper Extremity of the Femur. In: Whittle M, Harris D, editors. Biomechanical Measurement in Orthopaedic Practice. Oxford: Oxford University Press, 1985:36-43.

Burny F, Zucman J, Bourgois R, Aubriot JH, Sedel J. Utilisation des jauges extensometriques pour la mesure de la consolidation des fractures du tibia traitees par enclouage centromedullaire. *Acta Orthop Belg* 1971; 37:266-277.

Burturla E, Pope M. A finite element wave propagation model of pathogenic and healing bone. In: Anonymous Proceedings. 1st Annual New England Bioengineering Conference. Oxford: Pergamon Press, 1973:36-45.

Carter DR, Hayes WC. The compressive behavior of bone as a two-phase porous structure. *J Bone Joint Surg* 1977; 59:954-962.

Chehade MJ, Lawes TJ, and Pohl AP. Influence of shaker static preload on resonant frequency determinations using BRA. *Proceedings of the AOA annual scientific meeting (SA branch)*.1993.

Chehade MJ, Pohl AP. Update on BRA: An improved reproducible technique. *Proceedings of the AOA annual scientifc meeting (SA branch)*.1992.

Chen II, Saha S. Wave propagation characteristics in long bones to diagnose osteoporosis. *J Biomech* 1987; 20:523-527.

Cheng S, Komi PV, Kyrolainen H, Kim DH, Hakkinen K. In vivo vibrational wave propatation in human tibiae at different ages. *Eur J Appl Physiol* 1989; 59:128-130.

Chibber SR, Singh I. Asymmetry in muscle weight in the human lower limbs. *J Anat London* 1970; 106:553-556.

Chibber SR, Singh I. Asymmetry in muscle weight in the human uper limbs. *Acta Anat (Basel)* 1971; 81:462-465.

Chrisman OD, Snook GA. The problem of refracture of the tibia. *Clin Orthop* 1968; 60:217-219.

Christensen AB, Ammitzboll F, Dyrbye C. Resonance of Human Tibia - Assessment to Fracture Healing. In: Woo SL, Mates RE, editors. American Society of Mechanical Engineers Biomechanics Symposium. 56th ed. New York: A.S.M.E. 1983:205-208.

Christensen AB, Ammitzboll F, Dyrbye C, Cornelissen M, Cornelissen P, Van der Perre G. Assessment of tibial stiffness by vibration testing in situ--I. Identification of mode shapes in different supporting conditions. *J Biomech* 1986; 19:53-60.

Collier RJ, Donarski RJ. Non-invasive method of measuring resonant frequency of a human tibia in vivo. Part 1. *J Biomed Eng* 1987; 9:321-328.

Collier RJ, Donarski RJ. Non-invasive method of measuring the resonant frequency of a human tibia in vivo. Part 2. *J Biomed Eng* 1987; 9:329-331.

Collier RJ, Nadav O, Thomas TG. The mechanical resonances of a human tibia: part I--in vitro. *J Biomech* 1982; 15:545-553.

Cornelissen M, Cornelissen P, Van der Perre G. A Dynamic Model For A Healing Fractured Tibia. In: Huiskes R, Van Campen DH, de Wijn JR, editors. Biomechanics: Principles and Applications. The Hague: Martinus Nijhoff, 1982:213-218.

Cornelissen M, Cornelissen P, Van der Perre G, Ammitzboll F, Christensen AB, Dyrbye C. Vibration measurements correlated with mechanical stability characteristics II. An experimental study. In: Van Der Perre G, Borgwardt Christensen A, editors. Monitoring of Fracture Healing by Vibrational Analysis and other Mechanical Methods. leuven: acco, 1985:91-97.

Cornelissen M, Cornelissen P, Van der Perre G, Christensen AB, Ammitzboll F, Dyrbye C. Assessment of tibial stiffness by vibration testing in situ--III. Sensitivity of different modes and interpretation of vibration measurements. *J Biomech* 1987; 20:333-342.

Cornelissen M, Cornelissen P, Van der Perre G, Christensen AB, Ammitzboll F, Dyrbye C. A healing simulation technique. Experimental study concerning usability on dry and in situ tibiae. In: Cornelissen M, Van Der Perre G, Borgwardt A, editors. Monitoring of Bone Condition by Vibration Testing. Leuven: K.U.Leuven, 1988:127-141.

Cornelissen M, Huybrechs D, Van der Perre G. Reproducibility of Frequency Measurements made with the Impact Dynamic Measurement System. In: Cornelissen M, Van Der Perre G, Borgwardt A, editors. Monitoring of Bone Condition by Vibration Testing. Leuven: K.U.Leuven, 1988:37-47.

Cornelissen M, Mulier M, Cornelissen P, Van der Perre G. A study of the dynamic behaviour of healing long bones experiments and mathematical model. In: Cornelissen M, Van Der Perre G, Borgwardt A, editors. Monitoring of Bone Condition by Vibration Testing. Leuven: K.U.Leuven, 1988:79-101.

Cornelissen M, Van der Perre G, Martens M. Vibration measurements correlated with mechanical stability characteristics I. On the influence of parameters on the mechano-dynamic relations. In: Van Der Perre G, Borgwardt Christensen A, editors. Monitoring of Fracture Healing by Vibration Analysis and other Mechanical Methods. leuven: acco, 1985:75-90.

Cornelissen P, Cornelissen M, Van der Perre G. Development of a new technique: preliminary results. In: Van Der Perre G, Borgwardt Christensen A, editors. Monitoring of Fracture Healing by Vibrational Analysis and other Mechanical Methods. leuven: acco, 1985:101-112.

Cornelissen P, Cornelissen M, Van der Perre G, Christensen AB, Ammitzboll F, Dyrbye C. Assessment of tibial stiffness by vibration testing in situ--II. Influence of soft tissues, joints and fibula. *J Biomech* 1986; 19:551-561.

Courpron P. Bone tissue mechanisms underlying osteoporoses. *Orthop Clin North Am* 1981; 12:513-545.

Cruess RL, Dumont J. Current concepts. Fracture healing. *Can J Surg* 1975; 18:403-413.

Cunningham JL. The Oxford Experience with the Impact Dynamic Measurement System. In: Cornelissen M, Van Der Perre G, Borgwardt A, editors. Monitoring of Bone Condition by Vibration Testing. Leuven: K.U.Leuven, 1988:29-35.

Cunningham JL, Kershaw CJ. Clinical Measurements of Fracture Healing using IFR Method. In: Van Der Perre G, Lowet G, Borgwardt Christensen A, editors. In Vivo Assessment of Bone Quality by Vibration and Wave Propogation Techniques. Leuven: K.U. Leuven, 1991:127-138.

Dickson GR. Methods of calcified tissue preparation. New York: Elsevier Science, 1984.

Dogra SK, Singh I. Asymmetry in bone weight in the human upper limbs. *Anat Anz.Bd.* 1970; 127:210-212.

Dogra SK, Singh I. Asymmetry in bone weight in the human lower limbs. *Anat Anz.Bd.* 1971; 128:278-280.

Edholm P, Hammer R, Hammerby S, Lindholm B. The stability of union in tibial shaft fractures: its measurement by a non-invasive method. *Arch Orthop Trauma Surg* 1984; 102:242-247.

Emmanual J, Hornbeck C, Emmanual JG, Campbell P. Techniques for large bone specimens and bone with implants. In: National Workshop Manual. National Society of Histotechnoology, 1987:

Evans EJ. Vibratory properties and resonances of the isolated human ulna. *J Biomed Eng* 1985; 7:144-148.

Evans M, Gwillim J, Harris D, Tanner KE. The Monitoring of Fracture Stiffness with External Fixation. In: Whittle M, Harris D, editors. Biomechanical Measurement in Orthopaedic Practice. Oxford: Oxford University Press, Oxford, 1985:29-35.

Frost HM. The regional acceleratory phenomenon: A review. *Henry Ford Hospital Med J* 1983; 31:3

Frost HM. Structural adaptations to mechanical usage. A proposed "three-way-rule" for BMU-based remodelling of lamellar bone. Part 1. *Veterinary and Comparative Orthopaedic Traumatology* 1988; 1:9

Frost HM. The biology of fracture healing. An overview for clinicians. Part I. *Clin Orthop* 1989; 283-293.

Goodship AE, Kenwright J. The influence of induced micromovement upon the healing of experimental tibial fractures. *J Bone Joint Surg Br* 1985; 67:650-655.

Goodship AE, Watkins PE, Rigby HS, Kenwright J. The role of fixator frame stiffness in the control of fracture healing. An experimental study. *J Biomech* 1993; 26:1027-1035.

Guzelsu N, Saha S. Electro-mechanical wave propagation in long bones. *J Biomech* 1981; 14:19-33.

Hammer R, Norrbom H. Evaluation of fracture stability. A mechanical simulator for assessment of clinical judgement. *Acta Orthop Scand* 1984; 55:330-333.

Harris JD, Kenwright J, Evans M. Fracture stiffness monitoring with external fixation using strain gauge transducers and forceplate. In: Van Der Perre G, Borgwardt Christensen A, editors. Monitoring of Fracture Healing by Vibration Analysis and other Mechanical Methods. Leuven: K.U.Leuven, 1985:177-186.

Hecker JF. The sheep as an experimental animal. London: Academic Press, 1983.

Henry AN, Freeman MAR, Swanson SAV. Studies on the Mechanical Properties of Healing Experimental Fractures. *Proc Roy Soc Med* 1968; 61:902-906.

Hight TK, Piziali RL, Nagel DA. Natural frequency analysis of a human tibia. *J Biomech* 1980; 13:139-147.

Jernberger A. Measurement of stability of tibial fractures. *Acta Orthop Scand Suppl* 1970; 135:

Jorgensen TE. Measurement of stability of crural fractures treated with Hoffmann osteotaxis. 2. Measurements on crural fractures. *Acta Orthop Scand* 1972; 43:207-218.

Jorgensen TE. Measurement of stability of crural fractures treated with Hoffmann osteotaxis. 3. The uncomplicated, terminal phase of healing of crural fractures. *Acta Orthop Scand* 1972; 43:264-279.

Jurist JM, Dymond AM. Reproducibility of ulnar resonant frequency measurement. *Aerosp Med* 1970; 41:875-878.

Jurist JM, Kianian K. Three models of the vibrating ulna. *J Biomech* 1973; 6:331-342.

Kenwright J. Biomechanical measurement of fracture repair. In: Whittle M, Harris JD, editors. Biomechanical Measurement in Orthopaedic Practice. Oxford: Oxford University Press, 1985:3-9.

Kenwright J, Goodship AE. Controlled mechanical stimulation in the treatment of tibial fractures. *Clin Orthop* 1989; 36-47.

Kenwright J, Richardson JB, Cunningham JL, White SH, Goodship AE, Adams MA, et al. Axial movement and tibial fractures. A controlled randomised trial of treatment. *J Bone Joint Surg Br* 1991; 73:654-659.

Khalil TB, Viano DC, Taber LA. Vibrational characteristics of the embalmed human femur. In: Anonymous Advances in Bioengineering. New York: ASME, 1980:57

Larsen J, Borgwardt A, Ammitzboll F, Dyrbye C. The BRA-setup - A detailed description. In: Van Der Perre G, Borgwardt Christensen A, editors. Monitoring of Fracture Healing by Vibration Analysis and other Mechanical Methods. leuven: acco, 1985:47-50.

Lawes TJ, Chehade MJ. New BRA hand-held shaker: improved design and performance. *Proceedings of the AOA annual scientific meeting (SA branch).*1993.

Lettin AWF. The effects of axial compression on the healing of experimental fractures of the rabbit tibia. *Proc Roy Soc Med* 1965; 58:882-886.

Lewis JL. A dynamic model of a healing fractured long bone. *J Biomech* 1975; 8:17-25.

Lim MK. Effect of swollen soft tissue on the impedance of bone for fracture healing diagnosis. *J Biomed Eng* 1989; 11:517-519.

Lowet G, Van Audekercke R, Van der Perre G, Geusens P, Dequeker J, Lammens J. The correlation between resonant frequency analysis and torsional stiffness of long bones. In: Van Der Perre G, Lowet G, Borgwardt Christensen A, editors. In Vivo Assessment of Bone Quality by Vibration and Wave Propagation Techniques. Part II. Leuven: K.U.Leuven, 1992:111-125.

Lowet G, Van Audekercke R, Van der Perre G, Geusens P, Dequeker J, Lammens J. The relation between resonant frequencies and torsional stiffness of long bones in vitro. Validation of a simple beam model. *J Biomech* 1993; 26:689-696.

Markel MD, Wikenheiser MA, Chao EY. A study of fracture callus material properties: relationship to the torsional strength of bone. *J Orthop Res* 1990; 8:843-850.

Markel MD, Wikenheiser MA, Chao EY. Formation of bone in tibial defects in a canine model. Histomorphometric and biomechanical studies. *J Bone Joint Surg [Am]* 1991; 73:914-923.

Markey EL, Jurist JM. Tibial resonant frequency measurements as an index of the strength of fracture union. *Wis Med J* 1974; 73:62-65.

Mather BS. The symmetry on the mechanical properties of the human femur. *J Surg Res* 1967; 7:222-225.

Matthews LS, Kaufer H, Sonstegard DA. Manual sensing of fracture stability: a biomechanical study. *Acta Orthop Scand* 1974; 45:373-381.

Matthews MG, King JB, Collier RJ, Donarski RJ. The objective monitoring of stiffness of healing fractures by acoustic resonance scanning - initial clinical experience. In: "Institute of Mechanical Engineers.", editor. The Changing Role of Engineers in Orthopaedics. Proceedings of the Instititon of Mechanical Engineers. London: 1989:127-132.

Mayer G, Wolf E. Animal experiments to examine the histology of fracture healing in osteosynthesis with external fixation and compression. *Arch Orthop Trauma Surg* 1983; 101:111-120.

McKibbin B. The biology of fracture healing in long bones. *J Bone Joint Surg* 1978; 60-B:150-162.

Nokes LD, Fairclough JA, Mintowt Czyz WJ, Mackie I, Williams J. Vibration Analysis of Human Tibia: The Effect of Soft Tissue on the Output from Skin-Mounted Accelerometers. *J Biomed Eng* 1984; 6:223-226.

Nokes LD, Mintowt Czyz WJ, Mackie I, Fairclough JA, Williams J. Direct and indirect determination of tibial natural frequency -a comparison of frequency domain analysis and fast fourier transform. *J Biomed Eng* 1994; 6:45-48.

Nunamaker DM, Perren SM. A radiological and histological analysis of fracture healing using prebending of compression plates. *Clin Orthop* 1979; 167-174.

Orne D. The in vivo, driving-point impedance of the human ulna--a viscoelastic beam model. *J Biomech* 1974; 7:249-257.

Orne D, Mandke J. The influence of musculature on the mechanical impedance of the human ulna, an in vivo simulated study. *J Biomech* 1975; 8:143-149.

Orne D, Young DR. The effects of variable mass and geometry, pretwist, shear deformation and rotatory inertia on the resonant frequencies of intact long bones: a finite element model analysis. *J Biomech* 1976; 9:763-770.

Parfitt AM, Drezner MK, Glorieux FH, Kanis JA, Malluche H, Meunier PJ, et al. Bone histomorphometry: standardization of nomenclature, symbols, and units. Report of the ASBMR Histomorphometry Nomenclature Committee. *J Bone Miner Res* 1987; 2:595-610.

Pelker R, Saha S. A theoretical investigation of wave propagation in long bones. In: Bell AC, Nerem RM, editors. Advances in Bioengineering. New York: American Society of Mechanical Engineers, 1975:98-100.

Pelker RR, Saha S. Stress wave propagation in bone. *J Biomech* 1983; 16:481-489.

Pelker RR, Saha S. Wave propagation across a bony discontinuity simulating a healing fracture. *J Biomech* 1985; 18:745-753.

Perren SM. Physical and biological aspects of fracture healing with special reference to internal fixation. *Clin Orthop* 1979; 175-196.

Perren SM, Rahn BA. Biomechanics of fracture healing. *Can J Surg* 1980; 23:228-232.

Pohl AP, Cain CM, Latham JM, and Casse J. Bone resonance analysis of the human tibia: an accurate non-invasive technique. *Transactions 42nd Annual Meeting Orthopaedic Research Society,* 1991; 119.

Reilly DT, Burstein AH. The elastic and ultimate properties of compact bone tissue. *J Biomech* 1975; 8:393-405.

Reilly DT, Burstein AH, Frankel VH. The elastic modulus for bone. *J Biomech* 1974; 7:271-275.

Richards J, Brandon JA, Mackie I. Vibration methods for assessing fracture healing. In: Anonymous The Changing Role of Engineering in Orthopaedics. Proceedings of the Institution of Mechanical Engineers. London: "Institute of Mechanical Engineers.", 1989:123-125.

Richardson JB, Cunningham JL, Goodship AE, O'Connor BT, Kenwright J. Measuring stiffness can define healing of tibial fractures. *J Bone Joint Surg Br* 1994; 76:389-394.

Richardson JB, Kenwright J, Cunningham JL, Beavis A, Evans M, Tew T. Clinical applications of fracture stiffness measurements. *Annu Rep Oxford Eng Cent* , 1987; 14:61-65.

Rubin CT, Lanyon LE. Regulation of bone formation by applied dynamic loads. *J Bone Joint Surg [Am]* 1984; 66-A:397-401.

Saha S, Lakes RS. A non-invasive technique for detecting stress waves in bone using the piezoelectric effect. *IEEE Trans Biomed Eng* 1977; 24:508-512.

Saha S, Lakes RS. The effect of soft tissue on wave-propagation and vibration tests for determining the in vivo properties of bone. *J Biomech* 1977; 10:393-401.

Sarmiento A, Schaeffer JF, Beckerman L, Latta LL, Enis JE. Fracture healing in rat femora as affected by functional weight-bearing. *J Bone Joint Surg [Am]* 1977; 59-A:369-375.

Schaffler MB, Burr DB. Stiffness of compact bone: effects of porosity and density. *J Biomech* 1988; 21:13-16.

Seimon LP. Re-fracture of the shaft of the femur. *J Bone Joint Surg* 1964; 46 B:32-39.

Sevitt S. Healing of fractures in man. In: Owen R, Goodfellow J, Bullough P, editors. Scientific foundations of orthopaedics and traumatology. Philadelphia: W.B.Saunders, 1980:258-272.

Sonstegard DA, Matthews LS. Sonic diagnosis of bone fracture healing--a preliminary study. *J Biomech* 1976; 9:689-694.

Spiegl PV, Jurist JM. Prediction of ulnar resonant frequency. *J Biomech* 1975; 8:213-217.

Steele CR, Zhou LJ, Guido D, Marcus R, Heinrichs WL, Cheema C. Noninvasive determination of ulnar stiffness from mechanical response--in vivo comparison of stiffness and bone mineral content in humans. *J Biomech Eng* 1988; 110:87-96.

Tencer AF, Johnson KD, Kyle RF, Fu FH. Biomechanics of fractures and fracture fixation. *Instr Course Lect* 1993; 42:19-55.

Thompson GA. In vivo determination of bone properties from mechanical impedance measurements. *Aerospace Medical Association Annual Science Meeting, 7-10 May, Las Vegus, Nevada* 1973; Abstract.

Thompson GA, Orne D, Young DR. In vivo determination of mechanical properties of the human ulna by means of mechanical impedance tests: experimental results and improved mathematical model. *Med Biol Eng* 1976; 14:253-262.

Thomsen JJ. Modelling human tibia structural vibrations. *J Biomech* 1990; 23:215-228.

Tower SS, Beals RK, Duwelius PJ. Resonant Frequency Analysis of the Tibia as a Measure of Fracture Healing. *J Orthop Trauma* 1993; 7:552-557.

Van der Perre G. Dynamic analysis of human bones. In: Ducheyne P, Hastings GW, editors. Functional Behaviour of Orthopedic Biomaterials. Boca Raton, Florida: CRC Press, 1984:99-159.

Van der Perre G, Cornelissen P. On the mechanical resonances of a human tibia in vitro. *J Biomech* 1983; 16:549-552.

Van der Perre G, Van Audekercke R, Martens M, Mulier JC. Identification of in-vivo vibration modes of human tibiae by modal analysis. *J Biomech Eng* 1983; 105:244-248.

Vandecasteele J, Van der Perre G, Van Audekercke R, Martens M. Evaluation of bone strength and integrity by vibration methods. In: Stokes IAF, editor. Mechanical Factors and the Skeleton. London: John Libbey, 1981:98-105.

White AA, Panjabi MM, Hardy RJ. Analysis of mechanical symmetry in rabbit long bones. *Acta Orthop Scand* 1974; 45:328-336.

White AA, Panjabi MM, Southwick WO. The four biomechanical stages of fracture repair. *J Bone Joint Surg Am* 1977; 59:188-192.

Wong AT, Goldsmith W, Sackman JL. Flexural wave propagation in discontinuous model and in vitro tibiae. *J Biomech* 1976; 9:813-825.

Wong FY, Pal S, Saha S. The assessment of in vivo bone condition in humans by impact response measurement. *J Biomech* 1983; 16:849-856.

Wright TM, Hayes WC. Tensile testing of bone over a wide range of strain rates: effects of strain rate, microstructure and density. *Med Biol Eng* 1976; 14:671-680.

Ziegert JC, Lewis JL. The Effect of Soft Tissue on Measurements of Vibrational Bone Motion by Skin-Mounted Accelerometers. *J Biomech* 1979; 101:218-220.